

**POSITRON
EMISSION
TOMOGRAPHY
OF NOVEL
RADIOTRACERS
FOR THE
CENTRAL
NERVOUS
SYSTEM**

**RADIATION DOSIMETRY AND
TRANSLATIONAL IMAGING STUDIES**

JASPER VAN DER AART

POSITRON EMISSION TOMOGRAPHY OF NOVEL RADIOTRACERS
FOR THE CENTRAL NERVOUS SYSTEM

VRIJE UNIVERSITEIT

POSITRON EMISSION TOMOGRAPHY OF NOVEL RADIOTRACERS FOR THE CENTRAL NERVOUS SYSTEM

Radiation Dosimetry and Translational Imaging Studies

ACADEMISCH PROEFSCHRIFT

ter verkrijging van de graad Doctor of Philosophy aan
de Vrije Universiteit Amsterdam,
op gezag van de rector magnificus
prof.dr. V. Subramaniam,
in het openbaar te verdedigen
ten overstaan van de promotiecommissie
van de Faculteit der Geneeskunde
op maandag 30 september 2019 om 11.45 uur
in de aula van de universiteit,
De Boelelaan 1105

door
Jasper van der Aart
geboren te Lisse

Design: Caroline de Lint, Voorburg (caro@delint.nl)

All rights reserved. No part from this thesis may be reproduced, distributed or transmitted in any form or by any means, without prior written permission of the author.

Publication of this thesis was financially supported by the foundation
Centre for Human Drug Research in Leiden, the Netherlands

promotoren: prof.dr. A.A. Lammertsma
prof.dr. B.N.M. van Berckel

copromotor: dr. G.J. Groeneveld

	CHAPTER 1
7	INTRODUCTION
	CHAPTER 2
25	RADIATION DOSE ESTIMATES FOR CARBON-11 LABELLED PET TRACERS
	CHAPTER 3
45	HUMAN DOSIMETRY OF THE NMDA RECEPTOR LIGAND [¹¹ C]GMOM
	CHAPTER 4
55	EVALUATION OF THE NOVEL PET TRACER [¹¹ C]HACH242 FOR IMAGING THE GLUN2B NMDA RECEPTOR IN NON-HUMAN PRIMATES
	CHAPTER 5
72	FIRST IN HUMAN EVALUATION OF [¹⁸ F]PK-209, A PET LIGAND FOR THE ION CHANNEL BINDING SITE OF NMDA RECEPTORS
	CHAPTER 6
95	QUANTIFICATION OF HUMAN BRAIN PDE4 OCCUPANCY BY GSK356278: A [¹¹ C](R)-ROLIPRAM PET STUDY
	CHAPTER 7
109	DISCUSSION AND CONCLUSIONS
	CHAPTER 8
127	SUMMARY IN DUTCH / NEDERLANDSE SAMENVATTING
137	CURRICULUM VITAE
139	LIST OF PUBLICATIONS

CHAPTER 1

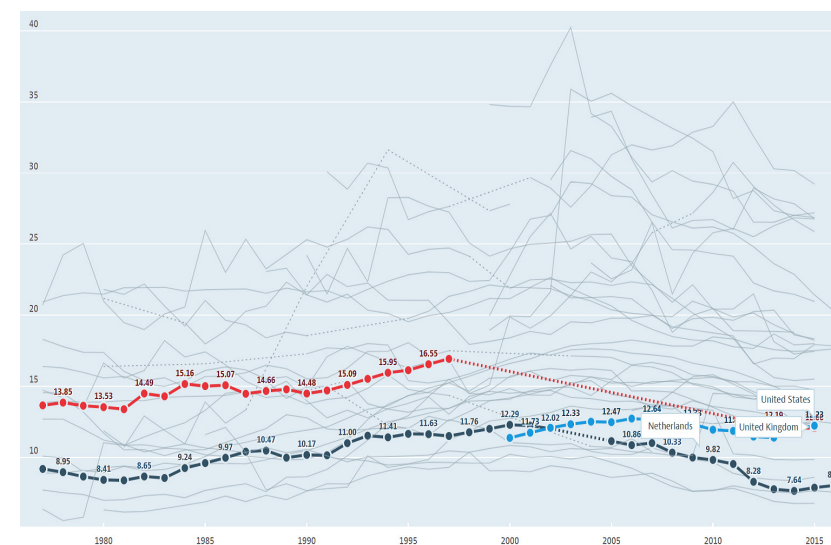
INTRODUCTION

Leescommissie: prof.dr. M. Lubberink
prof.dr. K. van Laere
prof.dr. R. Boellaard
prof.dr. H.W.H.G. Kessels
dr. J. Doorduyn
dr. E. A. Rabiner

Healthcare has the characteristics of an industry susceptible to disruption. The unsustainable rise in healthcare costs is a key challenge that is high on the agenda of politicians and entrepreneurs around the world. Already, Americans spend 17% of gross domestic product on health care, compared with 11% in the Netherlands¹. Ten of the twenty occupations that will grow the fastest in the u.s. by 2020 are related to healthcare, largely due to an aging population². Solutions to curtail healthcare expenditures include the digitisation of patient records, amassing data from clinical trials, and the development of big-data algorithms that can provide the most robust evidence for patient treatment and research and development (R&D) investment decisions.

Another area where gains can be made is the reduction of drug development cost. There has been substantial media interest in the price of a small number of medicines, partly triggered by scandals concerning the hiked prices of old drugs. However, as Figure 1 shows, pharmaceutical spending as part of total healthcare spending has decreased in most countries in the past 20 years. For example the u.s. and the Netherlands saw a decrease of approximately 4% to 12.2% and 8.0% of total healthcare spending respectively³. Nevertheless, despite a rise in drug development R&D spending, new product approvals have been low, especially of drugs that intent to treat central nervous system (CNS) disorders. The likelihood of approval of a novel drug for a neurological indication that is in Phase 1 of clinical development is currently just 9%⁴. The two most important reasons for failures between Phase 2 and submission to regulatory authorities were a lack of efficacy (52%) or safety (24%)⁵. Failure of compounds in late phase development reduces R&D efficiency substantially. However, failure in Phase 1 does not necessarily need to be interpreted as a negative trend. The early timing of attrition in the pipeline can be a powerful lever for driving R&D productivity by avoiding the need for costly late-stage clinical trials. Fortunately, success rates of new drugs across the industry are up in the three years up to 2014⁶. Forty-five new molecular entities were approved in 2015 by the United States Food and Drug Administration (FDA) Center for Drug Evaluation and Research. The size of the overall portfolio of novel clinical-stage compounds has increased as well to 3,823 compounds in 2015⁶. However, operations in the pharmaceutical industry are far from optimised. A recent report⁷ showed that against a standardised portfolio of clinical trials, a ‘poor’ company performing at –1 standard deviation (SD) spends 1.9 times as much money, takes 1.5 times as long and has 2.3 times as many regulatory findings per audit as a ‘good’ company performing at +1 SD. These results highlight that product value and the rate of pipeline attrition

FIGURE 1 Pharmaceutical spending from 1976 to 2016 as % of total health spending.³



are not the only important determinants of R&D productivity, but also the optimisation of clinical development operations such as speed (e.g. reducing inter-trial intervals) and regulatory submission quality.

Drug development in neurology and psychiatry has been particularly unsuccessful. The decline in new drug has largely been driven by a high failure rate in the translation of preclinical efficacy findings, caused by inadequate animal models, poor protocol design, data robustness, data generalisability and target engagement⁸. In fact, when scientists at Pfizer reviewed 44 on the company’s Phase II programmes across several therapeutic areas for evidence of target engagement, they found that 43% of clinical proof-of-concept (POC) studies that failed to show efficacy did not adequately demonstrate whether the mechanism of the drug-target interaction was tested⁹. Similarly, an analysis of the use of biomarkers in the development of novel treatments for schizophrenia showed that for 80% of 72 novel drugs tested in POC studies between 1994 and 2014 there was no evidence of biomarker-driven dose selection⁸. The analysis of a longitudinal internal review of AstraZeneca’s small-molecule drug projects¹⁰ concluded that 40% of projects

that failed in Phase 2 could be ascribed to a lack of target linkage to the disease or no availability of validated animal models. 29% of failures could be attributed to absence of evidence that supported exposure of the drug to the target tissue. Clearly, a drug's exposure, binding, and functional modulation of the target site (that is relevant for the chosen indication) must be established as early on as possible in order to minimise attrition in Phase 1 and 2 clinical trials.

Following pre-clinical development, novel compounds are conventionally implemented in four consecutive phases of clinical development. The objectives are generally to provide information on (I) safety, tolerability and pharmacokinetics in healthy subjects, (II) modulation of disease activity in patients, (III) the drug's therapeutic index and covariate effects leading to marketing approval, and (IV) post-approval trials, e.g. competitor comparisons. This framework reduces the risk of unknown findings, yet offers only incremental confidence in the drug. Data intensive (and hence more informative) early phase studies could reduce the risk of performing a subsequent larger clinical trial at either non-pharmacological doses or at doses that produce side effects. The European Medicines Agency (EMA) published in July 2017 a guideline for first-in-human drug studies, which has been comprehensively discussed by Van Gerven and Bonelli¹¹ with a focus on the identification and mitigation of risks inherent to administration of investigational medicinal products in humans.

In addition to safety and tolerability objectives that are traditionally the primary objectives in first-in-human studies, clinical development programmes may benefit from the quantitative measurements of pharmacodynamic (PD) effects to explore drug efficacy early on. However, the inclusion of PD endpoints in Phase 1 that are relevant to the drug's mechanism of action has only slowly gained traction over the past decades. For example, in a review of 81 Phase 1 studies in healthy volunteers that were submitted in 2009 to the competent authority for clinical trials in the Netherlands, 32 were first-in-human studies with safety and tolerability as the primary endpoints, and in only 13 studies biomarkers were investigated¹². Biomarkers can aid the identification of molecular and cellular mechanisms of disease pathogenesis processes. By exploring pharmacological modification in Phase 1, biomarkers that are relevant to the disease may mitigate the risk of clinical trial failure. A more cyclical, instead of linear Phase 1 to 3 approach to drug development may be more suitable to novel compounds^{12,13}. One that incorporates biomarker identification and measurement into the scientific objectives of the clinical programme.

The criteria for fit-for-purpose biomarkers in early drug development have been reviewed extensively in the literature^{14,15}. A valuable biomarker offers insight into the timing, magnitude, and location of pharmacological effects. It can help to answer important questions early in the drug development process such as:

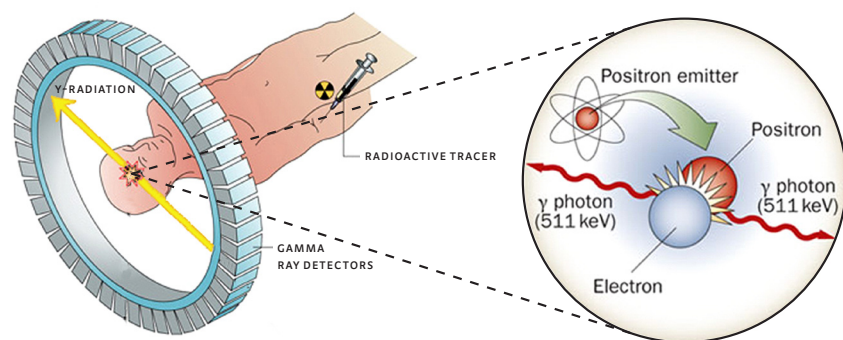
- Does a new drug molecule reach the tissue of interest in potentially pharmacologically active concentrations?
- Is it interacting with the target of interest?
- What is the quantitative relationship between the extent of this interaction and the administered dose?
- What are the consequent pharmacological and physiological effects and how long do they last?
- Do patients express the target differently than healthy volunteers?

With regards to development of drugs targeting the CNS, a wide range of pharmacodynamic tools and biomarkers can be used to establish effects on the brain. Pharmacological functional magnetic resonance imaging (fMRI)¹⁶ can show how compounds affect downstream physiology, in this case the haemodynamic response to neuronal activity. In addition, computerised, repeatable drug-sensitive tests such as those incorporated in the NeuroCart battery developed by the Centre for Human Drug Research (Leiden, the Netherlands) have been implemented in Phase 1 studies. Using the NeuroCart, the pharmacodynamic profile of more than 40 CNS compounds has been determined, by using tests that measure cognitive, psychomotor, neurophysiological and subjective drug effects¹⁷. Such tests offer the chance to explore both dose-response and time specific drug effects, including generating evidence to answer key questions related to blood-brain-barrier penetration and the pharmacokinetic-pharmacodynamic (PK-PD) relationship.

Positron Emission Tomography

The highest level of confidence and direct evidence that engagement of the target (e.g. a receptor, transporter or enzyme) is achieved, can be provided with in vivo molecular imaging experiments with positron emission tomography (PET). Important discoveries in nuclear physics, neurophysiology and radiotracer development in the 20th century revolutionised non-invasive imaging techniques that led to the invention of the first human positron imaging devices in the 1950s and the

FIGURE 2 Tomography of positron emission using gamma ray detectors following injection of a radiotracer.



Adapted from reference 22.

introduction of the first PET scanner in 1975¹⁸. The technique relies on the concept of imaging molecules that are labelled with positron emitting radionuclides called radiotracers, or radioligands if they bind with high affinity to a specific molecular target. Following intravenous administration, a radiotracer is distributed throughout the body in a matter of minutes. The gamma radiation emitted by the radiotracer can be detected and localised by a PET scanner, and its distribution followed over time. Radioactive isotopes such as carbon-11 have unstable nuclei that decay to stable form by converting excess protons to neutrons. This process, where a proton is converted into a neutron, a positron, and an electron neutrino is known as β^+ decay or positron emission. Carbon-11 for example decays to boron-11 mainly by positron emission (99.8%) with a half-life ($T_{1/2}$) of 20.334 minutes¹⁹. Radioactivity refers to the nuclear transformation rate, i.e., the number of disintegrations of unstable atomic nuclei per second. The SI unit is the Becquerel (Bq) which equals to one disintegration per second. When a positron annihilates with an electron, the mass of the positron and electron (both $9.1091 \cdot 10^{-31}$ kg) is converted into energy as described by $E=mc^2$ ^{20,21} in the form of two photons with 511keV energy in nearly opposite directions (Figure 2)²². Combining PET with computed tomography (CT) or MRI facilitates anatomic localisation of the signal and direct mapping to functional pathways. However, PET spatial resolution is ultimately limited by the positron range before annihilation (~ 1 -2mm) and the non-collinearity of the annihilation ($180^\circ \pm 0.25^\circ$).

Only minute amounts of radioligand (tracer amounts) are sufficient to illuminate processes in the human body using modern PET scanners. These have the ability to measure gamma ray photons with a high temporal and spatial resolution. Microdosing of the radiotracer eliminates the risk that routine toxicological safety screening prohibits the administration of a small molecule PET imaging agents in humans. Tracer amounts further ensure that the radioligand engages only a fraction of the target, and therefore should not influence the pharmacokinetics of the drug under investigation. Only for the most potent agonist radiotracers such as [¹¹C]PHNO there is a risk that the injected mass is outside the tracer range, which could present potential confounding factors in imaging²³.

Quantification of the tissue radioactivity data allows inferences to be made about biochemical and physiological processes reflected in the distribution and kinetics of the labelled molecule in humans in vivo. However, in order to allow appropriate quantification in the organ of interest (e.g. the brain), a radiotracer with sufficient radioactivity (in the order of megaBecquerels) needs to be administered. This exposes the subject's body tissue to a source of ionising radiation. Short-lived positron emitting isotopes such as carbon-11 and fluorine-18 ($T_{1/2}=109.77$ min) enable optimal use of imaging photons to capture the kinetics of the radiotracer in the body, while keeping the radiation dose relatively low. Furthermore, through state-of-the-art radiochemistry, these isotopes can be incorporated into pharmaceuticals without altering their biological activity. However, despite the relatively short half-lives of carbon-11 and fluorine-18 (compared with e.g. zirconium-89), estimates are still required of the radiation dose and associated risk arising from the radiotracer administration. In CHAPTER 2 of this thesis, we describe in more detail the biological effects of radiation and the methods to estimate radiation dose for carbon-11 labelled PET tracers. Furthermore, we summarise the published radiation dose estimates for a wide range of carbon-11 labelled radiotracers and relate them to most commonly used dose limits from regulatory guidelines.

In CHAPTER 3, we present human PET experiments that have been performed to assess the radiation dose of the novel brain N-methyl-D-aspartate (NMDA) receptor radiotracer [¹¹C]GMOM. Although there are methods available to scale radiation dose estimates from preclinical species to man, potentially significant interspecies differences mean that extrapolation from rodent data should be considered with care. When a new radiotracer is implemented in a clinical setting, with potentially repeated imaging in a single (healthy) subject, this should not incur a safety risk to the subject. PET biodistribution studies can help to understand the

radiopharmaceutical's administration, distribution, metabolism or elimination profile (ADME). Put simply, a dynamic PET scan allows for the measurement of the concentration-time course in the tissue of interest, which in the case of [¹¹C]GMOM is the NMDA receptor in the brain. It was therefore important not only to assess radiation dosimetry, but also to confirm blood-brain-barrier (BBB) penetration of the radiotracer in humans.

The strength of PET lies not in biodistribution studies, but rather in its potential for "precision pharmacology"²⁴. Using a labelled tracer molecule that specifically binds to the same target as the investigational compound, PET imaging can indirectly visualise the interaction between the investigational compound and its target by showing changes in radiotracer binding. It is comparable to competitive antagonism – the higher the affinity of the compound to the target, the more the tracer signal will be reduced. PET can provide excellent quantitative accuracy and high sensitivity, provided that the utilised radiotracer has the right characteristics for the objective of PET imaging. The availability of specific radiotracers is paramount to successful bridging of preclinical and early clinical drug development, and for the application of PET in the clinical setting. The increased accessibility in the 1990s to lab facilities sufficiently equipped for radiopharmaceutical research spurred development of high-quality PET radiotracers as well as pharmacological challenge tools with suitable characteristics to evaluate radiotracer binding. Nowadays there are well-validated PET radioligands available for more than 40 CNS targets, including neurotransmitter targets (receptors, transporters, synthesis and activity) such as dopamine, serotonin, noradrenaline, GABA, glutamate, acetylcholine, histamine, opioids, and many others^{25,26}. Table 1 shows a selection of radiotracers that have been implemented in clinical studies at the VU University Medical Center (Amsterdam UMC, The Netherlands) which span therapy areas such as neurology, cardiology and oncology.

Unfortunately, radiotracer development is often a time-consuming process with considerable attrition, akin to processes in drug development. The requirements for optimal characteristics of CNS radiotracers and its targets are well described in the literature⁴⁷. In brief, the tracer should have good brain delivery, good (rapid) tissue kinetics, low non-specific binding (e.g. from radiometabolites), and sufficiently high affinity for the target. The target itself should have high concentration in the tissue (i.e. B_{MAX}) to provide a useful signal-to-noise ratio. Furthermore, the timing of the availability of a well validated PET ligand for a novel target is crucial for it to have maximum benefit in drug development. For example the recent interest in P2X7

receptor antagonists, which target the neuroinflammatory cascade, has engaged the pursuit of PET ligands for this target^{48,49}. In 2016, the candidate tracers that were in development were not ready for clinical implementation, despite the completion of Phase 1 studies with P2X7 antagonists such as JNJ-54175446⁵⁰. Clinical availability of a P2X7 radiotracer would have allowed confirmation of JNJ-54175446 BBB penetration. In addition, data on target occupancy could be related to plasma exposure, safety and tolerability outcomes, and (if present) pharmacodynamic effects. The development and validation of PET radiotracers requires significant resources and expertise, and the discovery and clinical implementation of the right radiotracer at the right time is a major challenge for the field of PET.

TABLE 1 A selection of radiotracers that have been implemented in clinical studies at the VU University Medical Center.

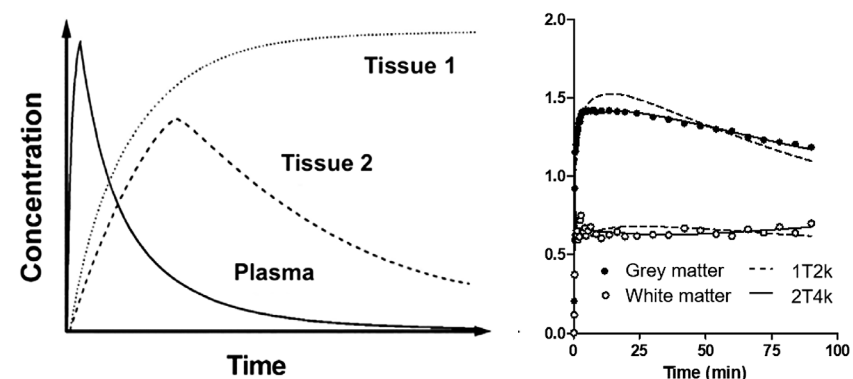
Radiotracer	Target	Reference
[¹¹ C]Flumazenil	Brain GABA _A receptor	27
[¹¹ C]Raclopride	Brain Dopamine D ₂ /D ₃ receptor	28
[¹¹ C]PK11195	Brain Microglial activation	29
[¹⁸ F]DPA-714	Brain Microglial activation	30
[¹¹ C]SMW139	Brain P2X7 receptor	31
[¹¹ C]GMOM	Brain PCP site of the NMDA receptor	32
[¹⁸ F]PK-209	Brain PCP site of the NMDA receptor	33
[¹¹ C]PIB	Brain Beta-amyloid	34
[¹⁸ F]Flutemetamol	Brain Beta-amyloid	35
[¹⁸ F]Florbetapir	Brain Beta-amyloid	36
[¹⁸ F]AV1451	Brain Tau	37
[¹¹ C]Phenytoin	P-glycoprotein	38
[¹¹ C]Verapamil	P-glycoprotein	39
[¹¹ C]Laniquidar	P-glycoprotein	40
[¹¹ C]HED	Norepinephrine, myocardium	41
[¹¹ C]Erlotinib	Oncology tyrosine kinase inhibitor	42
[¹⁸ F]FLT	Oncology tumor proliferation	43
[¹⁸ F]FAZA	Oncology tumor hypoxia	44
[¹⁸ F]FDG	Glucose metabolism	45
[¹⁵ O]H ₂ O	Blood flow	46

In Vivo Radiotracer Quantification

The exposure and regional distribution of radiotracers in the brain can be measured with a high resolution PET system and quantified using standard pharmacokinetic parameters such as C_{max} , T_{max} , AUC and brain/blood ratios. However, target binding also depends on the affinity of the ligand for its target (the inverse of K_D) and the density of the target (B_{max}). Quantification of binding can be achieved with kinetic analysis using compartmental modelling. A radiotracer that is suitable to measure drug occupancy at its target ideally has reversible, high specific binding (S) and low non-specific binding (NS, e.g. binding to other proteins). Non-specific and free unbound radiotracer in the tissue are together referred to as the non-displaceable (ND) fraction, as they cannot be blocked by competitive binding. The non-displaceable fraction is often assumed to be equal in regions of interest (ROIs) that are target-rich and target-free. For example, [^{11}C]raclopride has high affinity for dopamine D_2/D_3 receptors, which are expressed in the striatum but not in the cerebellum. The binding potential is the equilibrium concentration of specific binding as a ratio to another concentration, e.g. non-displaceable radioligand (BP_{ND}), and is unitless⁵¹. In the case of [^{11}C]raclopride, the BP_{ND} in the region with the highest D_2 fraction (putamen) is approximately 3.0 when using a reference region devoid of the target (cerebellum)²³. The molecular targets that are investigated in this thesis, i.e. the NMDA receptor and the PDE4 enzyme, are expressed throughout the CNS, and therefore reference regions devoid of the targets are not available. However, the non-displaceable fraction of the radiotracer can also be quantified if there is a blocking agent available that competes with the radioligand at the target. In this case, 'baseline' radiotracer binding is compared to binding after administration of the blocking agent, regardless of the existence of a reference region. The fraction of non-displaceable binding can be derived from the (modified) Lassen plot⁵² after a full block of the specific signal, under the assumption that there is a range of regions with differing target density.

The radiotracer concentrations in plasma and tissue (Figure 3) can be described by PET pharmacokinetic models which simplify the physiological interactions by using compartments that can characterise the kinetics of the tracer. Kinetic parameter estimates can be calculated by minimising the sum of squares between measured data and (non-linear) models. The amount of radioactivity in the tissue is dependent on the amount supplied to it via the plasma. Figure 4 shows a schematic diagram of a two-tissue compartment model (in contrast to clinical pharmacology,

FIGURE 3 A. Example of time-activity curves (TACs) showing radioactivity concentrations in plasma following intravenous administration of the radiotracer, and uptake, distribution and elimination in two different tissues of interest. B. Example TACs corrected for injected radioactivity and bodyweight (i.e. standardised uptake values, SUV) in grey matter (closed circles) and white matter (open circles) and kinetic fits using one compartment (1t2k) or two compartment models (2t4k), the latter showing a superior fit of the grey matter TAC).



the plasma component does not represent a third component in radioligand imaging). K_1 is the rate constant that represents the influx from plasma to tissue, whereas k_2 represents the clearance from tissue to plasma. By using dynamic PET data and a compartmental description of the tracer, the model parameters are able to decouple tracer delivery and binding information. For example, assuming a cerebral blood flow of $50 \text{ ml} \cdot 100 \text{ g} \cdot \text{min}^{-1}$ and a density of brain tissue of $1 \text{ g} \cdot \text{cm}^{-3}$, the first pass extraction of [^{11}C]raclopride from plasma is approximately 30%⁵³. The free and non-specifically bound ligand can be kinetically distinguished by rate constants k_3 and k_4 . The latter equals 0 for an irreversible two tissue compartment model.

FIGURE 4 Schematic diagram of a two-tissue reversible compartment model with 4 kinetic parameters (2t4k).



When there are no suitable reference regions or blocking agents, the total volume of distribution (V_T) is an appropriate endpoint for quantification. Volume of distribution in radioligand imaging refers to the concentration in the target region (e.g. brain) in relation to the concentration in plasma, at equilibrium, and is expressed as $\text{ml} \cdot \text{cm}^{-3}$ of tissue. V_T includes both the specific (V_S) and nonspecific (V_{ND}) binding signals (Figure 5). The V_T is equal to $V_{ND} + V_S$ and is calculated by the formula,

$$V_T = \frac{K_1}{k_2} \left(1 + \frac{k_3}{k_4} \right)$$

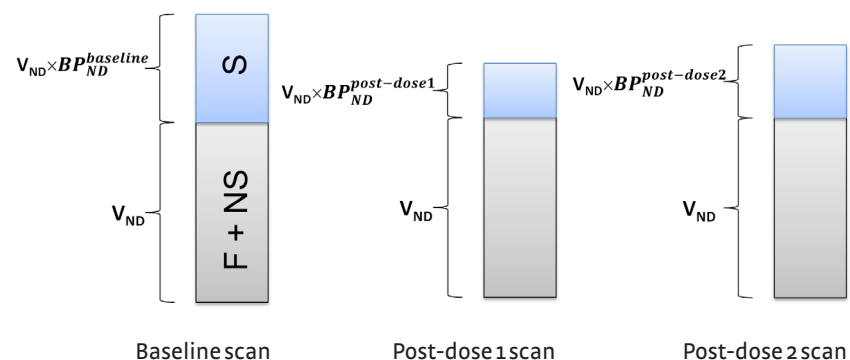
where

$$V_{ND} = \frac{K_1}{k_2}$$

The V_S can further be represented as the product of V_{ND} and the binding potential (BP_{ND}), therefore $V_S = V_{ND} \times BP_{ND}$.

When a drug competes with specifically bound radiotracer in the brain it can lead to a reduction of the BP_{ND} and consequently the V_T (Figure 5). After the time of maximum drug concentration in plasma (T_{MAX}), the concentration is normally reduced by processes of metabolism and elimination. In case of reversible binding of the drug to the target, the concentration at the target will therefore also decrease following T_{MAX} , thereby increasing the fraction of radiotracer binding.

FIGURE 5 Schematic representation of the total volume of distribution of the radiotracer before drug administration and at two timepoints post drug administration, for example at T_{max} and after two half-lives.

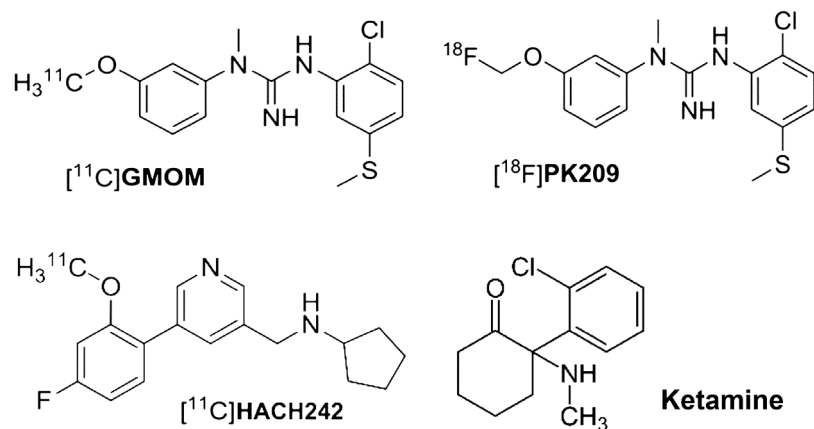


The PET scanner cannot distinguish between positrons that are emitted from radiotracer molecules that are specifically bound or non-displaceable. Neither can it distinguish between emission from intact radiotracer or from its *metabolites* that carry the radioactive label and emit positrons. Should radiometabolites pass the BBB, they may bind off-target, compromising the signal-to-noise ratio and hindering kinetic analysis of the PET data. An arterial input function takes into account radiotracer metabolism and the amount of radioactivity in blood and plasma. Experiments in CHAPTER 4, 5 and 6 of this thesis describe the measurement of radiometabolites and the parent fraction using high performance liquid chromatography (HPLC). The individual subject's metabolite corrected arterial plasma input function describes the concentration of intact radiotracer that is available in plasma during the course of the scan. The input function is then combined with the subject's PET data for quantification of tissue uptake in ROIs using the optimal kinetic model.

NMDA Receptor Imaging

In the last two decades, a significant effort in drug development has focused on the NMDA receptor, and specifically the negative allosteric modulation of the NMDA receptor's ion channel activity via the GluN2B binding site (previously known as NR2B). Glutamate is an important mediator of excitatory neurotransmission in the CNS and GluN2B modulators may have therapeutic potential for the treatment of a wide range of CNS pathologies, including acute and chronic pain, stroke, dementias and major depressive disorder^{54,55}. At present, there is no well validated GluN2B binding PET radiotracer available. The majority of radiotracers tested in the past exhibited poor brain penetration, high non-specific uptake in the brain and extensive metabolism⁵⁶. In CHAPTER 4, we present the initial PET assessment in non-human primates of [¹¹C]HACH242, a new GluN2B antagonist radiotracer⁵⁷. Prior preclinical experiments with [¹¹C]HACH242 ex vivo have shown that the ligand enters the brain and that distribution in tissue is consistent with the known distribution of the GluN2B binding site⁵⁸. These results gave confidence to continue with the next steps in tracer evaluation, which included the assessment of the kinetic profile, the measurement of plasma parent radiotracer and metabolites, and the attempt to block the specific signal. To this end, a pharmacological dose of radioprodil was administered intravenously, which was expected to reduce the specific signal of [¹¹C]HACH242 at GluN2B binding sites in the brain.

FIGURE 6 Chemical structures of the three radiotracers tested and described in chapters 3, 4 and 5. [¹¹C]GMOM (i.e. [¹¹C]N-(2-chloro-5-thiomethylphenyl)-n'-(3-methoxy-phenyl)-n'-methylguanidine), [¹⁸F]PK-209 (i.e. 3-(2-chloro-5-(methylthio)-phenyl)-1-(3-([¹⁸F]fluoromethoxy)phenyl)-1-methylguanidine), and [¹¹C]HACH242 (i.e. n-((5-(4-fluoro-2-[¹¹C]methoxyphenyl)pyridin-3-yl)methyl)-cyclopentanamin). Ketamine (i.e. 2-(2-chlorophenyl)-2-(methylamino)cyclohexanone) was used as a blocking compound in chapter 5.



PET in non-human primate is highly amenable to clinical translation, and successful imaging of the NMDA receptor in primate species warrants further investigation in humans. A second promising novel NMDA receptor ligand, [¹⁸F]PK-209, has recently been synthesised at the VUMC (Figure 6) and successfully tested in non-human primates⁵⁹.

The radiotracer binds to the phencyclidine (PCP) binding site of the NMDA receptor, which sits within the ion channel in the transmembrane domain. Primate studies with [¹⁸F]PK-209 have shown that the regional binding of [¹⁸F]PK-209 can be quantified with acceptable between-subject variability and evidence for specific binding, albeit modest⁵⁹. This data provided a stimulus for the evaluation of [¹⁸F]PK-209 in humans, enabling further insight into glutamatergic neurotransmission in the brain. In **CHAPTER 5**, we describe and report the first-in-human experiments which aimed to assess test-retest variability and specific binding following intravenous ketamine infusion. The interest in ketamine as a treatment for mood disorders such as treatment-resistant depression, as well as suicidal ideation and post-traumatic stress disorder has greatly expanded⁶⁰. The study included a cohort in which a

subanaesthetic dose of S-ketamine (0.5 mg/kg) was administered to healthy volunteers in order to reduce the specific binding of [¹⁸F]PK-209. Compartmental models were used to simplify the complex pharmacological processes in vivo. As the NMDA receptor is expressed throughout the CNS, a reference region devoid of NMDA receptors was not available. Arterial blood sampling was performed in combination with PET imaging for the parallel measurement of radioactivity in whole blood, plasma and brain, as well as radiotracer metabolism.

The relationship between target (e.g. receptor) occupancy profiles and the plasma concentration of the drug over time can guide dose selection for subsequent clinical trials in order to find the optimal balance between therapeutic efficacy in patients and unwanted safety and tolerability effects. In **CHAPTER 6** we report and interpret the results of a PET experiment which aimed to evaluate the relationship between the plasma concentration of GSK356278, a novel inhibitor of the phosphodiesterase-4 (PDE4) enzyme, and the occupancy of PDE4 by GSK356278 in healthy male subjects. PDE enzyme activity dysfunction has been implicated in disease states such as asthma, ischemic stroke and CNS disorders⁶¹. Upregulation of the cAMP cascade through long-term pharmacological inhibition of the PDE4 enzyme is a promising therapeutic intervention for a range of conditions. The imaging probe that was used, [¹¹C]R-rolipram, is suitable for in vivo quantification of PDE4 availability and activity. We present the first human data of PDE4 occupancy measured directly in the human brain with PET. The results of this study were used in conjunction with plasma GSK356278 pharmacokinetics to determine optimal doses to be used in future clinical development.

Finally, the main findings of this thesis are summarised, discussed, and put into context of recent scientific developments in **CHAPTER 7**.

REFERENCES

- World Health Organisation – Global Health Expenditure Database [Internet]. [cited 2017 Apr 6].
- Healthcare Occupations: Occupational Outlook Handbook: u.s. Bureau of Labor Statistics [Internet]. [cited 2017 Apr 6].
- Health at a Glance 2017. OECD Publishing; 2017. Available from: https://doi.org/10.1787/health_glance-2017-en
- Hay M, Thomas DW, Craighead JL, Economides C, Rosenthal J. Clinical development success rates for investigational drugs. *Nat Biotech.* 2014;32(1):40-51. Available from: <https://doi.org/10.1038/nbt.2786>
- Harrison RK. Phase II and phase III failures: 2013-2015. *Nature Reviews Drug Discovery.* 2016;15(12):1-2. Available from: <https://doi.org/10.1038/nrd.2016.184>
- Smietana K, Siatkowski M, Møller M. Trends in clinical success rates. *Nature Reviews Drug Discovery.* 2016;15(6):379-80. Available from: <https://doi.org/10.1038/nrd.2016.85>
- Ringel M, Martin L, Hawkins C, Panier V, Denslow M, Buck L, Schulze U. What drives operational performance in clinical R&D? *Nature Reviews Drug Discovery.* 2016;15(3):155-6. Available from: <https://doi.org/10.1038/nrd.2016.2>
- Bespalov A, Steckler T, Altevogt B, Koustova E, Skolnick P, Deaver D, Millan MJ, Bastlund JF, Doller D, Witkin J, Moser P, O'Donnell P, Ebert U, Geyer MA, Prinssen E, Ballard T, Macleod M. Failed trials for central nervous system disorders do not necessarily invalidate preclinical models and drug targets. *Nature Reviews Drug Discovery.* 2016;15(7):516-516. Available from: <https://doi.org/10.1038/nrd.2016.88>
- Morgan P, Van Der Graaf PH, Arrowsmith J, Feltner DE, Drummond KS, Wegner CD, Street SA. Can the flow of medicines be improved? Fundamental pharmacokinetic and pharmacological principles toward improving Phase II survival. *Drug Discovery Today.* 2012;17(9-10):419-24. Available from: <https://doi.org/10.1016/j.drudis.2011.12.020>
- Cook D, Brown D, Alexander R, March R, Morgan P, Satterthwaite G, Pangalos MN. Lessons learned from the fate of AstraZeneca's drug pipeline: a five-dimensional framework. *Nature reviews Drug discovery.* 2014;13(6):419-31. Available from: <https://doi.org/10.1038/nrd4309>
- van Gerven J, Bonelli M. Commentary on the EMA Guideline on strategies to identify and mitigate risks for first-in-human and early clinical trials with investigational medicinal products. *British Journal of Clinical Pharmacology.* 2018;84(7):1401-9. Available from: <https://doi.org/10.1111/bcp.13550>
- Cohen AF. Developing drug prototypes: pharmacology replaces safety and tolerability? *Nature reviews Drug discovery.* 2010;9(11):856-65. Available from: <https://doi.org/10.1038/nrd3227>
- CHMP. General Considerations for Clinical Trials. European Medicines Agency (EMA). 2006;(September 1997):1-37. Available from: <https://doi.org/10.2165/00128413-200615320-00004>
- Cohen AF, Burggraaf J, van Gerven JM, Moerland M, Groeneveld GJ. The Use of Biomarkers in Human Pharmacology (Phase I) Studies. *Annual Review of Pharmacology and Toxicology.* 2015;55(1):55-74. Available from: <https://doi.org/10.1146/annurev-pharmtox-011613-135918>
- Townsend MJ, Arron JR. Reducing the risk of failure: biomarker-guided trial design. *Nature Reviews Drug Discovery.* 2016;15(8):517-8. Available from: <https://doi.org/10.1038/nrd.2016.124>
- Klaassens BL, Rombouts sARB, Winkler AM, van Gorsel HC, van der Grond J, van Gerven JMA. Time related effects on functional brain connectivity after serotonergic and cholinergic neuro-modulation. *Human Brain Mapping.* 2017 Jan;38(1):308-25. Available from: <https://doi.org/10.1002/hbm.23362>
- Groeneveld GJ, Hay JL, Van Gerven JM. Measuring blood-brain barrier penetration using the NeuroCart, a CNS test battery. *Drug Discovery Today: Technologies.* 2016;20:27-34. Available from: <https://doi.org/10.1016/j.ddtec.2016.07.004>
- Portnow LH, Vaillancourt DE, Okun MS. The history of cerebral PET scanning: From physiology to cutting-edge technology. *Neurology.* 2013;80(10):952-6. Available from: <https://doi.org/10.1212/WNL.0b013e318285c135>
- Scobie J, Lewis GM. K-capture in carbon 11. *Philosophical Magazine.* 1957 Sep;2(21):1089-99. Available from: <https://doi.org/10.1080/14786435708242737>
- Einstein A. Das Prinzip von der Erhaltung der Schwerpunktsbewegung und die Trägheit der Energie. *Annalen der Physik.* 1906 Jan 1;325(8):627-33. Available from: <https://doi.org/10.1002/andp.19063250814>
- Moylan P, Lombardi J, Moylan S. Einstein's 1905 Paper on E=mc². 2016.
- Gonzalez-Escamilla G. A drawing of positron emission tomography [Internet]. Available from: <https://doi.org/10.6084/m9.figshare.6452777>
- Shotbolt P, Tziortzi AC, Searle CE, Colasanti A, van der Aart J, Abanades S, Plisson C, Miller SR, Huibman M, Beaver JD, Gunn RN, Laruelle M, Rabiner EA. Within-subject comparison of [(11)C]-(+)-PHNO and [(11)C]raclopride sensitivity to acute amphetamine challenge in healthy humans. *Journal of cerebral blood flow and metabolism.* 2012 Jan;32(1):127-36. Available from: <https://doi.org/10.1038/jcbfm.2011.115>
- Matthews PM, Rabiner I, Gunn R. Non-invasive imaging in experimental medicine for drug development. *Current opinion in pharmacology.* 2011 Oct;11(5):501-7. Available from: <https://doi.org/10.1016/j.coph.2011.04.009>
- Finnema SJ, Scheinin M, Shahid M, Lehto J, Borroni E, Bang-Andersen B, Sallinen J, Wong E, Farde L, Halldin C, Grimwood S. Application of cross-species PET imaging to assess neurotransmitter release in brain. *Psychopharmacology.* 2015; Available from: <https://doi.org/10.1007/s00213-015-3938-6>
- Jones T, Rabiner EA. The development, past achievements, and future directions of brain PET. *Journal of cerebral blood flow and metabolism.* 2012 Jul;32(7):1426-54. Available from: <https://doi.org/10.1038/jcbfm.2012.20>
- Froklage FE, Syvänen S, Hendrikse NH, Huisman MC, Molthoff CF, Tagawa Y, Reijneveld JC, Heimans JJ, Lammertsma AA, Eriksson J, de Lange EC, Voskuyl RA. [(11)C]Flumazenil brain uptake is influenced by the blood-brain barrier efflux transporter P-glycoprotein. *EJNMMI research.* 2012 Mar 28;2:12. Available from: <https://doi.org/10.1186/2191-219X-2-12>
- Te Beek ET, de Boer P, Moerland M, Schmidt ME, Hoetjes NJ, Windhorst AD, van Berckel BNM, Cohen AF, van Gerven JM, Lammertsma AA. In vivo quantification of striatal dopamine D2 receptor occupancy by JNJ-37822681 using [(11)C]raclopride and positron emission tomography. *Journal of psychopharmacology.* 2012 Aug;26(8):1128-35. Available from: <https://doi.org/10.1177/0269881111435251>
- van Berckel BNM, Bossong MG, Boellaard R, Kloet R, Schuitmaker A, Caspers E, Luurtsema G, Windhorst AD, Cahn W, Lammertsma AA, Kahn RS. Microglia Activation in Recent-Onset Schizophrenia: A Quantitative (R)-[(11)C]PK11195 Positron Emission Tomography Study. *Biological Psychiatry.* 2008 Nov 1;64(9):820-2. Available from: <https://doi.org/10.1016/j.biopsych.2008.04.025>
- Golla SS V., Boellaard R, Oikonen V, Hoffmann A, van Berckel BNM, Windhorst AD, Virta J, te Beek ET, Groeneveld GJ, Haaparanta-Solin M, Luoto P, Savisto N, Solin O, Valencia R, Thiele A, Eriksson J, Schuit RC, Lammertsma AA, Rinne JO. Parametric Binding Images of the TSPO Ligand [(18)F]-DPA-714. *Journal of Nuclear Medicine.* 2016 Oct 1;57(10):1543-7. Available from: <https://doi.org/10.2967/jnumed.116.173013>
- Janssen B, Vugts DJ, Wilkinson SM, Ory D, Chalou S, Hoozemans JJM, Schuit RC, Beaino W, Kooijman EJM, van den Hoek J, Chishty M, Doméné A, Van der Perren A, Villa A, Maggi A, Molenaar GT, Funke U, Shevchenko R V, Baekelandt V, Bormans G, Lammertsma AA, Kassou M, Windhorst AD. Identification of the allosteric P2X7 receptor antagonist [(11)C]SMW139 as a PET tracer of microglial activation. *Scientific reports.* 2018 Apr 26;8(1):6580. Available from: <https://doi.org/10.1038/s41598-018-24814-0>
- Doef TF van der, Golla SS, Klein PJ, Oropeza-Seguias GM, Schuit RC, Metaxas A, Jobse E, Schwarte LA, Windhorst AD, Lammertsma AA, Berckel BNM van, Boellaard R. Quantification of the novel N-methyl-D-aspartate receptor ligand [(11)C]CMOM in man. *Journal of Cerebral Blood Flow & Metabolism.* 2015;0271678X15608391. Available from: <https://doi.org/10.1177/0271678X15608391>
- van der Aart J, Golla SS V, Pliuim M Van Der, Schwarte LA, Schuit RC, Klein PJ, Metaxas A, Windhorst AD, Boellaard R, Lammertsma AA, van Berckel BNM. First in human evaluation of [(18)F]PK-209, a PET ligand for the ion channel binding site of NMDA receptors. *EJNMMI research.* 2018; Available from: <https://doi.org/10.1186/s13550-018-0424-2>
- van Berckel BNM, Ossenkoppelle R, Tolboom N, Yaqub M, Foster-Dingley JC, Windhorst AD, Scheltens P, Lammertsma AA, Boellaard R. Longitudinal Amyloid Imaging Using [(11)C]-PiB: Methodologic Considerations. *Journal of Nuclear Medicine.* 2013 Sep 1;54(9):1570-6. Available from: <https://doi.org/10.2967/jnumed.112.113654>
- Zwan MD, Bouwman FH, Konijnenberg E, van der Flier WM, Lammertsma AA, Verhey FRJ, Aalten P, van Berckel BNM, Scheltens P. Diagnostic impact of [(18)F]flutemetamol PET in early-onset dementia. *Alzheimer's research & therapy.* 2017 Jan 17;9(1):2. Available from: <https://doi.org/10.1186/s13195-016-0228-4>
- Golla SS, Verfaillie SC, Boellaard R, Adriaanse SM, Zwan MD, Schuit RC, Timmers T, Groot C, Schober P, Scheltens P, van der Flier WM, Windhorst AD, van Berckel BNM, Lammertsma AA. Quantification of [(18)F]florbetapir: A test-retest tracer kinetic modelling study. *Journal of Cerebral Blood Flow & Metabolism.* 2018 Jun 13. Available from: <https://doi.org/10.1177/0271678X18783628>
- Golla SS V., Timmers T, Ossenkoppelle R, Groot C, Verfaillie S, Scheltens P, van der Flier WM, Schwarte LA, Mintun MA, Devous M, Schuit RC, Windhorst AD, Lammertsma AA, Boellaard R, van Berckel BNM, Yaqub M. Quantification of Tau Load Using [(18)F]AV1451 PET. *Molecular Imaging and Biology.* 2017 Dec 3;19(6):963-71. Available from: <https://doi.org/10.1007/s1107-017-1080-z>
- Mansor S, Boellaard R, Froklage FE, Bakker EDM, Yaqub M, Voskuyl RA, Schwarte LA, Verbeek J, Windhorst AD, Lammertsma AA. Quantification of Dynamic [(11)C]-Phenitoin PET Studies. *Journal of nuclear medicine, Society of Nuclear Medicine.* 2015 Sep;56(9):1372-7. Available from: <https://doi.org/10.2967/jnumed.115.158055>
- van Assema DM, Lubberink M, Boellaard R, Schuit RC, Windhorst AD, Scheltens P, van Berckel BNM, Lammertsma AA. Reproducibility of quantitative (R)-[(11)C]verapamil studies. *EJNMMI Research.* 2012 Jan 17;2(1):1. Available from: <https://doi.org/10.1186/2191-219X-2-1>
- Froklage FE, Boellaard R, Bakker E, Hendrikse NH, Reijneveld JC, Schuit RC, Windhorst AD, Schober P, van Berckel BNM, Lammertsma AA, Postnov A. Quantification of [(11)C]-Laniquidar Kinetics in the Brain. *Journal of Nuclear Medicine.* 2015 Nov 1;56(11):1730-5. Available from: <https://doi.org/10.2967/jnumed.115.157586>
- Harms HJ, Huisman MC, Rijnerse MT, Greuter H, Hsieh Y-L, de Haan S, Schuit RC, Knaapen P, Lubberink M, Lammertsma AA. Noninvasive Quantification of Myocardial [(11)C]-Meta-Hydroxyephedrine Kinetics. *Journal of Nuclear Medicine.* 2016 Sep 15;57(9):1376-81. Available from: <https://doi.org/10.2967/jnumed.115.167437>
- Bahce I, Yaqub M, Errami H, Schuit RC, Schober P, Thunnissen E, Windhorst AD, Lammertsma AA, Smit EF, Hendrikse NH. Effects of erlotinib therapy on [(11)C]erlotinib uptake in EGFR mutated, advanced NSCLC. *EJNMMI Research.* 2016 Dec 9;6(1):10. Available from: <https://doi.org/10.1186/s13550-016-0169-8>
- Iqbal R, Kramer GM, Frings V, Smit EF, Hoekstra OS, Boellaard R, QuIC-ConCePT Consortium. Validation of [(18)F]FLT as a perfusion-independent imaging biomarker of tumour response in EGFR-mutated NSCLC patients undergoing treatment with an EGFR tyrosine kinase inhibitor. *EJNMMI Research.* 2018 Dec 27;8(1):22. Available from: <https://doi.org/10.1186/s13550-018-0376-6>
- Verwer EE, van Velden FHP, Bahce I, Yaqub M, Schuit RC, Windhorst AD, Raijmakers P, Lammertsma AA, Smit EF, Boellaard R. Pharmacokinetic analysis of [(18)F]FAZA in non-small cell lung cancer patients. *European Journal of Nuclear Medicine and Molecular Imaging.* 2013 Oct 6;40(10):1523-31. Available from: <https://doi.org/10.1007/s00259-013-2462-3>
- Verfaillie SCJ, Adriaanse SM, Binnewijzend MAA, Benedictus MR, Ossenkoppelle R, Wattjes MP, Pijnenburg YAL, van der Flier WM, Lammertsma AA, Kuijjer JPA, Boellaard R, Scheltens P, van Berckel BNM, Barkhof F. Cerebral perfusion and glucose metabolism in Alzheimer's disease and frontotemporal dementia: two sides of the same coin? *European Radiology.* 2015 Oct 22;25(10):3050-9. Available from: <https://doi.org/10.1007/s00330-015-3696-1>

- 46 Koopman T, Yaqub M, Heijtel DF, Nederveen AJ, van Berckel BN, Lammertsma AA, Boellaard R. Semi-quantitative cerebral blood flow parameters derived from non-invasive [¹⁵O]H₂O PET studies. *Journal of Cerebral Blood Flow & Metabolism*. 2017 Sep 13. Available from: <https://doi.org/10.1177/0271678X17730654>
- 47 Honer M, Gobbi L, Martarello L, Comley RA. Radioligand development for molecular imaging of the central nervous system with positron emission tomography. *Drug discovery today*. 2014 Aug 27;00(00). Available from: <https://doi.org/10.1016/j.drudis.2014.08.012>
- 48 Fantoni ER, Dal Ben D, Falzoni S, Di Virgilio F, Lovestone S, Gee A. Design, synthesis and evaluation in an LPS rodent model of neuroinflammation of a novel ¹⁸F-labelled PET tracer targeting P2X7. *EJNMMI Research*. 2017 Dec 4;7(1):31. Available from: <https://doi.org/10.1186/s13550-017-0275-2>
- 49 Han J, Liu H, Liu C, Jin H, Perlmutter JS, Egan TM, Tu Z. Pharmacologic characterizations of a P2X7 receptor-specific radioligand, [¹¹C]CSK1482160 for neuroinflammatory response. *Nuclear Medicine Communications*. 2017 May;38(5):372-82. Available from: <https://doi.org/10.1097/MNM.0000000000000660>
- 50 Van der Aart J, Recourt K, Jacobs G, de Kam M, Khoshchin A, Kanhai K, Siebenga P, Zuiker R, Vets E, Timmers M, de Boer P, van Gerven J. Pharmacodynamic effects of the P2X7 receptor antagonist JNJ-54175446 in a translational human dexamphetamine challenge model. *Journal of Psychopharmacology*. 2017;8(31):A62.
- 51 Innis RB, Cunningham VJ, Delforge J, Fujita M, Gjedde A, Gunn RN, Holden J, Houle S, Huang S-C, Ichise M, Iida H, Ito H, Kimura Y, Koeppe RA, Knudsen GM, Knuuti J, Lammertsma AA, Laruelle M, Logan J, Maguire RP, Mintun MA, Morris ED, Parsey R, Price JC, Slifstein M, Sossi V, Suhara T, Votaw JR, Wong DF, Carson RE. Consensus nomenclature for in vivo imaging of reversibly binding radioligands. *Journal of Cerebral Blood Flow & Metabolism*. 2007 Sep 9;27(9):1533-9. Available from: <https://doi.org/10.1038/sj.jcbfm.9600493>
- 52 Cunningham VJ, Rabiner EA, Slifstein M, Laruelle M, Gunn RN. Measuring drug occupancy in the absence of a reference region: the Lassen plot re-visited. *Journal of cerebral blood flow and metabolism*. Jan;30(1):46-50. Available from: <https://doi.org/10.1038/jcbfm.2009.190>
- 53 Farde L, Eriksson L, Blomquist G, Hallidin C. Kinetic Analysis of Central [¹¹C]Raclopride Binding to D₂-Dopamine Receptors Studied by PET—A Comparison to the Equilibrium Analysis. *Journal of Cerebral Blood Flow & Metabolism*. 1989;9(5):696-708. Available from: <https://doi.org/10.1038/jcbfm.1989.98>
- 54 Paoletti P, Bellone C, Zhou Q. NMDA receptor subunit diversity: impact on receptor properties, synaptic plasticity and disease. *Nature reviews Neuroscience*. 2013 Jun;14(6):383-400. Available from: <https://doi.org/10.1038/nrn3504>
- 55 Rammes G, Seeser F, Mattusch K, Zhu K, Haas L, Kummer M, Heneka M, Herms J, Parsons CG. The NMDA receptor antagonist Radiprodil reverses the synaptotoxic effects of different amyloid-beta (Aβ) species on long-term potentiation (LTP). *Neuropharmacology*. 2018;140:184-92. Available from: <https://doi.org/10.1016/j.neuropharm.2018.07.021>
- 56 Fuchigami T, Nakayama M, Yoshida S. Development of PET and SPECT probes for glutamate receptors. Vol. 2015, *Scientific World Journal*. 2015. p. 1-19. Available from: <https://doi.org/10.1155/2015/716514>
- 57 Van der Aart J, Yaqub M, Kooijman EJM, Bakker J, Langermans JAM, Schuit RC, Hofman MBM, Christiaans JAM, Lammertsma AA, Windhorst AD, Van Berckel BNM. Evaluation of the Novel PET Tracer [¹¹C]HACH242 for Imaging the GluN2B NMDA Receptor in Non-Human Primates. *Mol Imaging Biol*. 2018; Available from: <https://doi.org/10.1007/s11307-018-1284-x>
- 58 Christiaans JAM, Klein PJ, Metaxas A, Kooijman EJM, Schuit RC, Leysen JE, Lammertsma AA., van Berckel BNM, Windhorst AD. Synthesis and preclinical evaluation of carbon-11 labelled N-(5-(4-fluoro-2-[¹¹C]methoxyphenyl)pyridin-3-yl)methyl)cyclopentanamine as a PET tracer for NR2B subunit-containing NMDA receptors. *Nuclear Medicine and Biology*. 2014;41(8):670-80. Available from: <https://doi.org/10.1016/j.nucmedbio.2014.04.131>
- 59 Golla SSV, Klein PJ, Bakker J, Schuit RC, Christiaans J a. M, van Geest L, Kooijman EJM, Oropeza-Seguias GM, Langermans J a. M, Leysen JE, Boellaard R, Windhorst AD, van Berckel BNM, Metaxas A. Preclinical evaluation of [¹⁸F]PK-209, a new PET ligand for imaging the ion-channel site of NMDA receptors. *Nuclear Medicine and Biology*. 2015;42(2):205-12. Available from: <https://doi.org/10.1016/j.nucmedbio.2014.09.006>
- 60 Veen C, Jacobs G, Philippens I, Vermetten E. Subanesthetic Dose Ketamine in Posttraumatic Stress Disorder: A Role for Reconsolidation During Trauma-Focused Psychotherapy? In Vermetten E., Baker D., Risbrough V. (eds) *Behavioral Neurobiology of PTSD*. Current Topics in Behavioral Neurosciences, vol 38. Springer, Cham 2018. Available from: https://doi.org/10.1007/7854_2017_34
- 61 Menniti FS, Faraci WS, Schmidt CJ. Phosphodiesterases in the CNS: targets for drug development. *Nature Reviews Drug Discovery*. 2006 Aug 1;5(8):660-70. Available from: <https://doi.org/10.1038/nrd2058>
- 62 Bradford AM. Molecular pharmacology of a Novel NR2B-selective NMDA Receptor Antagonist. Durham University; 2006.
- 63 Weatherall D, Goodfellow P, Harris J, Hinde R, Johnson L, Morris R, Ross N, Skehel J, Tickell C. The use of non-human primates in research. *Medical Research Council*. 2006;(December):1-153. Available from: [https://doi.org/10.1016/0047-2484\(75\)90100-1](https://doi.org/10.1016/0047-2484(75)90100-1)
- 64 Klein PJ, Christiaans JAM, Metaxas A, Schuit RC, Lammertsma AA, van Berckel BNM, Windhorst AD. Synthesis, structure activity relationship, radiolabeling and preclinical evaluation of high affinity ligands for the ion channel of the N-methyl-D-aspartate receptor as potential imaging probes for positron emission tomography. *Bioorganic & Medicinal Chemistry*. 2015;23(5):1189-206. Available from: <https://doi.org/10.1016/j.bmc.2014.12.029>
- 65 The 2007 recommendations of the International Commission on Radiological Protection. International Commission on Radiological Protection (ICRP) publication 103.:7-8.

Cover visual production credits: iStock.com/Rick_Jo.

CHAPTER 2

RADIATION DOSE ESTIMATES FOR CARBON-11 LABELLED PET TRACERS

PUBLISHED IN NUCLEAR MEDICINE & BIOLOGY

Jasper van der Aart, William A. Hallett, Eugenii A. Rabiner, Jan Passchier, Robert A. Comley

Glaxosmithkline, Clinical Imaging Centre (Invivo), Imperial College London, Hammersmith Hospital, London, UK

© 2012 Elsevier Inc. Creative Commons Attribution Non-Commercial No Derivatives License.

DOI 10.1016/j.nucmedbio.2011.08.005

Abstract

INTRODUCTION Carbon-11 labelled PET tracers commonly used in biomedical research expose subjects to ionising radiation. Dosimetry is the measurement of radiation dose, but also commonly refers to the estimation of health risk associated with ionising radiation. This review describes radiation dosimetry of carbon-11 labelled molecules in the context of current PET research and the most widely used regulatory guidelines.

METHODS A MEDLINE literature search returned 42 articles, 32 of these were based on human PET data dealing with radiation dosimetry of carbon-11 molecules. Radiation burden expressed as effective dose and maximum absorbed organ dose was compared between tracers.

RESULTS All but one of the carbon-11 labelled PET tracers have an effective dose under 9 $\mu\text{Sv}/\text{MBq}$, with a mean of 5.9 $\mu\text{Sv}/\text{MBq}$. Data show that serial PET scans in a single subject are feasible for the majority of radiotracers.

CONCLUSION Although differing in approach, the two most widely used regulatory frameworks (those in the USA and the EU) do not differ substantially with regard to the maximum allowable injected activity per PET study. The predictive validity of animal dosimetry models is critically discussed in relation to human dosimetry. Finally, empirical PET data is related to human dose estimates based on homogeneous distribution, generic models and maximum cumulated activities. Despite the contribution of these models to general risk estimation, human dosimetry studies are recommended where continued use of a new PET tracer is foreseen.

Introduction

PET is an imaging technique which allows the visualisation and quantification of the time-dependent distribution of molecules labelled with positron-emitting isotopes. Appropriate quantification of the tissue radioactivity data allows inferences to be made about biochemical and physiological processes reflected in the distribution and kinetics of the labelled molecule in humans *in vivo*. In addition to its use in research¹ and clinical practice², PET makes a significant contribution to pharmaceutical development³. However, the administration of radiotracers to human subjects exposes them to an additional source of ionising radiation. In order for research ethics committees and other regulatory bodies to be able to adequately review research protocols, and for potential research subjects to be able to make an informed decision about their participation, it is necessary to estimate the risk to the subject posed by that exposure. In addition, restrictions are typically placed on the doses which can be administered to subjects who are not anticipated to benefit personally from a scanning procedure. Therefore, estimates of the radiation dose and associated risk arising from the administration of a particular radiotracer are required. In this review, we summarise the published radiation dose estimates for carbon-11 labelled PET tracers, discuss radiation dosimetry in the context of the research applications of PET imaging, and relate the doses required to meet common research objectives to the most widely used guidelines.

Radiation measures

Radiation dose estimates are based on four concepts which we will briefly introduce: radioactivity, absorbed radiation dose, equivalent dose and effective dose.

- **Radioactivity** refers to the nuclear transformation rate, i.e. the number of disintegrations of unstable atomic nuclei per second. The SI unit, becquerel (1 Bq = 1 disintegration per second) has superseded the curie (Ci) as the unit of radioactivity (1 Ci = 37000 Bq).
- The **absorbed radiation dose** for a material as a result of its exposure to ionising radiation is the absorbed energy per unit mass. The SI unit, gray (1 Gy = 1 Joule/kilogram), has superseded the rad (1 Gy = 100 rad).
- For living tissues exposed to radiation, **dose equivalent**, a term introduced by the International Commission on Radiation Protection (ICRP) in Publication

30^4 , equals the absorbed dose multiplied by a radiation ‘quality factor’ which expresses relative biological damage from a particular type of radiation. The SI unit of dose equivalent (also referred to as equivalent dose) is the sievert (Sv), which has superseded the rem (1 Sv = 100 rem). It should be noted that in estimating exposure from PET, dose equivalent is numerically equal to absorbed dose as the radiation quality factor is 1 for both gamma rays and positrons at all energies.

- **Effective dose (E)** The total or whole body absorbed dose, i.e. the total amount of radiation absorbed by the body divided by the mass of the body, is not adequate to estimate the risks associated with exposure to radiation since it does not take into account non-uniform irradiation or differences in tissue radiosensitivity. In the ICRP scheme^{4,5} the relative overall harm to health or detriment from the exposure of different organs to low doses of radiation is taken into account through tissue weighting factors (w_T , table 1) that represent the relative risk contribution arising from each organ or tissue should the whole body be irradiated uniformly. Summation of the weighted dose equivalents over all tissues gives the *effective dose equivalent* (EDE). The ICRP subsequently renamed EDE *effective dose* (E), and introduced revised tissue weighting factors⁵ more appropriate for biomedical research, which have recently been revised again⁶. EDE however is still mentioned regularly in dosimetry calculations, sometimes exclusively. E can in principle be used prospectively for any procedure involving low doses of ionising radiation (therefore excluding high dose exposures in procedures such as radiotherapy), allowing easy comparison between radiation dose from different radiotracers. Perhaps confusingly, the unit of E is also the sievert (Sv).

Biological effects of radiation

The biological effects of ionising radiation can be classified as deterministic, teratogenic and stochastic, and depend on the magnitude and duration of exposure. Deterministic effects occur when a radiation dose threshold is exceeded. Examples include erythema and hair loss. The threshold for deterministic effects is relatively high (of the order of several Sv), although some tissues have lower thresholds (e.g. the eye lens). Teratogenic effects are caused by *in utero* exposure, and can be stochastic or deterministic. The complexity of teratogenic effects is beyond the scope of this review.

TABLE 1 Tissue weighting factors.

Organ or tissue	w_T ICRP 30 (1979) *	w_T ICRP 60 (1991)	w_T ICRP 103 (2007)
Gonads	0.25	0.20	0.08
Red bone marrow	0.12	0.12	0.12
Large intestine		0.12	0.12
Lung	0.12	0.12	0.12
Stomach		0.12	0.12
Bladder		0.05	0.04
Breast	0.15	0.05	0.12
Liver		0.05	0.04
Oesophagus		0.05	0.04
Thyroid	0.03	0.05	0.04
Skin		0.01	0.01
Bone surface	0.03	0.01	0.01
Rest †	0.30	0.05	0.12
Brain			0.01
Total	1.00	1.00	1.00

* ICRP 30 w_T are used to calculate EDE, whereas ICRP 60 w_T and ICRP 103 w_T give E values.

† ‘Rest’ includes adrenals, small intestine, kidney, muscle, brain (except ICRP 103 w_T), pancreas, spleen, thymus, and uterus.

Stochastic effects

The radiation doses administered in PET studies are so low that any harmful effects are likely to be stochastic in nature, meaning that as the dose increases the probability of harm increases, rather than the severity of symptoms. Stochastic effects arise from radiation induced chromosomal changes, leading to cancers and (in theory at least) genetic disorders in future generations. Stochastic effects associated with doses from 60 mSv have been described by extrapolation in epidemiological studies of atomic bomb survivors and other populations known to have been exposed to high doses of radiation⁷. However, effects below 60 mSv are not well characterised as they are hard to detect. There has been a long debate⁸ about how best to estimate the effects of low doses of radiation. Currently ICRP guidance uses a linear-no-threshold model (LNT), which assumes a linear relationship between dose and risk even at low radiation doses, i.e. there is no dose that does not carry a risk. However, there is no *single* dose-effect relationship, i.e. each link in the chain of radiation effect will have its own dose-effect relationship (e.g. mechanisms

of suppression, amplification, destabilisation and feedback), and those effects will combine to form the biological endpoint^{8,9}.

One study estimated that among 400 000 nuclear workers with a mean accumulated total dose of about 20 mSv, 1-2% of all cancer deaths may be attributable to occupational radiation exposure¹⁰. Nevertheless the added cancer risks from PET studies performed under the current guidelines are so low as to be practically unobservable⁹. Furthermore, everyone is exposed to some level of ionising radiation from environmental sources (background radiation) in addition to any occupational or medical exposure one may receive. The worldwide average dose is estimated to be 2.4 mSv per year¹¹ with a sizeable portion of the population receiving 10-20 mSv. Most variation in dose is explained by the level of natural radionuclide content in the soil and concentration of radon gas in indoor air.

Guidelines concerning radiation exposure in research studies

The three basic principles of radiation protection in biomedical research are (i) justification of irradiation, (ii) administration of a dose that is as low as reasonably achievable (ALARA) or practicable (ALARP, used in the UK) consistent with the aim of the investigation, and (iii) adhering to dose constraints specified by the appropriate regulatory body. The fundamental issues pertaining to human research involving ionising radiation have been previously described^{12,13}.

Research in the USA and Europe is subject to different local and national regulations, and as such the acceptable/ permissible radiation exposure differs from country to country. For studies performed in the USA, the Food and Drug Administration (FDA) Code of Federal Regulations (CFR) Title 21 Part 361¹⁴ states that the maximal absorbed dose for the whole body should not exceed 30 mSv per study, or 50 mSv annual total dose. Importantly, the FDA puts limits on specific organs, e.g. 30 mSv for the red marrow, testes, ovaries, and the lens of eye (although the eye is commonly ignored in dosimetry studies where PET tracers are injected intravenously), 50 mSv per study for all other organs, or a total annual dose of 150 mSv. The ICRP guidance was largely adopted in a directive from the European Commission¹³. In the UK for example this directive has been enacted in the Ionising Radiation (Medical Exposures) Regulations¹⁶. In addition to ethical review, permission must also be obtained from the Administration of Radioactive Substances Advisory Committee (ARSAC) under the terms of the Medicines (Administration of

Radioactive Substances) Regulations. There is no dose limit for research purposes, but like many EU member states, the UK follows the ICRP 62 guidance that indicates a constraint of 10 mSv (or less) per study where research subjects are not expected to benefit personally¹⁵. Perhaps the most notable distinction between regulation in Europe and the US is the absence of organ limits in Europe and the increased emphasis on effective dose.

Methods to calculate exposure

Methods to estimate the absorbed radiation dose following radiotracer injection have been used since the medical use of radiolabelled compounds began in the 1940s¹⁷. Today dosimetry methods applicable to PET, radionuclide therapy, and the exposure of different populations (i.e. children, females)¹⁸ are all available. In addition, guidelines concerning dose estimation at the sub-organ, voxel, and cellular levels have been published¹⁹. In the simplest terms, the dose will depend on both the biological half-life (residual time in various organs) of the radiolabelled compound (and any labelled metabolites) and radioactive half-life of the nuclei attached to the molecule. Various methods are available, each having its own pros (e.g. external validity) and cons (e.g. cost). However, up until now a concise overview of the methods used to obtain animal and human dosimetry for carbon-11 labelled PET tracers (at the organ and whole body level) has been lacking.

Dosimetry for a homogeneously distributed carbon-11 labelled molecule

Calculations can be made *a priori* about radiation energy deposition per MBq of injected activity for a whole body. The simplest way to estimate dose is to assume homogeneous distribution of the radiotracer in the body, where radioactivity is only removed by physical decay and not by excretion. Radiation dose then equals the total number of transitions multiplied by the energy per transition divided by the mass of the body. Assuming a reference body with a target mass of 70kg, deposition of 100% beta energy and 50% gamma energy in tissue, the total body dose of an injected carbon-11 labelled radiotracer would equal 3.6 μ Sv/MBq.

In reality the assumption of homogeneous radiotracer distribution rarely holds. However, given the relatively short half-life of carbon-11 (20.4 min) compared to fluorine-18 or iodine-123 tracers (109.8 min and 13.22 hour half-lives respectively), the total radiation burden (the effective dose E) depends largely on the initial organ perfusion and retention. Highly perfused organs with a high blood flow as

a percentage of cardiac output (brain, heart, lung, liver, kidney) receive the majority of the absorbed dose while less perfused organs (muscle, fat) and small organs receive a smaller fraction. Therefore the worst case scenario would be for all activity to decay in one organ with a high tissue weighting factor. For example, in the case of the serotonin transporter radiotracer [^{11}C]DASB ($E = 6.4 \mu\text{Sv}/\text{MBq}$)²⁰, it was shown that E would be $670 \mu\text{Sv}/\text{MBq}$ if one assumes that all activity decays in the testes/ovaries ($w_T=0.2$), whereas E would be $2.7 \mu\text{Sv}/\text{MBq}$ if all activity decayed in the skin or bone ($w_T=0.01$). This variability highlights the effect of inhomogeneous tracer distribution on E , and the need to account for the biological half-life of the tracer per organ in addition to energy deposition within the body.

Pre-clinical experiments and scaling to humans

Biodistribution data for an intravenously administered radiotracer can be obtained in rodents without the use of PET imaging, by classical dissection or direct measurement techniques such as gamma or liquid scintillation counting and quantitative whole body autoradiography (QWBA). For a tritiated molecule, classical dissection is often preferable due to the relatively low cost and high sensitivity. Extrapolating data obtained with a tritium labelled tracer does require the assumption that a difference in the labelling position (compared to carbon-11) does not lead to different radio-labelled metabolites. However, given the short half-life of carbon-11 and other sources of inter species variation this assumption is normally deemed to be acceptable. QWBA has the advantage of providing detailed distribution data in pictorial form allowing quantification with similar accuracy to classical approaches. With either method typically pairs of rats (e.g. one male and one female) are dosed and sacrificed at each of several times post-dose (e.g. 5, 10, 20, 60 and 120 minutes) and all tissues/organs taken or sampled from each carcass are measured for total radioactivity.

Various methods can be used to scale the normalised cumulated activities to man; the simplest being to assume that they are the same in both species. However, various interspecies differences can introduce errors. Differences in anatomy are perhaps the most obvious. Rats lack a gallbladder, and in general relative organ size decreases as animal size increases. In addition other factors may affect the rate of drug/tracer elimination, for example: both the level of hepatic enzymes and the number of nephrons as a fraction of kidney weight are thought to be higher in small animals than in humans²¹; In addition, biliary excretion and bladder exposure varies substantially between species; and blood circulation time is shorter in

small animals than in man. Therefore human residence times extrapolated from rat data are estimated using conservative assumptions. For example, Parsey *et al.*²² notes that rats have a 60.6 times lower absorbed bladder dose than humans (Mathis *c*, as described in²²) following injection of the 5-HT_{1A} receptor tracer [^{11}C]WAY100635. The majority of injected activity in human subjects accumulated in the bladder within 1 hr of injection, indicating that differences in radiotracer binding to the target (between species) may lead to substantially different absorbed organ doses. [^{11}C]WAY100635 also provides an example of a radiotracer that is subject to different metabolic rates and/or fates in different species, potentially leading to the presence of different radiolabelled metabolites. The rate at which the [^{11}C]WAY100635 radioactivity in plasma decreases is contrary to the order expected on the basis of body weight, i.e. human > monkey > rat²³. Indeed, it has been proposed that animal data require an interval of factor 10 to reliably predict human organ dose estimates 90% of the time²⁴. Several other examples exist in the literature of substantial differences between calculated effective doses based on rodent versus human data. For example, E for [^{11}C]CP126,998 was found to be $3.9 \mu\text{Sv}/\text{MBq}$ based on human PET data²⁵, whereas mouse data returned an estimate of $7.7 \mu\text{Sv}/\text{MBq}$. For the α 7 nicotinic receptor tracer [^{11}C]CHIBA-1001, mouse data underestimated human data; 3.8 versus $6.9 \mu\text{Sv}/\text{MBq}$ respectively^{26,27}. Human dosimetry estimates for [^{11}C]PBR28 based on monkey biodistribution data were overestimated by 60%, as the absorbed activity in the monkey was greater than in humans for organs with high PBR densities²⁸. Taken together, these studies suggest that although animal studies may highlight cases which do not conform to the homogenous distribution model and provide information about the kinetics of the PET tracer in an organ of interest such as the brain, they add relatively little to human dose estimates in terms of effective dose. For these reasons, preclinical data was not included in this review where human data was available.

Typical Human Dosimetry

In vivo PET studies can provide biokinetic input data such as fractional long term retention of labelled molecules, turnover of the radiopharmaceutical and its metabolites, and distribution within different organs. A PET dosimetry protocol for a carbon-11 labelled tracer will typically specify the acquisition of images from multiple overlapping bed positions collected over consecutive passes lasting up to 120 minutes, after which time less than 2% of the injected activity remains throughout the body. The short half-life of carbon-11 in combination with a scan duration of

120 minutes avoids the need to extrapolate time-activity data. If scanning time is insufficient (e.g. if other radionuclides are used) and more data post scan is needed, it is conservatively assumed that the area under the time activity curves of organs from the end of the scan to infinity follows a declining mono-exponential function. Whole-body scanning may miss an early perfusion phase for organs with a low retention of the tracer; however the energy deposition from the tracer in these tissues is likely to be minimal.

Organs to be included in the image analysis are often determined by visual inspection, with regions of interest being drawn for organs showing uptake (activity levels) above the tissue background. 'Residence time' or 'normalised cumulated activity'²⁹, which refers to the number of nuclear transitions per injected amount of activity, can be obtained directly from PET studies. Data is corrected for organ volume using anatomical models and subsequently entered into dose estimation software such as those developed by the ICRP, the Medical Internal Radiation Dose (MIRD) committee, or the Radiation Dose Assessment Resource (RADAR). The most widely used publicly available software packages are MIRDose³⁰ and in revised form OLINDA/EXM (Organ Level Internal Dose Assessment/Exponential Modeling)³¹. It should be noted that the output uses ICRP 60 (1991) w_T to calculate E instead of revised ICRP 103 (2007) w_T .

Methods

The PubMed search engine (<http://www.pubmed.gov>) was used to query the MEDLINE bibliographic database (U.S. National Library of Medicine) using the terms "Dosimetry AND ¹¹C", returning 120 articles. Studies were selected after inspection of titles and abstracts. The search was then complemented by manually cross-checking the reference list of the selected papers. In the cases where preclinical dosimetry experiments were conducted, the calculated human dose estimates are given.

Results

Effective dose reviewed

Two main conclusions can be drawn from the dosimetry data presented in table 2. First, the analysis of 37 effective dose estimates available from 42 dosimetry articles shows a narrow range of values (mean $E=5.9 \pm 2.0 \mu\text{Sv}/\text{MBq}$, 95% confidence

interval of 5.2-6.6 and range 3.2-8.9 with one outlier at 14, Figure 1), supporting the assertion that the half-life of carbon-11 is the major determinate of E for PET tracers based on small molecules. Compared with an estimated E of around $15 \mu\text{Sv}/\text{MBq}$ for most fluorine-18 tracers (data summarised in ICRP 53⁶⁸), and $19 \mu\text{Sv}/\text{MBq}$ for [¹⁸F] fluorodeoxyglucose (data summarised in ICRP 80^{69,70}), carbon-11 tracers generally display a relatively modest radiation dose profile. EDE values are higher than E for all studies where both are computed, suggesting that the use of older weighting factors overestimates radiation risk for carbon-11 tracers. Second, organ perfusion and the mechanism of clearance is a major determinant of tracer biokinetics in humans and hence effective dose. For institutions following US FDA legislation¹⁴, the maximum injected activity per study may be limited by the critical organ rather than the (whole body) effective dose as used by many EU PET centres. Organs which exhibit the highest absorbed dose differ markedly between radiotracers, and are not confined to major visceral organs such as the kidneys, liver, and lung. Indeed, the bladder-wall and gallbladder-wall are frequently reported to be the limiting organs, despite both delayed filling and the short half-life of carbon-11. Many radiotracers seem to be excreted rapidly in urine, which in turn contributes considerably to E. However, closer inspection of the data in the articles shows that dose estimates for organs involved in excretory pathways generally display a large variability between subjects. The effective dose of one radiotracer appeared to be an outlier,

FIGURE 1 Effective dose estimates for 37 carbon-11-labelled PET tracers.

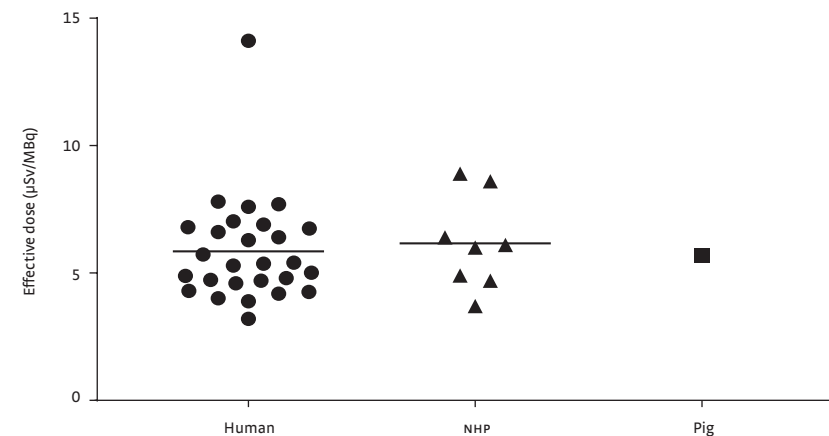


TABLE 2 DOSE ESTIMATES

Target	Radiotracer	E	EDE	Critical Organ	Max absorbed	us max*	Species	Ref
Receptors		μSv/MBq	μSv/MBq		μGy/MBq	MBq		
α2-adreno	Mirtazapine	6.8		lungs	34	1470	Human (n=1, 1 ♀)	32
α2-adreno	Yohimbe	5.7		urinary bladder	54.3	920	Pig (n=1)	33
Dopamine D1	NNC 112	5.7	9.2	gallbladder	32.4	1351	Human (n=7, 3 ♀)	34
Dopamine D2	Raclopride	6.3	8.7	gallbladder	31.5	1587	Human (n=6, 3 ♀)	35
Dopamine D2	Raclopride	6.7		kidney	40.6	1231	Human (n=3)	36
Dopamine D2	MNPA	6.4		urinary bladder	26	1923	NHP (n=2)	37
Dopamine D2	NMB	3.7	4.4	heart	10.5	4761	NHP (n=2)	38
Dopamine D2	NPA	3.2	6.7	gallbladder	28.1	1779	Human (n=6, 3 ♀)	39
GABA benzodiazepine	Flumazenil	7.6	11.2	urinary bladder	63.2	791	Human (n=6, 3 ♀)	40
GABA benzodiazepine	Flumazenil	5		urinary bladder	37	1351	Human (n=5, 2 ♀)	41
GABA benzodiazepine	MPGA	5.3		small intestine	33	1515	Human (n=3)	42
GABA benzodiazepine	lomazenil		15	urinary bladder	99	505	Human (n=2)	43
NK1	GR-205171	8.6	12.1	lung	55.4	902	NHP (n=3)	44
Opioid	Carfentanil	4.6	5.4	urinary bladder	36.5	1369	Human (n=5, 3 ♀)	45
Glutamate 5	ABP688		3.7	liver	16.4	3048	Human (n=5)	46
α7-Nicotinic	CHIBA-1001	6.9		small intestine	24.0	2083	Human (n=3)	27
Acetylcholine	MP4B	4.2		urinary bladder	18.6	2688	Human (n=7)	47
Angiotensin 2	Telmisartan	4.3		gallbladder	46.7	1071	Human (n=6)	48
Serotonin 5-HT _{1A}	WAY100635	14.1	17.4	urinary bladder	194	258	Human (n=6, 3 ♀)	22
Serotonin 5-HT ₆	GSK215083	7.7	7.8	lung	25.6	1172	Human (n=6, 3 ♀)	¥
TSPO (PRB)	PBR28	6.6	11	kidney	52.6	951	Human (n=6, 3 ♀)	28
TSPO (PBR)	PK11195	4.8	5.1	kidney	14.0	3571	Human (n=5)	49
(ICRP103)								
Transporters	Radiotracer	E	EDE	Maximum dose organ	Max dose	us max*	Species	Ref
Dopamine transporter	PE21	6.4		urinary bladder	18.0	2778	Human (n=3)	50
Pg-p	DLOP	7.8		kidney	50.1	998	Human (n=12, 8 ♀)	51
Serotonin transporter	DASB	7	8	lungs	32.8	1524	Human (n=7, 5 ♀)	52
Serotonin transporter	DASB	6	7.3	urinary bladder	25.2	1984	NHP (n=2)	20
VMAT 2	MTBZ			gonads	40.0	750	Human (n=6, 3 ♀)	53
VMAT 2	TBZ			gonads	27.6	1086	Rat (n=5)	54
VMAT 2	DTBZ	6.1		stomach	14.0	3571	NHP (n=5)	55

(CONTINUATION TABLE 2)

Protein targets, other	Radiotracer	E	EDE	Maximum dose organ	Max dose	us max*	Species	Ref.
Acetylcholinesterase inhibitors	CP126,998	3.9	5.1	liver	20.6	2427	Human (n=2)	25
Monoamine oxidase A	Harmine	8.9	11.1	lungs	39.9	1253	NHP (n=3)	56
Beta-Amyloid	PIB	5.3	8.9	gallbladder	44.8	1116	Human (n=6, 3 ♀)	57
Beta-Amyloid	PIB	4.7		gallbladder	41.5	1205	Human (n=8)	58
Beta-Amyloid	BTA-1	4.3		liver (n=4),	20.1	2488	Human (n=5, 3 ♀)	59
Beta-Amyloid	MES-IMPY	4.9		gallbladder	33.4	1497	NHP (n=2)	60
Metabolism	Glucose		3.3	Brain	11.0	4545	Human (n=33, 14 ♀)	61
Tumor Imaging Agent	MEAIB	4		pancreas	18.0	2778	Human (n=25, 7 ♀)	62
Tumor Imaging Agent	Methionine	5.2		urinary bladder	27.0	1852	Human (n=5)	63
Tumor Imaging Agent	Acetate	4.9	6.2	pancreas	17.0	2941	Human (n=6)	64
Tumor Imaging Agent	LY2181308	4.7	6.8	kidneys	32.0	1563	NHP (n=3)	65
Tumor Imaging Agent	DOCETAXEL	4.7		liver	35.2	1420	Human (n=7, 2 ♀)	66
Epidermal Growth Factor Receptor	PD153035	4.7	7.4	urinary bladder	60.1	832	Human (n=9, 5 ♀)	67

¥Comley, pers. comm. * us max activity per study

[¹¹C]WAY100635. The estimated effective dose of 14.1 μSv/MBq reported by Parsey et al.²¹ is more than four standard deviations above the mean of all tracers reviewed here. The absorbed dose for the bladder was on average 167 μGy/MBq for males and 220 μGy/MBq for females. A bladder dose of this magnitude is unusual but could in part be attributable to active secretion of the tracer into the renal tubule. One can speculate that for carbon-11 labelled tracers excreted via this route, an E of 14 μSv/MBq represents an upper limit.

Implications of us versus recent ICRP guidelines

us Federal Law guidelines state that the maximum absorbed dose per organ should be limited to either 30 mSv or 50 mSv depending on the organ. All but one of the radiotracers reviewed here fall into the 50 mSv organ limit category, the exception being [¹¹C]MTBZ. To illustrate the implication of organ limits; the 50 mSv single study organ limit would be reached following injection of 832 MBq [¹¹C]PD153035⁶⁷ or 505 MBq [¹¹C]iomazenil⁴³. Injected activity limits based on the critical organ for all tracers are given in Table 2. On average, the allowable injected activity equals 1713 MBq per study. This is comparable to the limit deduced from the average effective

dose (10 mSv dose deposited after 1692 MBq at 5.9 $\mu\text{Sv}/\text{MBq}$), suggesting that both regulatory bodies allow on average comparable maximum injected doses *per study*. However, US regulations allow the annual absorbed radiation dose to ‘other’ organs to be up to 150 mSv, which depending in the critical organ, is three times higher than the ICRP 62 recommendations. Finally, it should be emphasised that computerised tomography scans (CT) used for attenuation correction and sometimes anatomical localisation may contribute significantly to the radiation dose in PET studies where PET-CT systems are used⁷¹.

Models

Gatley⁷² proposed a model for carbon-11 labelled tracers that estimates the injected activity which could not, on *a priori* grounds, exceed the US organ limits. Factors such as tissue blood flow and arterial plasma data were included in the model which tried to estimate upper limits, rather than true organ doses. It proposed limiting administration of activity to humans from a novel molecule to 130 MBq in order not to exceed the organ limit of 50 mSv. As the author points out, calculated cumulated activities are unrealistically high, as the assumption of immediate uptake and trapping of the tracer until radioactivity has decayed in reality never holds. Nevertheless, 130 MBq of injected activity may allow derivation of physiologically meaningful parameters from PET experiments in humans.

A generic model to estimate effective dose for brain receptor studies was developed by Nosslin *et al.*^{73,74} with input data from thirteen carbon-11 labelled radiotracers. The model assumes rapid uniform distribution throughout the body, and an instantaneous 5% deposition in the brain. However, as data was lacking arbitrary judgements were made about biokinetic parameters. The model assumes that 25% of carbon-11 is excreted via the gallbladder and 75% in urine, with a biological half-life of 2 hours. The observation that brain uptake (between 1 and 9%) and organ doses of the selected radiotracers were sufficiently similar justified the attempt to formulate a generic model. Effective dose was estimated at 4.5 $\mu\text{Sv}/\text{MBq}$, a slight underestimation of the mean E of 5.9 $\mu\text{Sv}/\text{MBq}$ across all radiotracers reviewed here.

Individual Differences

In terms of health risks, the magnitude of stochastic effects, though difficult to predict at the lower end of the LNT model, are believed to be dependent on age and gender⁷⁵. Because uptake and distribution of tracers differs between individuals, and because the biological effects of low levels of radiation exposure are not directly observable, dosimetry calculations rest on the assumptions of mathematical

models that can at best only be representative of a population and should not be used to calculate the risk to a particular individual arising from a particular low level exposure.

These estimations may also not be generalisable across patient populations, e.g. tumour uptake in oncology patients will affect the distribution of absorbed dose. Moreover, radiation risks are estimated for a population of healthy individuals with normal lifespans that may not be applicable to patients. In addition it should be noted that fifteen human studies reviewed here only gathered dosimetry data for males. Because of the smaller size of the average female, conservative approaches should be taken (i.e. taking into account higher whole body dose relative to males) when administering PET tracers to female research subjects. Indeed, it has been suggested that biological half-life and fractional uptake differ across individuals with an estimated biokinetic variability factor of 2 for any carbon-11 labelled PET tracer⁷⁶. A clear example is [¹¹C]PBR28; individual differences in organ absorbed doses were so substantial that one human subject was not included in the effective dose calculation (based on the abnormal uptake in the kidneys, spleen and lungs, in addition to 4 times higher residence time in the gallbladder)²⁸. If the critical organ in one subject receives double the average dose, this would limit the US specified maximum allowable injected dose for this subject by half, were it to be applied at the individual level. PET centres following regulations based on effective dose are less affected by the maximum organ dose due to multiplication by tissue weighting factors. However, it has been shown⁷⁶ that the choice of factors (ICRP 30, 60, 103) can result in differences in effective dose of 20% to 40% depending on the radioisotope. The majority of studies reviewed here calculate the effective dose according to ICRP 60 (1990), with three studies reporting EDE and not E^{43,46,61} and two studies reporting neither^{53,54}. Only one study calculated E based on the newer ICRP 103 (2007) organ weighting factors⁴⁹.

Conclusion

Although it is difficult to estimate the risk that radiation exposure from PET studies poses to research subjects, radiation protection legislation and ethic committees demand an estimate of risk per radiotracer. In this paper we summarised the dosimetry of 42 carbon-11 labelled PET tracers. Radiation burden expressed as effective dose and maximum absorbed organ dose were compared. Estimated mean effective doses based on homogenous distribution (3.6 $\mu\text{Sv}/\text{MBq}$) or the generic model

(4.5 $\mu\text{Sv}/\text{MBq}$), and upper limits of cumulated activity contribute to our understanding of dose deposition for carbon-11 labelled tracers. However, despite the value of these models, in vivo dosimetry experiments remain crucial to the accurate estimation of health risks based on current guidance. Dosimetry estimates are affected by both biological and methodological sources of variability. In addition significant inter-species differences suggest that extrapolation from animal data should be considered to provide only preliminary dose estimates for humans.

For the studies examined, organs with peak uptake differed between tracers, though many irradiated excretory organs. Widely used radiation dose guidelines imply either an effective dose constraint of no more than 10 mSv per study, at least for healthy volunteers¹⁵, or a specific organ dose limit of 50 mSv per PET study¹⁴. With effective doses between 3.2-8.9 $\mu\text{Sv}/\text{MBq}$ for all but one of the radiotracers, serial PET scans in a single subject are feasible within the above constraints. For first time in human studies with a new carbon-11 labelled small molecule PET tracer where no human dosimetry data is available, one could assume an effective dose of 10 $\mu\text{Sv}/\text{MBq}$ (mean E plus two standard deviations). Where continued use of a new tracer is foreseen, it is recommended that a human study is performed to measure the spatiotemporal distribution of radioactivity and obtain a reliable estimate of effective dose.

REFERENCES

- Innis RB, Cunningham VJ, Delforge J, Fujita M, Gjedde A, Gunn RN et al. Consensus nomenclature for in vivo imaging of reversibly binding radioligands. *J Cereb Blood Flow Metab.* 2007;27:1533-9
- Mankoff DA, Eary JF, Link JM, Muzi M, Rajendran JG, Spence AM et al. Tumor-specific positron emission tomography imaging in patients: [¹⁸F] fluorodeoxyglucose and beyond. *Clin Cancer Res.* 2007;13:3460-9
- Cunningham VJ, Gunn RN, Matthews JC. Quantification in PET for research in pharmacology and drug development. *Nucl Med Commun.* 2004;643-6
- International Commission on Radiological Protection (ICRP). ICRP Publication 30, Part 1: Limits for Intakes of Radionuclides by Workers. Oxford, U.K. Pergamon Press; 1979
- International Commission on Radiological Protection (ICRP). ICRP Publication 60: 1990 Recommendations of the International Commission on Radiological Protection. Oxford, U.K.: Pergamon Press; 1991
- International Commission on Radiological Protection (ICRP). ICRP Publication 103: The 2007 recommendations of International Commission on Radiological Protection. 2007;37:1-333
- Pierce DA, Preston DL. Radiation-related cancer risk at low doses among atomic bomb survivors. *Radiat Res.* 2000;154:178-86
- Breckow J. Linear-no-threshold is a radiation-protection standard rather than a mechanistic effect model. *Radiat Environ Biophys.* 2006;44:257-60
- Land CE, Jeggo PA, Kellerer AM, Little JB, Pierce PD, Ullrich RL. Committee 1 Task Group Report. ICRP Publication 99: Low-dose Extrapolation of Radiation-Related Cancer Risk. 2005
- E Cardis, M Vrijheid, M Blettner, Gilbert E, Hakama M, Hill C, et al. Risk of cancer after low doses of ionising radiation: retrospective cohort study in 15 countries. *BMJ.* 2005;331:77
- Report of the United Nations Scientific Committee on the Effects of Atomic Radiation to the General Assembly. 2000. www.unscear.org/docs/reports/gareport.pdf
- Huda W, Scrimger JW. Irradiation of volunteers in nuclear medicine. *J Nucl Med.* 1989;30:260-4
- European Commission Radiation Protection 99: Guidance on Medical Exposures in Medical and Biomedical Research. 1998. http://ec.europa.eu/energy/nuclear/radiation_protection/doc/publication/099_en.pdf
- CFR - Code of Federal Regulations Title 21, part 361. <http://www.accessdata.fda.gov/scripts/cdrh/cfdocs/cfcr/cfrSearch.cfm?fr=361.1>
- International Commission on Radiological Protection (ICRP). ICRP Publication 62: Radiological Protection in Biomedical Research. Oxford, U.K.: Pergamon Press; 1991
- The Ionising Radiation (Medical Exposure) Regulations. 2000. <http://www.legislation.gov.uk/uksi/2000/1059/contents/made>
- Marinelli LD, Quimby EH, Hine CJ. Dosage determination with radioactive isotopes. *Nucleonics.* 1948;2:44-49
- Zanzonico PB. Internal radionuclide radiation dosimetry: a review of basic concepts and recent developments. *J Nucl Med.* 2000;41:297-308
- Howell RW, Wessels BW, Loevinger R, Watson EE, Bolch WE, Brill AB, et al. The MIRD perspective 1999. *J Nucl Med.* 1999;40:3S-10S
- Tipre DN, Lu JQ, Fujita M, Ichise M, Vines D, Innis RB. Radiation dosimetry estimates for the PET serotonin transporter probe ¹¹C-DASB determined from whole-body imaging in non-human primates. *Nucl Med Commun.* 2004;25:81-6
- Lin JH. Species similarities and differences in pharmacokinetics. *Drug Metab Dispos.* 1995. *J Nucl Med.* 2008;23:1008-21
- Parsey RV, Belanger MJ, Sullivan GM, Simpson NR, Stabin MG, Van Heertum R, et al. Biodistribution and radiation dosimetry of ¹¹C-WAY100,635 in humans. *J Nucl Med.* 2005;46:614-9
- Osman S, Lundkvist C, Pike VW, Halldin C, McCarron JA, Swahn CG, et al. Characterization of the radioactive metabolites of the 5-HT_{1A} receptor radioligand, [O-methyl-¹¹C]WAY-100635, in monkey and human plasma by HPLC: Comparison of the behaviour of an identified radioactive metabolite with parent radioligand in monkey using PET. *Nucl Med Biol.* 1996;23:627-34
- Sparks RB, Aydogan B. Comparison of the effectiveness of some common animal data scaling techniques in estimating human radiation dose. In: Stelson A, Stabin M, Sparks R, eds. Sixth International Radiopharmaceutical Dosimetry Symposium. Oak Ridge, TN: Oak Ridge Associated Universities; 1999:705-16
- Bencherif B, Endres CJ, Musachio JL, Villalobos A, Hilton J, Scheffel U, et al. PET imaging of brain acetylcholinesterase using [¹¹C]CP-126,998, a brain selective enzyme inhibitor. *Synapse.* 2002;45:1-9
- Toyohara J, Sakata M, Wu J, Ishikawa M, Oda K, Ishii K, et al. Preclinical and the first clinical studies on [¹¹C]CHIBA-1001 for mapping alpha7 nicotinic receptors by PET. *Ann Nucl Med.* 2009;23:301-9
- Sakata M, Wu J, Toyohara J, Oda K, Ishikawa M, Ishii K, et al. Biodistribution and radiation dosimetry of the $\alpha 7$ nicotinic acetylcholine receptor ligand [¹¹C]CHIBA-1001 in humans. *Nucl Med Biol.* 2011;38:443-8
- Brown AK, Fujita M, Fujimura Y, Liow JS, Stabin M, Ryu YH, et al. Radiation Dosimetry and Biodistribution in Monkey and Man of ¹¹C-PBR28: A PET Radioligand to Image Inflammation. *J Nucl Med.* 2007;48:2072-9
- Stabin MG. Fundamentals of Nuclear Medicine Dosimetry. 1st ed. Springer Science and Business Media; 2008:36
- Stabin MG. MIRDose: personal computer software for internal dose assessment in nuclear medicine. *J Nucl Med.* 1996;37:538-46
- Stabin MG, Sparks RB, Crowe E. OLINDA/EXM: The Second-Generation Personal Computer Software for Internal Dose Assessment in Nuclear Medicine. *J Nucl Med.* 2005;46:1023-7
- Marthi K, Hansen SB, Jakobsen S, Bender D, Smith SB, Smith DF. Biodistribution and radiation dosimetry of [N-methyl-¹¹C] mirtazapine, an antidepressant affecting adrenoceptors. *Appl Radiat Isot.* 2003;59:175-9
- Jakobsen S, Pedersen K, Smith DF, Jensen SB, Munk OL, Cumming P. Detection of alpha2-adrenergic receptors in brain of living pig with ¹¹C-yohimbine. *J Nucl Med.* 2006;47:2008-15
- Cropley VL, Fujita M, Musachio JL, Hong J, Ghose S, Sangare J, et al. Whole-body biodistribution and estimation of

- radiation-absorbed doses of the dopamine D1 receptor radioligand ^{11}C -NNC 112 in humans. *J Nucl Med.* 2006;47:100-4
- 35 Slifstein M, Hwang DR, Martinez D, Ekelund J, Huang Y, Hackett E, et al. Biodistribution and Radiation dosimetry of the dopamine D2 Ligand ^{11}C -raclopride determined from human whole-body PET. *J Nucl Med.* 2006;47:313-9
 - 36 Ribeiro MJ, Ricard M, Bourgeois S, Lièvre MA, Bottlaender M, Cervais P, et al. Biodistribution and radiation dosimetry of [^{11}C] raclopride in healthy volunteers. *Eur J Nucl Med Mol Imaging.* 2005;32:952-8
 - 37 Seneca N, Skinbjerg M, Zoghbi SS, Liow JS, Gladding RL, Hong J, et al. Kinetic brain analysis and whole-body imaging in monkey of [^{11}C]MNPAA: A dopamine agonist radioligand. *Synapse.* 2008;62:700-709
 - 38 Antenor-Dorsey JA, Laforest R, Moerlein SM, Videen TO, Perlmutter JS. Radiation dosimetry of N-([^{11}C]methyl)benperidol as determined by whole-body PET imaging of primates. *Eur J Nucl Med Mol Imaging.* 2007;35:771-8
 - 39 Laymon CM, Mason NS, Frankle WG, Carney JP, Lopresti BJ, Litschge MY, et al. Human Biodistribution and Dosimetry of the D2/3 Agonist ^{11}C -N-Propylnorapomorphine (^{11}C -NPA) Determined from PET. *J Nucl Med.* 2009;50:814-7
 - 40 Laymon CM, Narendran R, Mason NS, Carney JP, Lopresti BJ, Mathis CA, et al. Human Biodistribution and Dosimetry of the PET Radioligand [^{11}C]Flumazenil (FMZ). [Article in Press] *Mol Imaging Biol.* 2011
 - 41 Nugent AC, Neumeister A, Drevets WC, Eckelman WC, Channing MA, Herscovitch P. Human biodistribution and dosimetry of the PET benzodiazepine receptor ligand ^{11}C -flumazenil [abstract]. *J Nucl Med.* 2004;45(suppl):434P
 - 42 Santens P, De Vos F, Thierens H, Decoo D, Slegers G, Dierckx RA, et al. Biodistribution and dosimetry of carbon-11-methoxyprogabidic acid, a possible ligand for GABA-receptors in the brain. *J Nucl Med.* 1998;39:307-10
 - 43 Baldwin RM, Horti AG, Bremner JD, Stratton MD, Dannals RF, Ravert HT, et al. Synthesis and PET Imaging of the Benzodiazepine Receptor Tracer [N-Methyl- ^{11}C]iomazenil. *Nucl Med Biol.* 1995;22:659-65
 - 44 Ridler K, Rabiner EA, Kegeles L, Castrillon J, Hackett E, Laruelle M, et al. Biodistribution and radiation dosimetry of the NK1 ligand GR-205171 determined from Papio Anubis whole-body PET. *Journal of Cerebral Blood Flow and Metabolism* 2009 29 SUPPL. 1 (S362-3)
 - 45 Newberg AB, Ray R, Scheuermann J, Wintering N, Saffer J, Schmitz A, et al. Dosimetry of ^{11}C -carfentanil, a micro-opioid receptor imaging agent. *Nucl Med Commun.* 2009;30:314-8
 - 46 Treyer V, Streffer J, Ametamey SM, Bettio A, Bläuenstein P, Schmidt M, et al. Radiation dosimetry and biodistribution of ^{11}C -AVP688 measured in healthy volunteers. *Eur J Nucl Med and Mol Imaging.* 2008;35:766-70
 - 47 Virta JR, Tolvanen T, Nagren K, Brück A, Roivainen A, Rinne JO. ^{11}C -Methyl-4-Piperidinyln-Butyrate Radiation Dosimetry in Humans by Dynamic Organ-Specific Evaluation. *J Nucl Med.* 2008;49:347-53
 - 48 Yamane T, Shimizu K, Sasaki M, Kageyama H, Hashizume Y, Takashima T, et al. [^{11}C]telmisartan as a potential PET molecular imaging probe for human drug transporter OATP1B3. *Molecular Imaging and Biology* 2010 12 SUPPL. 2 (S926)
 - 49 Hirvonen J, Roivainen A, Virta J, Helin S, Nägren K, Rinne JO. Human biodistribution and radiation dosimetry of ^{11}C -(R)-PK11195, the prototypic PET ligand to image inflammation. *Eur J Nucl Med Mol Imaging.* 2010;37:606-12
 - 50 Ribeiro MJ, Ricard M, Lièvre MA, Bourgeois S, Emond P, Gervais P, et al. Whole-body distribution and radiation dosimetry of the dopamine transporter radioligand [^{11}C]PE21 in healthy volunteers. *Nucl Med Biol.* 2007;34:465-70
 - 51 Seneca N, Zoghbi SS, Liow J, Kreis W, Herscovitch P, Jenko K, et al. Human Brain Imaging and Radiation Dosimetry of ^{11}C -N-Desmethyl-Loperamide, a PET Radiotracer to Measure the Function of P-Glycoprotein. *J Nucl Med.* 2009;50:807-13
 - 52 Lu JQ, Ichise M, Liow JS, Ghose S, Vines D, Innis RB. Biodistribution and Radiation Dosimetry of the Serotonin Transporter Ligand ^{11}C -DASB Determined from Human Whole-Body PET. *J Nucl Med.* 2004;45:1555-9
 - 53 Vander Borgh T, Killbourn MR, Koeppe RA, DaSilva JN, Carey JE, Kuhl DE et al. In vivo imaging of the brain vesicular monoamine transporter. *J Nucl Med.* 1995;36:2252-60
 - 54 DaSilva JN, Carey JE, Sherman PS, Pisani TJ, Killbourn MR. Characterization of [^{11}C] tetraabenazine as an in vivo radioligand for the vesicular monoamine transporter. *Nucl Med Biol.* 1994;21:2151-6
 - 55 Murthy R, Harris P, Simpson N, Van Heertum R, Leibel R, Mann JJ, et al. Whole body [^{11}C]dihydrotetraabenazine imaging of baboons: biodistribution and human radiation dosimetry estimates. *Eur J Nucl Med Mol Imaging.* 2008;35:790-7
 - 56 Murthy R, Erlandsson K, Kumar D, Van Heertum R, Mann J, Parsey R. Biodistribution and radiation dosimetry of ^{11}C -harmine in baboons. *Nucl Med Commun.* 2007;28:748-54
 - 57 O'Keefe GJ, Saunderson TH, Ng S, Ackerman U, Tochon-Danguy HJ, Chan JG, et al. Radiation Dosimetry of Beta-Amyloid Tracers ^{11}C -PiB and ^{18}F -BAY94-9172. *J Nucl Med.* 2009;50:309-15
 - 58 Scheinin NM, Tolvanen TK, Wilson IA, Arponen EM, Nägren KA, Rinne JO. Biodistribution and Radiation Dosimetry of the Amyloid Imaging Agent ^{11}C -PiB in Humans. *J Nucl Med.* 2007;48:128-33
 - 59 Thees S, Neumaier B, Glatting G, Deisenhofer S, von Arnim CA, Reske SN, et al. Radiation dosimetry and biodistribution of the beta-amyloid plaque imaging tracer ^{11}C -BTA-1 in humans. *Nuklearmedizin.* 2007;46:175-80
 - 60 Seneca N, Cai L, Liow JS, Zoghbi SS, Gladding RL, Hong J, et al. Brain and whole-body imaging in nonhuman primates with [^{11}C] MeS-IMPY, a candidate radioligand for beta-amyloid plaques. *Nucl Med Biol.* 2007;34:681-9
 - 61 Graham MM, Peterson LM, Muzi M, Graham BB, Spence AM, Link JM, et al. 1-[Carbon-11]-glucose radiation dosimetry and distribution in human imaging studies. *J Nucl Med.* 1998;39:1805-1810
 - 62 Tolvanen T, Nägren K, Yu M, Sutinen E, Havu-Aurén K, Jyrkkö S, et al. Human radiation dosimetry of [^{11}C] MeAIB, a new tracer for imaging of system A amino acid transport. *Eur J Nucl Med Mol Imaging.* 2006;33:1178-84
 - 63 Deloar HM, Fujiwara T, Nakamura T, Itoh M, Imai D, Miyake M, et al. Estimation of internal absorbed dose of L-[methyl- ^{11}C] methionine using whole-body PET. *Eur J Nucl Med Mol Imaging.* 1998;25:629-33
 - 64 Seltzer MA, Jahan SA, Sparks R, Stout DB, Satyamurthy N, Dahlbom M, et al. Radiation Dose Estimates in Humans for (^{11}C) C-Acetate Whole-Body PET. *J Nucl Med.* 2004;45:1233-6
 - 65 Dence CS, Laforest R, Sun X, Sharp TL, Welch MJ, Mach RH. Radiochemical Synthesis, Rodent Biodistribution and Tumor Uptake, and Dosimetry Calculations of [^{11}C] Methylated LY2181308. *Mol Imaging Biol.* 2010 Dec;12(6):608-15
 - 66 Van der Veldt AA, Hendrikse NH, Smit EF, Mooijer MP, Rijnders AY, Gerritsen WR, et al. Biodistribution and radiation dosimetry of ^{11}C -labelled docetaxel in cancer patients. *Eur J Nucl Med Mol Imaging.* 2010 Oct;37(10):1950-8. Epub 2010 May 27
 - 67 Liu N, Li M, Li X, Meng X, Yang G, Zhao S, et al. PET-Based Biodistribution and Radiation Dosimetry of Epidermal Growth Factor Receptor-Selective Tracer ^{11}C -PD153035 in Humans. *J Nucl Med.* 2009;50:303-8
 - 68 International Commission on Radiological Protection (ICRP). ICRP Publication 53: Biokinetics and Dosimetry: General Considerations. 1987
 - 69 International Commission on Radiological Protection (ICRP). ICRP Publication 80: Radiation Dose to Patients from Radiopharmaceuticals (Addendum 2 to ICRP Publication 53. 1998
 - 70 Hays MT, Watson EE, Thomas SR, Stabin M. MIRD dose estimate report no. 19: radiation absorbed dose estimates from ^{18}F -FDG. *J Nucl Med.* 2002;43:210-4
 - 71 Brix G, Lechel U, Glatting G, Ziegler SI, Münzing W, Müller SP, et al. Radiation exposure of patients undergoing whole-body dual-modality ^{18}F -FDG PET/CT examinations. *J Nucl Med.* 2005;46:608-13
 - 72 Gatlery SJ. Estimation of upper limits on human radiation absorbed doses from carbon-11-labeled compounds. *J Nucl Med.* 1993;34:2208-15
 - 73 Nosslin B, Johansson L, Leide-Svegborn S, Liniecki J, Mattsson S, Taylor DM. A generic model for ^{11}C labelled radiopharmaceuticals for imaging receptors in the human brain. *Radiat Prot Dosimetry.* 2003;105:587-91
 - 74 International Commission on Radiological Protection (ICRP) Publication 106. Radiation Dose to Patients from Radiopharmaceuticals: Addendum 3 to ICRP Publication 53, Ann. ICRP 38(1-2). 2008
 - 75 International Commission on Radiological Protection (ICRP) Publication 99. Low-dose Extrapolation of Radiation-related Cancer Risk, Ann. ICRP 35(4). 2005
 - 76 Stabin MG. Uncertainties in Internal Dose Calculations for Radiopharmaceuticals. *J Nucl Med.* 2008;49:853-60

CHAPTER 3

HUMAN DOSIMETRY OF THE NMDA RECEPTOR LIGAND [¹¹C]GMOM

PUBLISHED IN THE JOURNAL OF NUCLEAR MEDICINE

Jasper van der Aart, Thalia F. van der Doef, Paul Horstman,
Marc C. Huisman, Robert C. Schuit, Arthur van Lingen, Albert D. Windhorst,
Bart N.M. van Berckel, Adriaan A. Lammertsma

Department Of Radiology And Nuclear Medicine, Vu University Medical Center,
Amsterdam UMC, The Netherlands

© 2017 The Society of Nuclear Medicine and Molecular Imaging. DOI 10.2967/jnumed.116.188250

Abstract

INTRODUCTION The methylguanidine derivative [^{11}C]GMOM has been used successfully to quantify N-methyl-D-aspartate (NMDA) receptor binding in humans. The purpose of the present study was to estimate the [^{11}C]GMOM radiation dose in healthy humans.

METHODS Following [^{11}C]GMOM injection, three female and two male subjects underwent 10 consecutive whole body PET scans in approximately 77 minutes. 7 source organs were defined manually, scaled to a gender specific reference, and residence times were calculated for input into OLINDA/EXM software. Accepted tissue weighting factors (ICRP103) were used to calculate the effective dose.

RESULTS Mean absorbed radiation doses in source organs ranged from 7.7 $\mu\text{Gy}\cdot\text{MBq}^{-1}$ in the brain to 12.7 $\mu\text{Gy}\cdot\text{MBq}^{-1}$ in the spleen. The effective dose (\pm SD) was $4.5 \pm 0.5 \mu\text{Sv}\cdot\text{MBq}^{-1}$.

CONCLUSION The effective dose of [^{11}C]GMOM is at the lower end of the range seen for other C-11 labelled ligands, allowing for serial PET scanning in a single subject.

Introduction

The phencyclidine (PCP) binding site within the pore of the glutamatergic N-methyl-D-aspartate (NMDA) receptor ion-channel is a target for NMDA antagonists such as MK-801 and ketamine. Imaging the PCP site using positron emission tomography (PET) with radiolabelled antagonists has been pursued avidly, but clinical implementation of these radiotracers has been held back by high nonspecific binding, high lipophilicity, low brain entrance, or rapid radioligand metabolism¹. Results from human molecular imaging studies with methylguanidine derivatives such as [^{11}C]CNS 5161² and [^{18}F]GE-179³ seem more promising. [^{11}C]GMOM (carbon-11 labelled N-(2-chloro-3-thiomethylphenyl)-N¹-(3-methoxyphenyl)-N³-methylguanidine) studies in awake rats showed that administration of the antagonist MK-801 decreased tracer binding in brain regions of interest (ROIs), whereas the channel activator D-serine increased binding⁴. Recent experiments in healthy subjects showed that intravenous administration of ketamine 0.3 mg·kg⁻¹ reduced the [^{11}C]GMOM inhibition constant (K_i) in total brain grey matter by, on average, 66%⁵. More human studies with [^{11}C]GMOM are planned, but at present no data on tracer distribution and radiation dose are available. Although various methods can be used to scale dose estimates from preclinical species to man, potentially significant interspecies differences mean that extrapolation from rodent data should be considered with care^{6,7}. The purpose of the present study was to calculate [^{11}C]GMOM effective dose in men and women for use in future clinical PET protocols.

Materials and Methods

Subjects and scan protocol

The study was approved by the Medical Ethics Review Committee of the VU University Medical Center Amsterdam and all subjects signed an informed consent form prior to inclusion. Five healthy subjects were included, two males and three females, with a mean (\pm standard deviation, SD) weight of 75.4 ± 7.0 kg, height of 177 ± 10 cm, and age of 24.9 ± 2.5 years. Subjects were screened and health status was confirmed by blood and urine tests (complete blood count, serum chemistry, drug screen), together with a physical examination and medical history. The scanning protocol was identical to that reported previously⁸. Subjects were positioned on the bed of a Philips Gemini TF-64 PET/CT scanner (Philips Medical Systems, Cleveland, OH, USA) and a 35 mAs low-dose whole body CT scan was acquired. [^{11}C]GMOM was

synthesized according to methods described previously⁵. Following intravenous injection of 376 ± 19 MBq [^{11}C]GMOM, a series of 10 whole-body sweeps was performed, taking 40 s per bed position and typically requiring 11 bed positions to cover the body from the top of the head to the upper thigh. Overlap between bed positions was approximately 50% to maintain a constant axial coverage. Total acquisition time was approximately 77 minutes, i.e. 3.8 times the half-life of carbon-11. Five 0.5 ml venous blood samples per subject were taken manually at 10, 27, 44, 60 and 77 minutes post [^{11}C]GMOM injection for measurement of whole blood radioactivity concentrations.

Data Analysis

All PET scans were reconstructed using the standard time-of-flight reconstruction algorithm, including normalization, and corrections for scatter, randoms, attenuation and dead-time⁸. Non-decay corrected radioactivity (Bq) in source organs was used to calculate [^{11}C]GMOM residence times. Source organs (ROIs) were defined manually on relevant slices of either CT or PET images depending on optimal visibility of those organs. ROIs included heart, liver, kidneys, spleen, lungs, thyroid and brain. Organ volume (ml) was derived automatically from the ROIs. The lung ROI was edited manually when its location on the respiration-averaged PET scan differed from that on the CT scan. Individual ROIs were projected onto each serially acquired PET frame, manually adjusted in case of patient motion, and [^{11}C]GMOM time-activity curves (TACs) were generated. Radioactivity per organ volume ($\text{Bq}\cdot\text{ml}^{-1}$) was calculated assuming that the distribution of radioactivity within an organ was uniform. TACs were extrapolated from the last whole-body scan to infinity, assuming only physical decay and no further organ clearance. Red marrow activity concentration was assumed to be one third of the whole blood radioactivity concentration¹⁰. Standardized uptake values (SUV) were calculated by dividing non-decay corrected tissue radioactivity concentration by injected dose per body weight. [^{11}C]GMOM residence times (i.e. normalized cumulated activities) in the seven source organs were obtained through multiplication of the areas under the TACs with each subject's organ mass. Mass was calculated by scaling reference organ weights from a standard male (73.7 kg) or female (56.9 kg) to each subject's body weight using the software package OLINDA/EXM 1.1¹¹. Residence times of the manually drawn source organs of each subject were entered into the software to calculate absorbed dose ($\mu\text{Gy}\cdot\text{MBq}^{-1}$) for the target organs, 24 in total. Multiplication of absorbed doses with tissue weighting factors gave the organ effective doses ($\mu\text{Sv}\cdot\text{MBq}^{-1}$). The

factors, which represent each organ's relative risk contribution should the whole body be irradiated uniformly, were taken from the International Commission on Radiological Protection (ICRP) publication 103¹². Total effective dose is the sum of the organ effective doses.

Results

Figure 1 shows coronal slices of the [^{11}C]GMOM distribution in a female subject as a function of time. Figure 2 shows subject-averaged SUVs for the manually delineated ROIs. In early time frames, [^{11}C]GMOM concentrations are highest in lungs, spleen, kidneys and thyroid. Mean residence times are shown in Table 1. The longest residence time (0.0368 ± 0.0093 hours) was observed in the liver, the shortest in the thyroid (0.0005 ± 0.0002 hours). In all subjects, the organ with the highest absorbed dose was the spleen (mean $12.7 \mu\text{Gy}\cdot\text{MBq}^{-1}$). The mean effective dose was $4.5 \pm 0.5 \mu\text{Sv}\cdot\text{MBq}^{-1}$ (males $4.3 \pm 0.8 \mu\text{Sv}\cdot\text{MBq}^{-1}$ and females $4.6 \pm 0.4 \mu\text{Sv}\cdot\text{MBq}^{-1}$).

Discussion

Organ radiation exposure for the NMDA-receptor radiotracer [^{11}C]GMOM was measured in five healthy subjects. The mean effective dose was $4.5 \pm 0.5 \mu\text{Sv}\cdot\text{MBq}^{-1}$. Therefore, a PET scan following an injection of 370 MBq [^{11}C]GMOM would lead, on average, to a radiation dose of 1.67 mSv, which is in the range of other carbon-11

FIGURE 1 Coronal PET/CT fusion images of [^{11}C]GMOM uptake in Bq per ml tissue (BQML) showing tracer bio-distribution at four different time points (2, 18, 36, and 52 mins) for a female subject. Each panel is a composite of 11 bed positions of 40 seconds each.

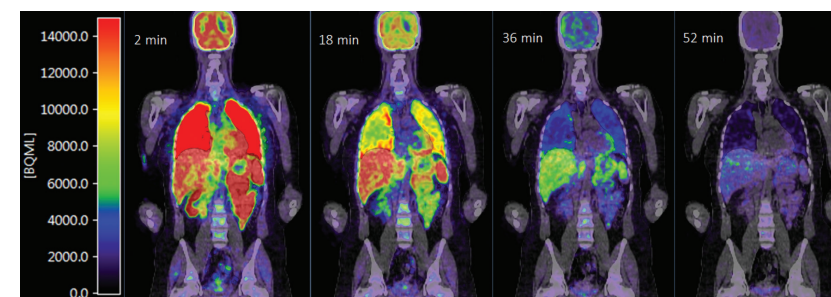
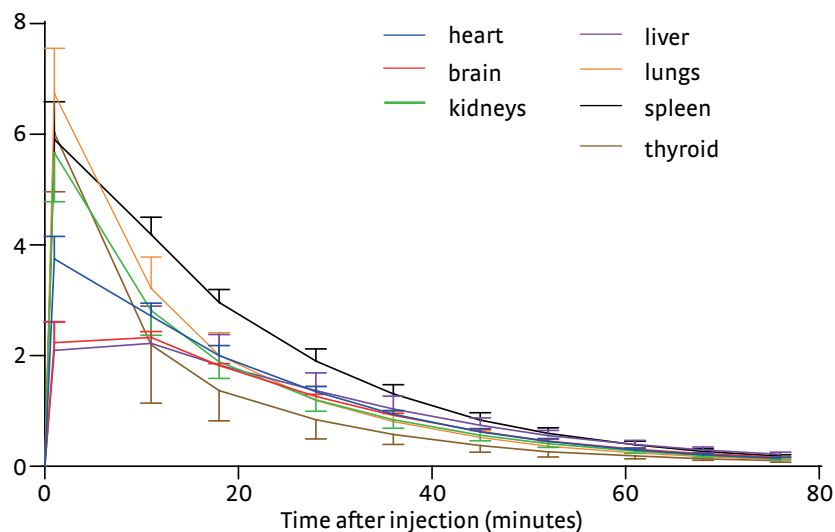


FIGURE 2 Time-standardised uptake value (SUV) curves (non-decay corrected) showing ^{11}C GMOM SUV (mean and standard deviation of 5 subjects) in manually delineated source organs.



labelled tracers^{7,13}. 2222 MBq injected activity would lead to a radiation dose of 10 mSv, which is the limit for proof of concept studies in normal subjects according to ICRP 62 guidelines and The Dutch Commission on Radiation Dosimetry¹⁴. For institutions following organ dose limits for radiopharmaceuticals that are administered under U.S. Radioactive Drug Research Committee regulations, the maximum injected activity per study would be limited by the critical organ rather than the (whole body) effective dose. The critical organ in this study was the spleen with an absorbed dose of $12.7 \mu\text{Gy}\cdot\text{MBq}^{-1}$, which is equivalent to 4.7 mSv for a typical injection of 370 MBq of ^{11}C GMOM.

Radiotracer dose deposition in tissue depends on both the biological half-life of the compound (and any radiolabelled metabolites) and half-life of the radionuclide. Given the relatively short half-life of carbon-11 (20.4 min), the effective dose mainly depends on organ perfusion and retention. Indeed, in the present study, the highest absorbed doses were found for highly perfused organs. Often, the urinary bladder-wall is reported as being the critical organ, despite delayed filling and the short half-life of carbon-11¹³. ^{11}C GMOM did not accumulate in the bladder, but rather in

TABLE 1 Mean \pm SD (N=5) ^{11}C GMOM residence times (in source organs), absorbed organ doses and effective organ doses. Organs are sorted from highest absorbed dose to lowest.

Target Organs	Residence Time (Hours)	Absorbed Dose ($\mu\text{Gy}\cdot\text{MBq}^{-1}$)	Effective Dose ($\mu\text{Sv}\cdot\text{MBq}^{-1}$)
Spleen	0.0065 ± 0.0009	12.7 ± 1.5	0.013
Lungs	0.0297 ± 0.0066	10.4 ± 1.9	1.252
Kidneys	0.0086 ± 0.0005	9.8 ± 0.4	0.010
Heart Wall	0.0072 ± 0.0011	9.3 ± 1.3	0.009
Liver	0.0368 ± 0.0093	9.1 ± 2.5	0.362
Thyroid	0.0005 ± 0.0002	8.0 ± 2.3	0.268
Brain	0.0283 ± 0.0033	7.7 ± 1.0	0.077
Pancreas		4.0 ± 0.4	0.004
Adrenals		3.9 ± 0.4	0.004
Gallbladder Wall		3.9 ± 0.4	0.004
Stomach Wall		3.5 ± 0.3	0.421
Total Body		3.5 ± 0.3	0.172
ULI Wall		3.4 ± 0.4	0.409
Ovaries		3.3 ± 0.3	0.261
Thymus		3.3 ± 0.3	0.003
Uterus		3.3 ± 0.3	0.013
LLI Wall		3.2 ± 0.3	0.384
Small Intestine		3.2 ± 0.2	0.003
Muscle		2.9 ± 0.3	0.003
Red Marrow	0.0016 ± 0.0008	2.8 ± 0.2	0.336
Urinary Bladder		2.8 ± 0.2	0.145
Breasts		2.7 ± 0.3	0.326
Skin		2.4 ± 0.2	0.024
Rest		3.5 ± 0.3	0.172
Total Effective Dose			4.5

LLI=lower large intestine, ULI=upper large intestine. 'Rest' includes Extrathoracic Region, Oesophagus, Stomach, Lymphatic Nodes and Salivary Glands.

the kidneys. This suggests that the main route of tracer excretion is not through the urinary system, and emptying of the bladder will not reduce the dose significantly. The results of the present study are in line with the dosimetry of another methylguanidine derivative, [¹¹C]CNS5161, of which the highest dose was also observed in lungs and spleen¹⁵.

A whole-body scan (from brain to upper thigh) typically required 11 bed positions taking about 7.5 minutes in total. The assumption was made that radiotracer kinetics between first and last bed positions were the same and that the main effect was decay, although this was not the case especially during the early phases of tracer distribution. The resulting uncertainty in organ dose estimates could have been minimized by using shorter PET frames for the first whole-body scans. However, organs with high uptake in the first frame were located towards the centre of a single bed position (i.e. mid-frame), and overlap between consecutive bed positions was approximately 50% to maintain a constant axial coverage.

Seven organs were designated source organs after visual inspection of the PET images. Absorbed radiation doses in these organs were low (e.g. 12.7 μGy·MBq⁻¹ in spleen) compared with other carbon-11 labelled radiotracers¹³. The mean absorbed dose in the critical organ of 32 radiotracers tested in humans was shown to be 40 μGy·MBq⁻¹ (range 11-194), a factor 3 higher than the spleen dose in the present study. Mean (± SD) effective dose of the 32 radiotracers was 5.3 ± 1.5 μSv·MBq⁻¹, half a standard deviation higher than the [¹¹C]GMOM effective dose.

Conclusion

With an effective dose of 4.5 μSv·MBq⁻¹ and relatively low organ doses, [¹¹C]GMOM has a dosimetry profile that allows for serial PET scanning in a single subject.

REFERENCES

- Fuchigami T, Nakayama M, Yoshida S: Development of PET and SPECT probes for glutamate receptors: *Scientific World Journal*. 2015. p.1-19. Available from: <https://doi.org/10.1155/2015/716514>
- Asselin M, Hammers A, Turton D, Osman S, Koeppe M BD: Initial kinetic analyses of the in vivo binding of the putative NMDA receptor ligand [C-11]CNS 5161 in humans: *NeuroImage*. 2004;22:T137.
- McGinnity CJ, Hammers A, Riaño Barros DA, Luthra SK, Jones PA, Trigg W, Micallef C, Symms MR, Brooks DJ, Koeppe MJ, Duncan JS: Initial evaluation of ¹⁸F-C E-179, a putative PET Tracer for activated N-methyl D-aspartate receptors. *Journal of Nuclear Medicine*. 2014 Mar;55(3):423-30. Available from: <https://doi.org/10.2967/jnumed.113.130641>
- Waterhouse RN, Slifstein M, Dumont F, Zhao J, Chang RC, Sudo Y, Sultana A, Balter A, Laruelle M: In vivo evaluation of [¹¹C]N-(2-chloro-5-thiomethylphenyl)-N'-(3-methoxyphenyl)-N'-methylguanidine ([¹¹C]GMOM) as a potential PET radiotracer for the PCP/NMDA receptor: *Nuclear Medicine and Biology*. 2004 Oct;31(7):939-48. Available from: <https://doi.org/10.1016/j.nucmedbio.2004.03.012>
- Doef TF van der, Golla SS, Klein PJ, Oropeza-Seguias GM, Schuit RC, Metaxas A, Jobse E, Schwarte LA, Windhorst AD, Lammertsma AA, Berckel BN van, Boellaard R: Quantification of the novel N-methyl-d-aspartate receptor ligand [¹¹C]GMOM in man: *Journal of Cerebral Blood Flow & Metabolism*: 2016;36:1111-21. Available from: <https://doi.org/10.1177/0271678X15608391>
- Sparks RB, Aydogan B: Comparison of the effectiveness of some common animal data scaling techniques in estimating human radiation dose: In: Stelson A, Stabin M, Sparks R, eds. *Sixth International Radiopharmaceutical Dosimetry Symposium*. Oak Ridge, TN: Oak Ridge Associated Universities; 1999:705-16
- Zanotti-Fregonara P, Innis RB: Suggested pathway to assess radiation safety of ¹¹C-labeled PET tracers for first-in-human studies: *European Journal of Nuclear Medicine and Molecular Imaging*. 2012;39(3):544-7. Available from: <https://doi.org/10.1007/s00259-011-2005-8>
- Postnov A, Froklage FE, van Lingen A, Reijneveld JC, Hendrikse NH, Windhorst AD, Schuit RC, Eriksson J, Lammertsma AA, Huisman MC: Radiation dose of the P-glycoprotein tracer ¹¹C-laniquidar: *Journal of Nuclear Medicine*. 2013 Dec;54(12):2101-3. Available from: <https://doi.org/10.2967/jnumed.113.120857>
- Surti S, Kuhn A, Werner ME, Perkins AE, Kolthammer J, Karp JS: Performance of Philips Gemini TF PET/CT scanner with special consideration for its time-of-flight imaging capabilities: *Journal of Nuclear Medicine*. 2007;48(3):471-80.
- Sgouros G: Bone marrow dosimetry for radioimmunotherapy: theoretical considerations: *Journal of Nuclear Medicine*. 1993;34(4):689-94.
- Stabin MG, Sparks RB, Crowe E: OLINDA/EXM: the second-generation personal computer software for internal dose assessment in nuclear medicine: *Journal of Nuclear Medicine*. 2005 Jun;46(6):1023-7.
- The 2007 recommendations of International the International Commission on Radiological Protection. International Commission on Radiological Protection (ICRP) publication 103.:7-8.
- Van der Aart J, Hallett WA, Rabiner EA, Passchier J, Comley RA: Radiation dose estimates for carbon-11-labelled PET tracers: *Nuclear Medicine and Biology*. 2012;39(2):305-14. Available from: <https://doi.org/10.1016/j.nucmedbio.2011.08.005>
- Publication of the Netherlands Commission on Radiation Dosimetry (Nederlandse Commissie Voor Stralingsdosimetrie NCS). Human Exposure to Ionising Radiation for Clinical and Research Purposes: Radiation Dose & Risk Estimates [Internet]. 2016 [cited 2016 Jul 29]. p20.
- Dhawan V, Robeson W, Bjelke D, Chaly T, Hellman M, Graf K, Zhuo L, Mackay M, Eidelberg D: Human Radiation Dosimetry for NMDA Receptor Radioligand ¹¹C-CNS5161: *Journal of Nuclear Medicine*. 2015 Apr 30; Available from: <https://doi.org/10.2967/jnumed.114.152447>

CHAPTER 4

**EVALUATION OF THE NOVEL
PET TRACER [11C]HACH242 FOR
IMAGING THE GLUN2B NMDA
RECEPTOR IN NON-HUMAN
PRIMATES**

PUBLISHED IN MOLECULAR IMAGING & BIOLOGY

Jasper van der Aart, Maqsood Yaqub, Esther J.M. Kooijman, Jaco Bakker,
Jan A.M. Langermans, Robert C. Schuit, Mark B.M. Hofman,
Johannes A.M. Christiaans, Adriaan A. Lammertsma, Albert D. Windhorst,
Bart N.M. van Berckel

Department of Radiology and Nuclear Medicine, vu University Medical Center,
Amsterdam UMC, The Netherlands

© 2018 The Authors. Open Access. This article is distributed under the terms of the Creative Commons
Attribution 4.0 International License. doi 10.1007/s11307-018-1284-x

Abstract

PURPOSE There are currently no positron emission tomography (PET) radiotracers for the GluN2B (NR2B) binding sites of brain N-Methyl-d-aspartate (NMDA) receptors. In rats, the GluN2B antagonist Ro25-6981 reduced binding of [¹¹C]HACH242. This paper reports the evaluation of [¹¹C]HACH242 PET in non-human primates at baseline and following administration of the GluN2B negative allosteric modulator radiprodil.

PROCEDURES Eight 90-min dynamic [¹¹C]HACH242 PET scans were acquired in 3 male anaesthetised rhesus monkeys, including a retest session of subject 1, at baseline and 10 min after intravenous 10 mg/kg radiprodil. Standardised uptake values (SUV) were calculated for 9 brain regions. Arterial blood samples were taken at 6 timepoints to characterise pharmacokinetics in blood and plasma. Reliable input functions for kinetic modelling could not be generated due to variability in the whole-blood radioactivity measurements.

RESULTS [¹¹C]HACH242 entered the brain and displayed fairly uniform uptake. The mean (\pm standard deviation, SD) T_{max} was 17 ± 7 min in baseline scans and 24 ± 15 min in radiprodil scans. The rate of radioligand metabolism in plasma (primarily to polar metabolites) was high, with mean parent fractions of $26 \pm 10\%$ at 20 min and $8 \pm 5\%$ at 85 min. Radiprodil increased [¹¹C]HACH242 whole-brain SUV in the last PET frame by 25%, 1%, 3% and 17% for subjects 1, 2, 3 and retest of subject 1, respectively. The mean brain to plasma ratio was 5.4 ± 2.6 , and increased by 39% to 110% in the radiprodil condition, partly due to lower parent plasma radioactivity of -11% to -56%.

CONCLUSIONS The present results show that [¹¹C]HACH242 has a suitable kinetic profile in the brain and low accumulation of lipophilic radiometabolites. Radiprodil did not consistently change [¹¹C]HACH242 brain uptake. These findings may be explained by variations in cerebral blood flow, a low fraction of specifically bound tracer, or interactions with endogenous NMDA receptor ligands at the binding site. Further experiments of ligand interactions are necessary to facilitate the development of radiotracers for *in vivo* imaging of the ionotropic NMDA receptor.

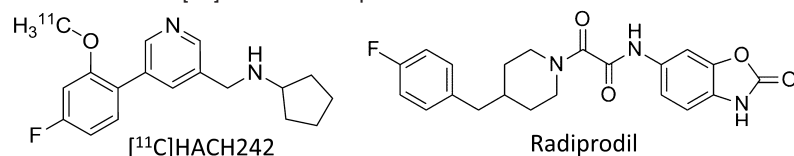
Introduction

N-Methyl-d-aspartate (NMDA) receptors are ionotropic glutamate receptors that mediate excitatory postsynaptic signaling and are expressed widely in the central nervous system (CNS). NMDA receptors are heterotetramers of mostly GluN1 and two GluN2(A-D) subunits in the CNS¹. In the last decade, a major effort in NMDA receptor drug development has focused on allosteric modulation of ion channel activity via the GluN2B (also known as NR2B) binding site which are located on the extracellular N-terminal domain (NTD) of the NMDA receptor. Ligands such as ifenprodil and derivatives are noncompetitive antagonists of the GluN2B site that stabilise a closed-cleft conformation of GluN2B NTD². Immunoblotting techniques showed that in the human brain, the GluN2B subunit is primarily expressed in forebrain structures, such as the cortex, hippocampus, striatum, thalamus, and olfactory bulb. Moderate levels of GluN2B subunit expression are evident in the midbrain, such as the hypothalamus, colliculi, and also the brain stem (rat only), and low expression occurs in the cerebellum and spinal cord^{3,4}. The interest in the therapeutic potential of GluN2B negative allosteric modulators has spurred drug development of ifenprodil derivatives in the past two decades. Second generation 'prodils' such as radiprodil (RGH-896), traxoprodil (CP-101,606), Besonprodil (CI-1041), CERC-301 (MK-0657), EVT-101, Ro 25-6981 and BMT-108908 have been developed for the treatment of a wide range of CNS pathologies, including acute and chronic pain, stroke, dementias and major depressive disorder.

The highest level of confidence and direct evidence that GluN2B engagement is achieved is acquired from *in vivo* molecular imaging experiments with positron emission tomography (PET). The development of PET tracers for imaging the NMDA receptor system has been reviewed in the past^{5,6,7}. Unfortunately, the majority of radiotracers exhibit poor *in vivo* applicability owing to poor brain penetration⁸, non-specific uptake in the brain and extensive metabolism^{9,10}. At present, there is no well validated GluN2B binding PET radioligand available. Recently, a new class of GluN2B antagonists with a wide range of potential 2,6-disubstituted aromatic and heteroaromatic compounds was described¹¹. Biodistribution and blocking studies with N-((5-(4-fluoro-2-[¹¹C]methoxyphenyl)pyridin-3-yl)methyl)-cyclopentanamin ([¹¹C]HACH242, Figure 1) were carried out in anaesthetised mice and in non-anaesthetised rats¹². The affinity of [¹¹C]HACH242 for GluN2B receptors was 12.4 ± 2.1 nM as shown in competition binding experiments against 5 nM [³H]ifenprodil, which is equal to ifenprodil and about 5 times lower than Ro25-6981. Brain

distribution studies in mice showed a 3-fold increase in activity uptake in forebrain regions vs. cerebellum at 15 min, which is the highest ratio that has been reported for candidate GluN2B site radiotracers. [^{11}C]HACH242 binding in non-anaesthetised rats was reduced by Ro25-6981, showing a regional distribution that is consistent both with the expression pattern of GluN2B subunits and the density of [^3H]Ro25-6981 binding sites in the adult rodent brain. However, high levels of non-specific uptake were observed in the thalamus¹².

FIGURE 1 Chemical structures of [^{11}C]HACH242 and radiprodil.



GluN2B ligands frequently exert off-target effects. For example ifenprodil dose-dependently reduces brain uptake of the sigma-1 receptor radiotracer [^{11}C]SA4503¹³. The selectivity of [^{11}C]HACH242 for GluN2B was investigated in an exhaustive pharmacological screen against 79 targets¹². The radioligand showed affinity > 1.1 μM for 78 of the targets. Sigma-1 was the exception, for which the tracer showed an affinity of 20 nM. Further studies with GluN2B specific antagonists are warranted to investigate the specific binding of [^{11}C]HACH242 *in vivo*. Radiprodil binds to GluN2B-containing receptors irrespective of the GluN2 subunit composition, analogous to Ro25-6981⁶². Furthermore, radiprodil binding is insensitive to 1,3-di-o-tolylguanidine (DTG), which suggests it does not bind to the sigma receptors¹⁴. Research on non-human primates (NHP) generates complementary data that can bridge translational imaging research from rodents to humans. This paper reports on the initial assessment of [^{11}C]HACH242 PET in NHP at baseline and following intravenous administration of a high dose of radiprodil.

Materials and Methods

Animals, housing and care

Three adult male rhesus monkeys (*Macaca mulatta*) were selected for this study. Subject and radiotracer injectate details are shown in Table 1. All animals originated from and were housed at the Biomedical Primate Research Centre (BPRC,

Rijswijk, The Netherlands), and underwent a complete physical, haematological, and biochemical examination before the study started. They remained under intensive veterinary supervision during the entire study period. Animals were housed in enriched cages at a temperature between 20–22°C, with a 12 hour light/12 hour dark cycle per day. Drinking water was provided ad libitum but food was withheld for 16 hours prior to anaesthesia. Ethics approval by the Animal Experiments Committee (DEC) of the BPRC was obtained prior to the commencement of the study. The procedures performed in this study were in accordance with the Dutch laws on animal experimentation, with the regulations for animal handling as described in the EU Directive 63/2010 and with the Weatherall report⁶³. The BPRC is accredited by the Association for Assessment and Accreditation of Laboratory Animal Care International.

TABLE 1 Subject and injectate details.

	Age (years)	Weight (kg)	Injected activity scan 1 (MBq)	A_m^{PET1} (MBq nmol ⁻¹)	Injected activity scan 2 (MBq)	A_m^{PET2} (MBq nmol ⁻¹)
s1	5.4	8.7	201	6.1	155	11.3
s2	8.6	11.3	86	17.9	78	13.9
s3	5.6	11.9	104	20.7	61	7.8
s1 re-test	5.7	8.7	113	23.6	72	22.7

A_m = molar activity, MBQ = megabecquerel.

Study design, anaesthesia and treatment

Three subjects underwent PET and magnetic resonance imaging (MRI) scans on a Philips Ingenuity Time-of-Flight PET/MRI scanner at the department of Radiology & Nuclear Medicine of the VU University Medical Center (Amsterdam, the Netherlands). Each subject was scanned twice on the same day, at baseline and 10 min post radiprodil IV administration. Subject 1 completed a second baseline and radiprodil PET scan 77 days after the first imaging session to investigate retest variability of PET and arterial blood measurements.

Monkeys were transported from the BPRC to the VUMC in the morning, underwent PET scanning at approximately 11:00 and 14:00, and were returned to the research colony of the BPRC at the end of the afternoon. The animals were trained to voluntarily enter their transit cages, and no anaesthesia was used during the 40 min transportation period. The animals were familiar with the procedures and

personnel involved. At the PET-MRI facility, monkeys were sedated with an injection of the α_2 -adrenoceptor agonist medetomidine hydrochloride (60 $\mu\text{g}/\text{kg}$; Sedastart 1 mg/ml, AST Farma BV, Oudewater, the Netherlands) and midazolam (0.3 mg/kg; Midazolam Actavis 5 mg/ml; Actavis BV, Baarn, the Netherlands), which were administered intramuscularly. Two cephalic lines were placed, first for the induction and maintenance of propofol anaesthesia, which was delivered at a rate of 0.2 mg/kg/min (PropoVet Multidose 10 mg/ml, Fresenius Kabi AB, Uppsala, Sweden). The second line was placed for to infuse NaCl/glucose for maintenance of fluid balance at a rate of 1 ml/kg/h (0.45% sodium chloride & 2.5% glucose 500ml, Baxter BV, Utrecht, the Netherlands). Two arterial lines were placed in the femoral artery for continuous and discrete blood sampling. Xylocaine 10% was used for endotracheal intubation to provide additional oxygen. The animals were allowed to breath freely during the anaesthesia. The monkeys were subsequently positioned in the scanner in the supine position, placed on a fluid heating system in order to maintain normothermia set at 38.5 ° (Small Animal Instruments Inc. [SAII], Stony Brook, NY, USA). SAII MR-compatible equipment was used to monitor haemoglobin oxygen saturation levels (SpO₂), heart rate, and body temperature. Monitoring data were transmitted out the magnet bore by optical fiber cables to a control/gating module which resided in the MR control room.

Radioprodil (ucb, Belgium) was used to block the GluN2B binding site of NMDA receptors. The drug was administered via the right cephalic vein 10 min prior to [¹¹C]HACH242 injection at a dose of 10 mg/kg (free-baseweight) in a concentration of 5 mg/ml. The solution contained 2.5% DMSO (dimethyl sulfoxide), 7.5% Tween 80 (polysorbate) and sodium dihydrogen phosphate (NaH₂PO₄).

Radiopharmaceutical Preparation and Injectate

Radiosynthesis of N-((5-(4-fluoro-2- [¹¹C] methoxyphenyl) pyridin-3-yl) methyl)cyclopentan-amine ([¹¹C]HACH242) was performed according to methods published previously¹². Synthesis time including HPLC purification was approximately 90 min and radiochemical purity of the final product > 98%. The radiotracer was formulated in a phosphate-buffered saline solution containing 8.6% ethanol, and administered by intravenous injection of ≤ 10 ml over a 10 second period.

Blood sampling and metabolite analysis

Blood was withdrawn from the femoral arteries using an iRadimed MRidium 3850 infusion pump with a controlled withdrawal rate of 2.5 ml·min⁻¹ for a period of 6 min following [¹¹C]HACH242 injection. Whole-blood radioactivity was measured

with an on-line blood sampler detection system (Swisstrace twilight, Switzerland). In addition, discrete 3 ml blood samples were collected at set timepoints (5, 10, 20, 40, 60, 85 min post injection) to measure plasma and whole-blood ratios, calibrate and extrapolate the whole-blood data, and determine metabolite fractions. Blood was collected into heparin tubes (Greiner Bio-One GmbH, Kremsmünster, Austria) and mixed by inversion. Plasma was separated from blood cells by centrifugation at 4000 rpm for 5 min at 4°C using a Hettich Universal 16 table centrifuge (Hettich Benelux BV, Geldermalsen, the Netherlands). Activity concentrations of whole blood and plasma were measured in a gammacounter (Wizard 2480, Perkin Elmer). For metabolite analysis, 1 ml of plasma was diluted with 2 ml of water and passed over an activated tC18 Sep-Pak cartridge (Waters, the Netherlands). The Sep-Pak cartridge was washed with 5 ml of water. Recovered fractions were defined as the polar and nonpolar radiolabelled metabolites. Thereafter, the tC18 Sep-Pak cartridge was eluted with 1.5 ml of methanol followed by 1.5 ml of water, and the fraction was further analysed by HPLC. The stationary phase consisted of a Phenomenex Gemini C18 5 μm 250*10 mm column (Phenomenex, Utrecht, the Netherlands). The mobile phase was A = acetonitrile B = H₂O / 0,1 % ammonium acetate in a gradient system from 70% B to 10% B in 9 min at a flow of 3 ml·min⁻¹. Fractions were collected and measured using a multiwell gammacounter (Wizard 2470, Perkin Elmer) and HPLC chromatograms were constructed.

Image Acquisition

The attenuation of the PET signal by tissues was derived from the MR data by performing a dedicated attenuation MR sequence. The scanner reconstruction software also accounts for the attenuation by the MR radiofrequency head coil using built-in template μ -map images. Ninety min dynamic PET data was acquired and binned into 38 time frames (1x10, 8x5, 4x10, 3x20, 5x30, 5x60, 4x150, 4x300, 2x600, 2x900 sec). Reconstruction was performed using line-of-response row-action maximum likelihood algorithm (LOR-RAMLA). All data were normalised and corrected for scatter, random coincidences, attenuation, decay and dead time. Images were reconstructed into a matrix of 128x128x90 voxels, with an isotropic voxel size of 2 mm. Subject motion was checked by visual inspection of the alignment of intrasubject PET frames and no frames needed to be adjusted or excluded. T1-weighted MRI scans were co-registered to an average of the PET frames from ~0-2 min post injection using VINC1 software. Individual whole-brain masks were manually drawn on each subject's T1 MRI scan and on each averaged PET image (25-150s frames) to ensure coregistration based on brain voxels only. Volumes of interest

(vois) were automatically delineated onto coregistered MRI scans using the INIA19 template for the rhesus monkey brain ^{16,17}. The following regions were defined and combined for the left and right hemispheres: frontal cortex, occipital cortex, temporal cortex, striatum (caudate and putamen), cerebellum, as well as all gray matter voxels in whole brain (global). vois were projected onto the dynamic PET images to extract the corresponding time-activity curves, using in-house software written in MATLAB® (R2007b, The MathWorks, Natick, MA, USA).

Statistical Analysis

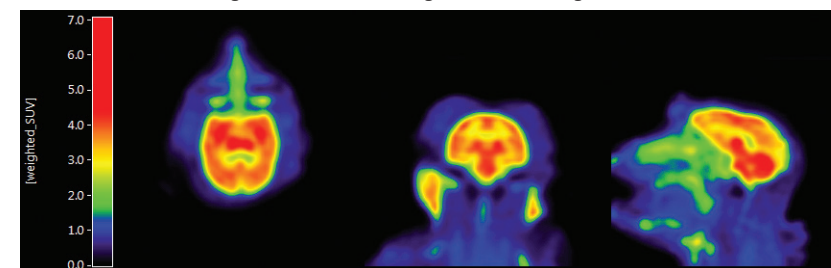
Radioactivity concentration was expressed as counts per second per mm³ of brain tissue (Bq/mm³). Standardised uptake values (suv, equaling measured activity divided by injected dose per body weight) were calculated from measured radioactivity in each voi. Area under the time-activity curves (AUC_{0-82.5}; frame midpoint times) was calculated as a simplified measurement of accumulated brain uptake of [¹¹C]HACH242-derived radioactivity. The between-subjects coefficient of variation (cv) was calculated as the ratio of standard deviation to mean suv values. The AUC of arterial parent [¹¹C]HACH242 fraction in plasma was estimated by means of the trapezoidal algorithm for each scan. Plasma suv at each time point was calculated as well as the AUC. Finally, the plasma parent fraction was multiplied by the corresponding plasma suv at each time point. Reliable input functions for kinetic modelling could not be generated because of variability in the whole blood radioactivity measurement during the first minutes post tracer injection. The brain to plasma partition coefficient, that is, the ratio of [¹¹C]HACH242 concentration in brain to that in plasma (K_p), was obtained by calculating the ratio between brain suv_{AUC} to the individual parent plasma_{AUC}. Results are presented as mean ± standard deviation (SD).

Results

[¹¹C]HACH242 readily entered the brain and displayed a fairly uniform pattern of uptake (Figure 2). Individual subject suvs at baseline and after radioprodil administration are shown in Figure 3 and summarised in Table 2. The peak uptake in whole brain gray matter during radioprodil scans was increased by 20% in subject 1 but reduced by 9%, 1%, and 20% for subjects 2, 3 and the retest of subject 1, respectively, compared to baseline. suv of in the last 15 min PET frame was 17 to 25% higher in the radioprodil condition for subject 1, but approximately equal (1 to 3%) in subjects

2 and 3. Covariance of suv_{AUC} between subjects for the 4 baseline scans was 12%. The suv of [¹¹C]HACH242 in whole brain, frontal cortex and cerebellum gray matter when normalised for individual peak uptake are shown in Figure 3b. Slower wash-out in the radioprodil condition resulted in slight suv increases in the last PET frame compared with peak uptake of 4 to 11% for subjects 1, 2 and 3 and 45% for the retest of subject 1.

FIGURE 2 Transaxial, coronal and sagittal views of time-weighted SUV PET images from 0-90 min.



Plasma analysis

Radioactivity measurements in blood and plasma, as well as tracer metabolism are shown in Figure 4. Blood could not be sampled from the artery during the radioprodil scan of subject 3, therefore results of four baseline scans and three radioprodil scans are reported. Mean parent fraction in all 7 scans was 52 ± 16% at 5 min, 35 ± 13% at 10 min, 26% ± 10 at 20 min, 15 ± 4% at 40 min, 13 ± 6% at 60 min, and 8 ± 5% at 85 min post injection. HPLC analysis demonstrated that the polar fraction and 1 major metabolite accounted for the remaining radioactivity (Figure 4b). Polar metabolites constituted 52 ± 10% at 10 min and 76 ± 8% at 85 min post injection. The mean nonpolar metabolite fraction was approximately 9% from 10 min p.i. until the end of the scan (not displayed). Mean AUC of [¹¹C]HACH242 parent fraction for baseline scans was 1316 (range 733-2025) and for radiopril scans 1689 (range 1170-2026). Total Plasma suv_{AUC} was reduced by 11%, 45% and 56% in the radioprodil scans compared to baseline.

suv_{AUC} of [¹¹C]HACH242 in the brain divided by the Plasma_{AUC} was 39%, 72% and 110% higher in the radioprodil condition for subjects 1, 2 and subject 1 retest, respectively. This change was partly driven by lower Plasma_{AUC} in the radioprodil scans (-11%, -45% and -56% respectively). Radioprodil administration did not affect the

TABLE 1 PET standardised uptake values (SUV) and areas under the curve (AUC) of brain and plasma parent fraction per subject and treatment.

		S1	S2	S3	S1 re-test	mean	SD	S1 TRT change
SUV _{peak}	Baseline	3.77	3.86	3.60	3.76	3.75	0.11	0%
	Radiprodil	4.51	3.51	3.55	3.03	3.65	0.62	-33%
	Change	20%	-9%	-1%	-20%	-3%	17%	
SUV _{75-90 min}	Baseline	1.91	2.67	3.08	1.43	2.27	0.74	-25%
	Radiprodil	2.39	2.70	3.16	1.68	2.48	0.62	-30%
	Change	25%	1%	3%	17%	11%	12%	
SUV _{75-90 min} / SUV _{peak}	Baseline	0.51	0.69	0.86	0.38	0.61	0.21	-25%
	Radiprodil	0.53	0.77	0.89	0.55	0.69	0.17	5%
	Change	4%	11%	4%	45%	16%	20%	
PLASMA _{auc} / PF	Baseline	44.3	56.2	30.9	79.9	52.8	20.8	80%
	Radiprodil	39.5	30.9		35.5	35.3	4.29	-10%
	Change	-11%	-45%		-56%	-37%	23%	
SUV _{auc} / PLASMA _{auc}	Baseline	5.32	4.83	8.79	2.62	5.39	2.55	-51%
	Radiprodil	7.37	8.28		5.52	7.06	1.41	-25%
	Change	39%	72%		110%	74%	36%	

TRT=test-retest, PF=parent fraction

FIGURE 3 A. Individual subject SUVs for whole-brain grey matter (global), frontal cortex and cerebellum and B. Normalised for peak uptake.

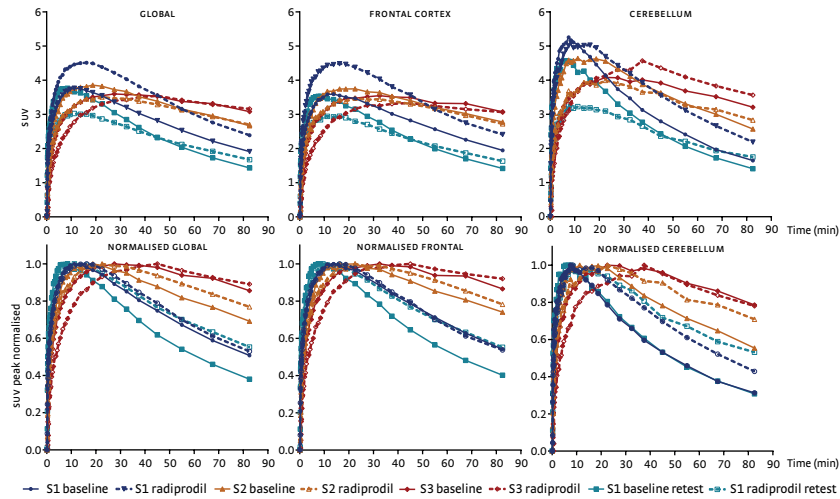
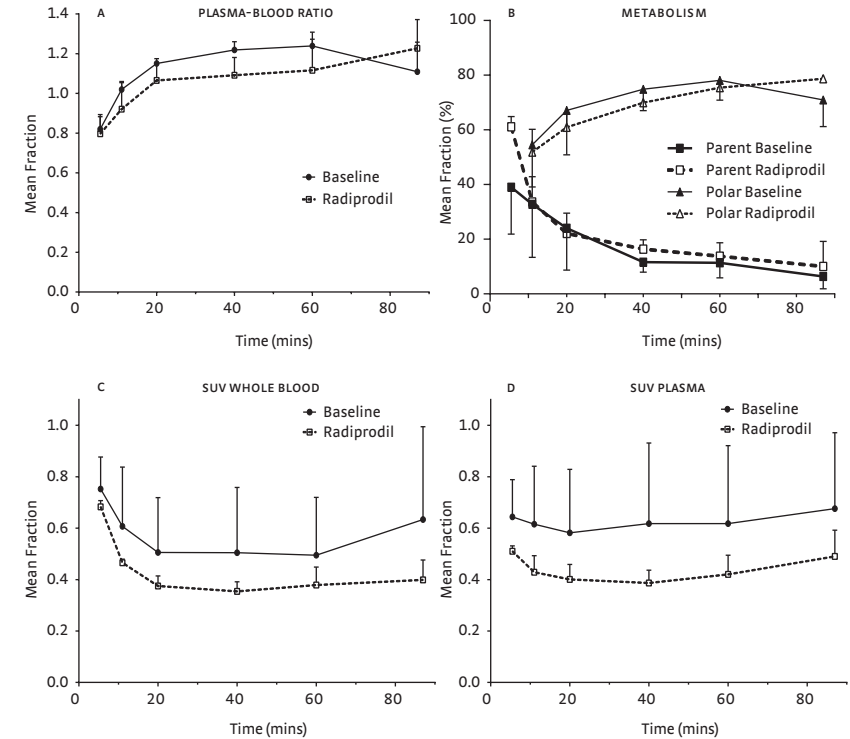


FIGURE 4 A. Plasma-to-blood ratio, B. the mean percentage of plasma radioactivity attributable to parent [¹¹C]HACH242 and polar metabolites, C. the standardised uptake value (SUV) of whole blood radioactivity and D. SUV of plasma radioactivity multiplied by the parent fraction. Results at each time-point are presented as the mean ± SD fractions from baseline (N=4) and radiprodil (N=3) scans.



change in [¹¹C]HACH242 brain-to-plasma ratio differently in the brain VOIs when compared to baseline brain-to-plasma ratios.

Figure 5 shows that the average [¹¹C]HACH242 uptake in the frontal cortex at baseline condition was initially 68% of cerebellum uptake (range 52-83%), and increased to 106% (range 96-118%) at the end of the scan. After radiprodil administration, the average SUV in the frontal cortex is more in line with the cerebellum SUV, starting at 80% (range 68-93%) and reaching 96% (range 86-110%) of the cerebellum uptake at the end of the scan.

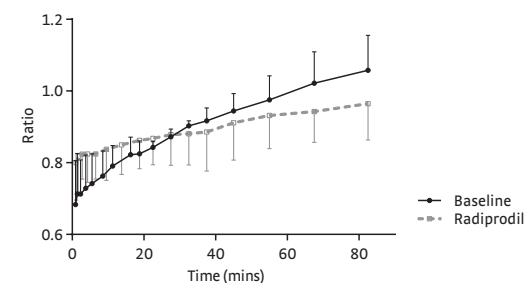
Discussion

This study describes the first *in vivo* evaluation of the radiotracer [^{11}C]HACH242 in the primate brain. [^{11}C]HACH242 TACS in the brain showed appropriate reversible pharmacokinetics within the timeframe of the PET scan. Systemic plasma clearance of the parent compound remained constant throughout the scan and was lower than clearance from brain VOIs. No consistent reduction was observed in [^{11}C]HACH242 SUVs after intravenous infusion of radiprodil, a GluN2B negative allosteric modulator. Radiprodil distribution studies in rodents showed that it has unrestricted access to the brain tissue with brain-to-plasma ratios of ~ 1 and a terminal half-life of 3.2h in dogs (UCB Pharma, unpublished communication). Radiprodil was therefore expected to decrease the SUV ratio at late time frames in VOIs with high versus low GluN2B binding sites. This could be suggestive of lower specific binding of [^{11}C]HACH242, under the assumption that the radiotracer kinetics in plasma are equal in both conditions. The main limitation of this study is that reliable input functions for kinetic modelling could not be generated because of variability in the whole blood radioactivity measurement during the first minutes post tracer injection. However, interpretation of the [^{11}C]HACH242 kinetics in different brain VOIs in relation to plasma metabolism and clearance allows for deductions to be made of the underlying physiological processes.

In previous studies in mice, [^{11}C]HACH242 showed high specific binding and heterogeneous distribution in brain slices that was similar to the expression of NMDA receptors. For example, a 3-fold increase in activity uptake was measured in fore-brain regions vs. cerebellum at 15 min⁶⁴. Results in the present study show that average [^{11}C]HACH242 peak uptake in the frontal cortex at baseline condition is 30% lower than cerebellum uptake and 10% higher at the end of the scan. This suggests a lower perfusion of the tracer into the frontal cortex and a somewhat slower wash-out. After radiprodil administration, the uptake in the cerebellum is more in line with the frontal cortex (Figure 5). The lower ratio from 30 min to the end of the scan could suggest that binding of [^{11}C]HACH242 to GluN2B in the frontal cortex is reduced relative to cerebellum binding. However, the ratio change can be explained largely by the change in the cerebellar TACS after radiprodil administration.

In another effort to compare the effect of radiprodil on [^{11}C]HACH242 binding, SUVs were normalised to the individual peak uptake (Figure 3B). GluN2B saturation was expected to accelerate the washoff and reveal the degree of specific binding. However, slower washout in the radiprodil condition was observed, resulting in SUV

FIGURE 5 Mean SUV ratio of the frontal cortex over cerebellum of all 4 baseline and Radiprodil scans. Error bars represent standard deviations.



increases in the last PET frame of 4 to 11% for subjects 1 to 3 and 45% for the retest of subject 1. The baseline TACS of the cerebellum were similar for subject 1 test and retest scans after normalization to peak uptake, indicating good TAC test-retest reproducibility in a VOI with relatively low density of the target. In situ hybridization studies of GluN2B have shown that mRNA expression patterns of the GluN2B subunit were similar between humans, monkeys, and mice in most brain regions¹⁸. The NR2B subunit is found predominantly in hippocampus, cerebral cortex, striatum and olfactory bulbs, as shown by immuno-cytochemical localisation studies¹⁹. The present baseline PET data indicate slower wash-out in cortex than in cerebellum, as could be expected based on the target density. Although *in vitro* autoradiography of [^{11}C]HACH242 in the brain of rhesus monkey has not been performed yet, the widespread distribution of GluN2B suggests that a reference region in the brain devoid of GluN2B binding sites is not available, which prevented the exploration of reference tissue compartmental models to fit to the PET data. An additional complexity in the interpretation of the current results is the affinity of [^{11}C]HACH242 to sigma-1 receptors (20 nM) in the brain. A postmortem human brain study found moderate levels of sigma-1 receptor mRNA distributed in the cortex, with the temporal cortex being particularly enriched²⁰. Although experiments to confirm the affinity of [^{11}C]HACH242 to sigma-1 in primates are warranted, it is reasonable to assume that the measured [^{11}C]HACH242 PET signal constitutes binding to both GluN2B and sigma-1, which could confound interpretation of (clinical) data. The degree of specific binding to GluN2B in mice was shown to vary between 3 and 40%¹². Dense labelling was observed in brain regions that do not express high levels of GluN2B subunit-containing NMDA receptors, suggesting binding to sigma-1 or other proteins. Future

research could employ a sigma-1 receptor compound such as the agonist fluvoxamine in combination with a GluN2B negative allosteric modulator to assess the binding potential of [¹¹C]HACH242. Importantly, however, a recent PET study in rats showed that the sigma-1 receptor agonist (1)-pentazocine abolished [¹¹C]Me-NB1 specific binding in the brain, despite the lack of direct competition *in vitro* and a 33-fold selectivity of [¹¹C]Me-NB1 for the human GluN2B receptor over sigma-1²¹. It was hypothesised that an interaction between sigma-1 agonism and GluN2B in the living brain could hamper binding of [¹¹C]Me-NB1, which is structurally comparable with [¹¹C]HACH242. It would be valuable to further investigate [¹¹C]HACH242 kinetics following administration of a sigma-1 agonist to confirm the findings of an *in vivo* PET signal block.

The change in [¹¹C]HACH242 brain uptake and washout following radioprodil administration may be a consequence of the drug's effect on the delivery of parent [¹¹C]HACH242 from blood to tissue. Results showed that SUV in blood and plasma, as well as the plasma-to-blood ratio were reduced in the radioprodil condition compared to baseline. A lower AUC of plasma parent fraction was also observed in the 3 radioprodil scans for which data was available (-11%, -45% and -56% compared to baseline). Binding in peripheral binding sites or to plasma proteins might have been altered by radioprodil, resulting in a different pattern of uptake in the brain, however a closer look at the individual TACS does not show a clear relationship between SUV_{AUC} in plasma and brain. Fast peripheral metabolism of [¹¹C]HACH242 and rapid clearance of the parent tracer from plasma hindered prolonged measurements of [¹¹C]HACH242 from arterial plasma. Errors in the estimation of arterial blood parameters are probable. For example the whole-blood activity at 85 min in the radioprodil retest scan of subject 1 was 40% higher than the previous samples resulting in aberrant group averages (Figure 4). Polar metabolites made up 50% of measured radioactivity in plasma at 10 min p.i., compared with 75% in previous *in vivo* [¹¹C]HACH242 experiments in mice⁶⁴. In general, it is assumed that polar metabolites do not cross the blood-brain barrier, but even if they do they will only increase the non-specific signal. The non-polar metabolite fraction remained less than 10% throughout the time of the scan. Therefore, even if these lipophilic metabolites cross the blood-brain barrier, they would constitute only a minor fraction of total cerebral uptake. Nevertheless, future studies are needed to assess the behaviour of the labelled metabolites in the brain.

It is possible that changes in cerebral blood flow (CBF) contributed to the difference between baseline and radioprodil [¹¹C]HACH242 SUV. There are currently

no scientific reports available that have investigated with PET or MRI the effect of 'prodils' or other GluN2B negative allosteric modulators on CBF in the healthy brain. One study on the protective effects of ifenprodil on ischemia used laser doppler flowmetry and showed that there was no significant change in cerebral blood flow²². In the present study, the anaesthetics medetomidine and midazolam were administered intramuscularly approximately 2 hours before the baseline PET scan, equating to ~6 hours before the radioprodil scan. Considering medetomidine's time to peak concentration and half-life of ~30 min following i.m. administration²³, the plasma and brain concentrations may still have been high enough to exert pharmacodynamic effects in the baseline scan. Reports of the effect of anaesthesia on CBF are important in this regard. A SPECT study in dogs showed that medetomidine increased the regional CBF in all brain regions bar the subcortical (thalamic) area²⁴. Consistent with increased CBF, [¹¹C]HACH242 TACS showed higher uptake and faster wash-out in the baseline scan. However, midazolam, which was co-administered with medetomidine, has been shown to reduce global CBF dose-dependently in humans²⁵. Propofol was injected intravenously at a constant rate during the entire scan day for maintenance of anaesthesia and therefore should not have affected CBF differently between the two [¹¹C]HACH242 PET scans on the same day. Polypharmacological effects, which potentially modulate multiple targets in the brain, complicate predictions of regional CBF effects. Ketamine is commonly used as a sole anaesthetic agent in NHP studies. However, this compound acts on the NMDA receptor²⁶ and therefore it was not suitable for implementation in the current study. Opioidergic compounds such as fentanyl can affect NMDA receptor function¹⁷, and hence propofol was deemed the most appropriate anaesthetic in the present study design. Future attempts at visualising the GluN2B binding site of the NMDA receptor are preferably performed in awake primates or humans to exclude potential CBF effects of anaesthetics. Simultaneous [¹¹C]HACH242 PET and fMRI could elucidate the relationship between NMDA receptor blockers, blood flow and radiotracer binding²⁷.

Preclinical experiments with [¹¹C]HACH242 have shown that anaesthesia in mice, administered as a mixture of fentanyl, fluanisone and midazolam, resulted in inconsistent effects on brain uptake of [¹¹C]HACH242 following pre-treatment with Ro25-6981⁶. Specifically, Ro25-6981 induced either a mean 22% decrease or a mean 29% increase in radioactivity uptake across all brain regions analysed in *ex vivo* brains 20 min after radiotracer injection. It is striking that in the present study there was considerable test-retest variability of subject 1 SUV in brain and plasma. PET

experiments performed in NHP under awake conditions with the carbon-11 labelled analogue of the GluN2B-selective ligand CP-101,606 showed no appreciable specific binding²⁸. Endogenous ligands of the NMDA receptor such as spermine and spermidine, as well as divalent cations, strongly inhibited radiolabelled CP-101,606 binding in the order of $Zn^{2+} > Mg^{2+} > Ca^{2+}$ at their physiological concentrations. L-glutamate and NMDA tended to slightly increase the binding, while glycine and D-serine showed no effect²⁸. Discrepancies between *in vitro* and *in vivo* binding properties of radiotracers developed for the GluN2B binding site have been reported for other NMDA receptor radiotracers^{21,29}. Ifenprodil and spermine inhibited the *in vitro* binding of ¹¹C-labelled bis(phenylalkyl)amines with potencies similar to those of non-radioactive ligand. *In vivo* however, pre-treatment with non-radioactive tracer caused an increase of binding in the cerebral cortex and hippocampus compared with the control group²⁹. Estimating the [¹¹C]HACH242 binding potential *in vivo* is complicated by the atypical mode of action of GluN2B containing NMDA receptors. For example, binding is context-dependent³⁰, such that strongly activated receptors are preferentially inhibited. In addition, GluN2B-selective antagonists can divide into two distinct classes according to binding pose, resulting in strikingly different ligand orientation and receptor interactions³¹. Taken together, there are various receptor interactions and biophysical factors that affect *in vivo* binding properties of NMDA receptor radioligands, which remain to be tested, for example using bolus-plus-infusion PET experiments in awake primates while monitoring hemodynamic changes²⁷.

Conclusions

The present results show that [¹¹C]HACH242 has a suitable kinetic profile in the brain and low accumulation of lipophilic radiometabolites. Under the tested conditions however, the specific binding of [¹¹C]HACH242 *in vivo* using PET could not be visualised. The divergent preclinical behavior in mice and primates could be a consequence of variations in cerebral blood flow, a low fraction of specifically bound tracer, or interactions of the radiotracer with the sigma-1 receptor or endogenous ligands at the binding site. The typical study design for neuroreceptor PET tracers executed here may not be applicable to such a dynamic and complex receptor system as the GluN2B site of the NMDA receptor. Further experiments of ligand interactions are necessary in order to facilitate the development of radiotracers for *in vivo* imaging of the ionotropic NMDA receptor.

REFERENCES

- Paoletti P, Bellone C, Zhou Q: NMDA receptor subunit diversity: impact on receptor properties, synaptic plasticity and disease: *Nature reviews Neuroscience*. 2013 Jun;14(6):383-400. Available from: <https://doi.org/10.1038/nrn3504>
- Mony L, Krzaczkowski L, Leonetti M, Le Goff A, Alarcon K, Neyton J, Bertrand H-O, Acher F, Paoletti P: Structural Basis of NR2B-Selective Antagonist Recognition by N-Methyl-D-aspartate Receptors: *Molecular Pharmacology*. 2009 Jan 1;75(1):60-74. Available from: <https://doi.org/10.1124/mol.108.050971>
- Loftis JM, Janowsky A: The N-methyl-d-aspartate receptor subunit NR2B: localization, functional properties, regulation, and clinical implications: *Pharmacology & Therapeutics*. 2003;97(1):55-85. Available from: [https://doi.org/10.1016/S0163-7258\(02\)00302-9](https://doi.org/10.1016/S0163-7258(02)00302-9)
- Laurie DJ, Bartke I, Schoepfer R, Naujoks K, Seeburg PH: Regional, developmental and interspecies expression of the four NMDAR2 subunits, examined using monoclonal antibodies: *Brain research Molecular brain research*. 1997 Nov;51(1-2):23-32.
- Sobrio F, Gilbert G, Perrio C, Barré L, Debruyne D: PET and SPECT imaging of the NMDA receptor system: an overview of radiotracer development: *Mini reviews in medicinal chemistry*. 2010 Aug;10(9):870-86.
- Klein PJ, Christiaans JAM, Metaxas A, Schuit RC, Lammertsma AA, van Berckel BNM, Windhorst AD: Synthesis, structure activity relationship, radiolabeling and preclinical evaluation of high affinity ligands for the ion channel of the N-methyl-d-aspartate receptor as potential imaging probes for positron emission tomography: *Bioorganic & Medicinal Chemistry*. 2015;23(5):1189-206. Available from: <https://doi.org/10.1016/j.bmc.2014.12.029>
- Fuchigami T, Nakayama M, Yoshida S: Development of PET and SPECT probes for glutamate receptors: *Scientific World Journal*. 2015. p. 1-19. Available from: <https://doi.org/10.1155/2015/716514>
- Labas R, Gilbert G, Nicole O, Dhilly M, Abbas A, Tirel O, Buisson A, Henry J, Barré L, Debruyne D, Sobrio F: Synthesis, evaluation and metabolic studies of radiotracers containing a 4-(4-[¹⁸F]-fluorobenzyl)piperidin-1-yl moiety for the PET imaging of NR2B NMDA receptors: *European Journal of Medicinal Chemistry*. 2011 Jun;46(6):2295-309. Available from: <https://doi.org/10.1016/j.ejmech.2011.03.013>
- Van der Aart J, Golla SSV, Pluijm M Van Der, Schwarte LA, Schuit RC, Klein PJ, Metaxas A, Windhorst AD, Boellaard R, Lammertsma AA, van Berckel BNM: First in human evaluation of [¹⁸F]PK-209, a PET ligand for the ion channel binding site of NMDA receptors: *EJNMMI research*. 2018;8(69). Available from: <https://doi.org/10.1186/s13550-018-0424-2>
- Roger G, Dollé F, De Bruin B, Liu X, Besret L, Bramoullé Y, Coulon C, Ottaviani M, Bottlaender M, Valette H, Kassiou M: Radiosynthesis and pharmacological evaluation of [¹¹C]EMD-95885: A high affinity ligand for NR2B-containing NMDA receptors: *Bioorganic and Medicinal Chemistry*. 2004;12(12):3229-37. Available from: <https://doi.org/10.1016/j.bmc.2004.03.065>
- Brown DG, Maier DL, Sylvester MA, Hoerter TN, Menhaji-Klotz E, Lasota CC, Hirata LT, Wilkins DE, Scott CV, Trivedi S, Chen T, McCarthy DJ, Maciag CM, Sutton EJ, Cumberledge J, Mathisen D, Roberts J, Gupta A, Liu F, Elmore CS, Alhambra C, Krumriner JR, Wang X, Ciaccio PJ, Wood MW, Campbell JB, Johansson MJ, Xia J, Wen X, Jiang J, Wang X, Peng Z, Hu T, Wang J: 2,6-Disubstituted pyrazines and related analogs as NR2B site antagonists of the NMDA receptor with anti-depressant activity: *Bioorganic & Medicinal Chemistry Letters*. 2011 (21). Available from: <https://doi.org/10.1016/j.bmcl.2011.03.117>
- Christiaans JAM, Klein PJ, Metaxas A, Kooijman EJM, Schuit RC, Leysen JE, Lammertsma AA, Van Berckel BNM, Windhorst AD: Synthesis and preclinical evaluation of carbon-11 labelled N-(5-(4-fluoro-2-[¹¹C]methoxyphenyl)pyridin-3-yl)methyl)cyclopentanamine as a PET tracer for NR2B subunit-containing NMDA receptors: *Nuclear Medicine and Biology*. 2014;41(8):670-80. Available from: <https://doi.org/10.1016/j.nucmedbio.2014.04.131>
- Toyohara J, Sakata M, Ishiwata K: Re-evaluation of *in vivo* selectivity of [¹¹C]SA4503 to $\sigma(1)$ receptors in the brain: contributions of emopamil binding protein: *Nuclear medicine and biology*. 2012 Oct;39(7):1049-52. Available from: <https://doi.org/10.1016/j.nucmedbio.2012.03.002>
- Bradford AM: Molecular pharmacology of a Novel NR2B-selective NMDA Receptor Antagonist: Durham University; 2006.
- Weatherall D, Goodfellow P, Harris J, Hinde R, Johnson L, Morris R, Ross N, Skehel J, Tickell C: The use of non-human primates in research: *Medical Research Council*. 2006;(Dec):1-153. Available from: [https://doi.org/10.1016/0047-2484\(75\)90100-1](https://doi.org/10.1016/0047-2484(75)90100-1)
- Rohlfing T, Kroenke CD, Sullivan E V, Dubach MF, Bowden DM, Grant KA, Pfefferbaum A: The INIA19 Template and NeuroMaps Atlas for Primate Brain Image Parcellation and Spatial Normalization: *Frontiers in Neuroinformatics*. 2012;6:27. Available from: <https://doi.org/10.3389/fninf.2012.00027>
- Golla SSV, Klein PJ, Bakker J, Schuit RC, Christiaans JAM, van Geest L, Kooijman EJM, Oropeza-Seguias GM, Langermans JM, Leysen JE, Boellaard R, Windhorst AD, Van Berckel BNM, Metaxas A: Preclinical evaluation of [¹⁸F]PK-209, a new PET ligand for imaging the ion-channel site of NMDA receptors: *Nuclear Medicine and Biology*. 2015;42(2):205-12. Available from: <https://doi.org/10.1016/j.nucmedbio.2014.09.006>
- Bai L, Hof PR, Standaert DG, Xing Y, Nelson SE, Young AB, Magnusson KR: Changes in the expression of the NR2B subunit during aging in macaque monkeys: *Neurobiology of Aging*. 2004 Feb;25(2):201-8. Available from: [https://doi.org/10.1016/S0197-4580\(03\)00091-5](https://doi.org/10.1016/S0197-4580(03)00091-5)
- Charton JP, Herkert M, Becker CM, Schröder H: Cellular and subcellular localization of the 2B-subunit of the NMDA receptor in the adult rat telencephalon: *Brain Research*. 1999 Jan 23;816(2):609-17. Available from: [https://doi.org/10.1016/S0006-8993\(98\)01243-8](https://doi.org/10.1016/S0006-8993(98)01243-8)
- Kitaichi K, Chabot JG, Moebius FF, Flandorfer A, Glossmann H, Quirion R: Expression of the purported sigma(1) receptor in the mammalian brain and its possible relevance in deficits induced by antagonism of the NMDA receptor complex as revealed using an antisense strategy: *Journal of chemical neuroanatomy*. 2000 Dec;20(3-4):375-87.

- 21 Krämer SD, Betzel T, Mu L, Haider A, Herde Müller A, Boninsegni AK, Keller C, Szermerski M, Schibli R, Wünsch B, Ametamey SM: Evaluation of [¹¹C]Me-NB1 as a potential PET radioligand for measuring GluN2B-containing NMDA receptors, drug occupancy and receptor crosstalk: *Journal of Nuclear Medicine*. 2017;59(4). Available from: <https://doi.org/10.2967/jnumed.117.200451>
- 22 Başkaya MK, Rao AM, Donaldson D, Prasad MR, Dempsey RJ: Protective effects of ifenprodil on ischemic injury size, blood-brain barrier breakdown, and edema formation in focal cerebral ischemia: *Neurosurgery*. 1997 Feb;40(2):364-70.
- 23 Kastner SBR, Wapf P, Feige K, Demuth D, Bettschart-Wolfensberger R, Akens MK, Huhtinen M: Pharmacokinetics and sedative effects of intramuscular medetomidine in domestic sheep: *Journal of Veterinary Pharmacology and Therapeutics*. 2003 Aug 1;26(4):271-6. Available from: <https://doi.org/10.1046/j.1365-2885.2003.00492.x>
- 24 Waelbers T, Peremans K, Vermeire S, Duchateau L, Dobbeleir A, Audenaert K, Polis I: The effect of medetomidine on the regional cerebral blood flow in dogs measured using Technetium-99m-Ethyl Cysteinate Dimer SPECT: *Research in Veterinary Science*. 2011;91(1):138-43. Available from: <https://doi.org/10.1016/j.rvsc.2010.08.003>
- 25 Veselis RA, Reinsel RA, Beattie BJ, Mawlawi OR, Feshchenko VA, DiResta GR, Larson SM, Blasberg RG: Midazolam changes cerebral blood flow in discrete brain regions: an H2(15)O positron emission tomography study: *Anesthesiology*. 1997 Nov;87(5):1106-17.
- 26 Van der Doef TF, Golla SS, Klein PJ, Oropeza-Seguias GM, Schuit RC, Metaxas A, Jobse E, Schwarte LA, Windhorst AD, Lammertsma AA, van Berckel BNM, Boellaard R: Quantification of the novel N-methyl-D-aspartate receptor ligand [¹¹C]GMOM in man: *Journal of Cerebral Blood Flow & Metabolism*. 2016;36:1111-21. Available from: <https://doi.org/10.1177/0271678X15608391>
- 27 Schoenberger M, Schroeder FA, Placzek MS, Carter RL, Rosen BR, Hooker JM, Sander CY: In Vivo [¹⁸F]GE-179 Brain Signal Does Not Show NMDA-Specific Modulation with Drug Challenges in Rodents and Nonhuman Primates: *ACS Chemical Neuroscience*. 2018;9(2):298-305. Available from: <https://doi.org/10.1021/acscemneuro.7b00327>
- 28 Haradahira T, Maeda J, Okauchi T, Zhang M-R, Hojo J, Kida T, Arai T, Yamamoto F, Sasaki S, Maeda M, Suzuki K, Suhara T: Synthesis, in vitro and in vivo pharmacology of a C-11 labeled analog of CP-101,606, (+/-)threo-1-(4-hydroxyphenyl)-2-[4-hydroxy-4-(p-[¹¹C]methoxyphenyl)piperidino]-1-propanol, as a PET tracer for NR2B subunit-containing NMDA receptors: *Nuclear Medicine and Biology*. 2002 Jul;29(5):517-25.
- 29 Sasaki S, Kurosaki F, Haradahira T, Yamamoto F, Maeda J, Okauchi T, Suzuki K, Suhara T, Maeda M: Synthesis of ¹¹C-labelled bis(phenylalkyl)amines and their in vitro and in vivo binding properties in rodent and monkey brains: *Biological & Pharmaceutical Bulletin*. 2004 Apr;27(4):531-7.
- 30 Yuan H, Myers SJ, Wells G, Nicholson KL, Swanger SA, Lyuboslavsky P, Tahirovic YA, Menaldino DS, Ganesh T, Wilson LJ, Liotta DC, Snyder JP, Traynelis SF: Context-Dependent GluN2B-Selective Inhibitors of NMDA Receptor Function Are Neuroprotective with Minimal Side Effects: *Neuron*. 2015 Mar 18;85(6):1305-1318. Available from: <https://doi.org/10.1016/j.neuron.2015.02.008>
- 31 Stroebel D, Buhl DL, Knafels JD, Chanda PK, Green M, Sciabola S, Mony L, Paoletti P, Pandit J: A Novel Binding Mode Reveals Two Distinct Classes of NMDA Receptor GluN2B-selective Antagonists: *Molecular Pharmacology*. 2016 Mar 31;89(5):541-51. Available from: <https://doi.org/10.1124/mol.115.103036>

CHAPTER 5

FIRST IN HUMAN EVALUATION OF [¹⁸F]PK-209, A PET LIGAND FOR THE ION CHANNEL BINDING SITE OF NMDA RECEPTORS

PUBLISHED IN EJNMMI RESEARCH

Jasper van der Aart, Sandeep S.V. Golla, Marieke van der Pluijm, Lothar A. Schwarte, Robert C. Schuit, Pieter J. Klein, Athanasios Metaxas, Albert D. Windhorst, Ronald Boellaard, Adriaan A. Lammertsma, Bart N.M. van Berckel

Department Of Radiology And Nuclear Medicine, vu University Medical Center, Amsterdam UMC, The Netherlands

© 2018 The Authors. Open Access. This article is distributed under the terms of the Creative Commons Attribution 4.0 International License. DOI 10.1186/s13550-018-0424-2

Abstract

BACKGROUND Efforts to develop suitable positron emission tomography (PET) tracers for the ion channel site of human N-methyl-D-aspartate (NMDA) receptors have had limited success. [¹⁸F]PK-209 is a GOM derivative that binds to the intrachannel phencyclidine site with high affinity and selectivity. Primate PET studies have shown that the volume of distribution in the brain was reduced by administration of the NMDA receptor antagonist MK-801, consistent with substantial specific binding. The purpose of the present study was to evaluate [¹⁸F]PK-209 in 10 healthy humans by assessing test-retest reproducibility and binding specificity following intravenous S-ketamine administration (0.5 mg·kg⁻¹).

METHODS Five healthy subjects underwent a test-retest protocol and five others a baseline-ketamine protocol. In all cases dynamic 120 min PET scans were acquired together with metabolite corrected arterial plasma input functions. Additional input functions were tested based on within-subject and population-average parent fractions.

RESULTS Best fits of the brain time-activity curves were obtained using an irreversible two-tissue compartment model with additional blood volume parameter. Mean test-retest variability of the net rate of influx K_i varied between 7 and 24% depending on the input function. There were no consistent changes in [¹⁸F]PK-209 PET parameters following ketamine administration, which may be a consequence of the complex endogenous ligand processes that affect channel gating.

CONCLUSION The molecular interaction between [¹⁸F]PK-209 and the binding site within the NMDA receptor ion channel is insufficiently reproducible and specific to be a reliable imaging agent for its quantification.

Background

Ionotropic glutamate receptors are subdivided into four groups: kainate, α-amino-3-hydroxy-5-methyl-4-isoxazolepropionate (AMPA), δ-receptors and N-methyl-D-aspartate receptors (NMDA-R). The NMDA-R is a heteromultimeric assembly of four subunits which, in the central nervous system, is primarily comprised of GluN1 and GluN2(A-D) subunits¹. The NMDA-R is different from other types of ligand-gated ionotropic receptors in that it functions as a molecular coincidence detector. To open the ion channel, relief of the voltage dependant magnesium block is required by activation of nearby AMPA and kainate receptors, as well as co-activation of the ligand-binding domain by glutamate (via GluN2) and either D-serine or glycine (via GluN1 or GluN3)^{2,3}. The phencyclidine (PCP) binding site sits within the ion channel in the transmembrane domain of the receptor⁴. It is an attractive target for pharmacological restoration of glutamatergic homeostasis in central nervous system disorders¹. For example, non-competitive NMDA-R channel blockers such as ketamine, MK-801, and memantine may attenuate excessive neuronal depolarization and prevent amyloid-β-induced excitotoxic cell death⁵.

Considerable interest has arisen in the development of a molecular imaging tool that can assess NMDA-R function in vivo. Positron emission tomography (PET) studies of radiolabelled NMDA-R antagonists in humans have been hampered by poor radiotracer selectivity and affinity, low brain entrance, rapid radioligand metabolism, and/or inability to establish specific NMDA-R targeting^{6,7,8,9}. However, recent studies using [¹¹C]GOM in humans demonstrated that intravenous administration of ketamine 0.3 mg·kg⁻¹ reduced the radiotracer net influx rate (K_i) in whole brain grey matter by, on average, 66%¹⁰. The structure of GOM^{11,12} was used as a template for a new series of substituted N, N'-diaryl-N-methylguanidines^{13,14}. Preclinical experiments showed that the fluorine-18 labelled analogue of GOM, [¹⁸F]PK-209 ([3-(2-chloro-5-(methylthio)phenyl)-1-(3-([¹⁸F]fluoromethoxy)phenyl)-1-methylguanidine]) was the most promising candidate ligand for imaging NMDA-R, with a high apparent affinity of 18 nM against [³H]MK-801 (K_i) compared with 15 to 22 nM for [¹¹C]GOM¹³. Lipophilicity of [¹⁸F]PK-209 (LogD_{OCT,7.4} = 1.45) was acceptable for a neuroreceptor tracer¹³ and the compound exhibited high selectivity for the ion-channel of NMDA-R over other targets¹⁵. A subsequent PET study in rhesus monkeys showed prolonged retention of [¹⁸F]PK-209 in NMDA-R rich cortical regions relative to the cerebellum¹⁵. IV administration of 0.3 mg·kg⁻¹ MK-801 30 min before [¹⁸F]PK-209 PET reduced the volume of distribution (V_T) compared with

baseline in two out of three subjects. These findings supported further evaluation of [¹⁸F]PK-209 as a PET radioligand for the PCP site of the NMDA-R in human subjects. To this end, test-retest reproducibility and specific binding following intravenous administration of ketamine were assessed in this first in human study.

Methods

Subjects

This was an open-label study in ten healthy volunteers aged 22 to 37 years (Table 1). Mean age ± standard deviation (SD) in the test-retest group was 27.6 ± 7.4 and in the ketamine group 24.4 ± 2.2. All subjects were free of medical and psychiatric illnesses based on medical history, neurological examination, blood tests (complete blood count and serum chemistry), urine analysis, and tested negative for drugs in urine. This study was approved by the Medical Ethical Review Committee of the VU University Medical Center (Amsterdam UMC) and conducted in accordance with ICH GCP and the 2008 revision of the Declaration of Helsinki. All participants included in this study provided consent to participate.

Radiopharmaceutical preparation

Precursor synthesis and radiolabelling procedures for [¹⁸F]PK-209 have been described previously¹³. The radiotracer was formulated in a phosphate-buffered saline solution containing 6.7% ethanol, and administered intravenously as a 0.5 to 15 ml bolus injection, which subsequently was flushed with a saline solution. The molar activity at time of injection was calculated against a calibration curve of PK-209 using the same high-performance liquid chromatography (HPLC) system and was 10 - 123 MBq/nmol. In all cases, synthesis time, including HPLC purification, was approximately 90 min, and radiochemical purity of the final product > 98%.

Positron emission tomography data acquisition

In total, 20 PET scans were acquired on a Gemini TF-64 PET/CT scanner (Philips Medical Systems, Cleveland, OH, USA). Five subjects underwent [¹⁸F]PK-209 test and retest (TRT) scans 31-61 days apart over a period of 211 days. Another 5 subjects underwent baseline and ketamine scans 13-161 days apart over a period of 258 days. At the start of each scan [¹⁸F]PK-209 was injected as an intravenous bolus with a mean injected activity of 187 ± 7 MBq. All scans were performed between 12:00 and 15:00 h to minimize diurnal variation. Duration of daylight on each scan day was calculated to investigate

TABLE 1 Subject demographics and injectate details.

	Subject	Gender	Weight (kg)	Age	Scan interval (days)	Injected activity PET1 (MBq)	Injected activity PET2 (MBq)	AM PET1 (MBq·nmol ⁻¹)	AM PET2 (MBq·nmol ⁻¹)	Mass PET1 (µg)	Mass PET2 (µg)
TEST-RETEST GROUP	1	F	70	37	47	191	185	41	87	1.6	0.8
	2	M	86	23	35	185	176	87	123	0.8	0.5
	3	M	62	23	28	187	185	88	77	0.7	0.8
	4	F	71	34	61	180	183	45	50	1.4	1.3
	5	M	93	22	31	173	172	60	64	1.0	1.0
					Mean	183	180	64	80	1.1	0.9
					SD	7	6	22	28	0.4	0.3
				Paired t-test (P value)		0.23		0.21		0.22	
KETAMINE GROUP	6	F	64	23	161	191	194	47	17	1.4	4.1
	7	M	83	28	28	189	187	89	44	0.8	1.5
	8	F	56	23	98	187	188	80	38	0.8	1.7
	9	M	81	23	49	202	195	52	56	1.4	1.2
	10	F	70	25	13	189	195	10	40	6.4	1.7
					Mean	192	192	56	39	2.2	2.1
					SD	6	4	31	14	2.4	1.1
				Paired t-test (P value)		0.92		0.31		0.94	

AM = molar activity, SD = standard deviation.

seasonal changes in tracer binding. Dynamic PET data were acquired for 120 min and binned into 25 time frames (1x15, 3x5, 3x10, 4x60, 2x150, 2x300, 10x600 s). PET was followed by a low dose CT (30 mAs, 120 kVp) for attenuation correction and localization. Data were reconstructed using a three-dimensional row action maximum likelihood reconstruction algorithm (3-D RAMLA). Acquired PET data were normalized and corrected for dead time, randoms, scatter, attenuation and decay¹⁶.

Blood sampling

All subjects received a radial artery cannula for continuous and manual arterial sampling. For each scan an arterial input function was obtained using an on-line blood sampler (Veenstra Instruments, Joure, The Netherlands) with a withdrawal rate of 5 ml·min⁻¹ during the first 5 min and 2.5 ml·min⁻¹ from 5 to 60 min post injection

(p.i.) in order to stay within blood volume sampling constraints. Continuous blood withdrawal was interrupted briefly to manually collect arterial blood samples (10 ml each) at set timepoints (5, 10, 20, 40, 60, 75, 90, 120 min p.i.). In several subjects, an arterial sample was taken immediately before PET and incubated with [¹⁸F]PK-209 at 37°C to compare radioactivity recovery fractions throughout the 120 min with extracted fractions of the arterial samples taken during PET. The samples were used to measure blood and plasma radioactivity concentrations, whole blood-to-plasma ratios, and plasma metabolite fractions of [¹⁸F]PK-209. For the latter purpose, samples were analyzed using solid-phase extraction combined with HPLC using off-line radioactivity detection.

The final arterial plasma input function was derived using both continuous and discrete arterial blood data. The input function was corrected for plasma to whole-blood ratio, metabolites and time delay. For each scan, two additional plasma input functions were generated to investigate the effect of within-subject and between-subject variability in plasma data. For the within-subject averaged input function, the mean of PET1 and PET2 [¹⁸F]PK-209 parent fractions per subject were used at each of the 8 sample time points for both scans. For the population averaged input function, the mean parent fractions for all 5 subjects in the TRT and ketamine groups (i.e. 10 scans) were taken at each timepoint. The manual arterial blood samples were also used for assessment of the plasma ketamine concentration. The area under the ketamine concentration-time curve was estimated by means of the trapezoidal rule.

Ketamine infusion

The (S+)-isomer of ketamine (0.5 mg·kg⁻¹) was dissolved in NaCl 50ml and administered intravenously in a pseudo-steady state model with a sub-acute loading dose. First, ketamine was administered for 40 min at a rate of 0.006 mg·kg⁻¹·min⁻¹ followed by a 130 min equilibrium phase at 0.002 mg·kg⁻¹·min⁻¹. [¹⁸F]PK-209 injection and start of PET were performed at 10 min into the equilibrium phase, following 0.26 mg·kg⁻¹ administration in the preceding 50 min.

Image acquisition and analysis

Prior to the PET studies, structural 3-dimensional coronal T1-weighted magnetic resonance images (MRI) were acquired for all subjects on a 1.5 T Sonata scanner (Siemens Medical Solutions, Erlangen, Germany) with 160 coronal slices using echo time 3.97 ms, repetition time 2700 ms, flip angle 8° and voxel size 1.0x1.5x1.0 mm³. Subject motion was checked by visual inspection of the alignment of intrasubject

PET frames and no frames were excluded due to excessive movement. T1-weighted MRI scans were co-registered to an average of the PET frames from ~4-70 min p.i. using VINC software¹⁷. The co-registered MRI scans were segmented into grey matter (GM), white matter and extra-cerebral fluid, using PVE-lab¹⁸. Subsequently 68 regions of interest (ROIs), including whole brain, were derived from the Hammers atlas¹⁹ and used to extract GM time activity curves (TACs). As a last step, the TACs of 60 out of the 67 ROIs were redefined into 9 volume weighted ROIs by combining the radioactivity at each timepoint according to the equation,

$$Bq = \frac{\sum_i \alpha_i \times Bq_i}{\sum_i \alpha_i},$$

where α_i is the volume (in mm³) of region i and the counts per mm³ of region i . The selection of ROIs was based on the widespread NMDA-R availability in the brain: frontal, temporal, occipital, and parietal cortices, hippocampus, thalamus, insula, brainstem, dorsal striatum, and cerebellum, as well as whole brain GM from the Hammers atlas. Standardized uptake values (SUV, equalling measured activity divided by injected dose per body weight) were calculated for whole brain GM.

Using the metabolite corrected arterial plasma input function, all GM TACs were fitted to single-tissue (1T2k), two-tissue irreversible (2T3k) and reversible (2T4k) compartmental models, both with and without an additional parameter for fractional blood volume (V_B). The non-metabolite corrected arterial whole blood curve was used as input function for V_B . The optimal tracer kinetic model for describing in vivo kinetics of [¹⁸F]PK-209 was determined according to the Akaike Information Criterion (AIC)²⁰. Depending on the model preference, outcome measures were the net influx constant ($K_i = K_1 k_3 / (k_2 + k_3)$) or the distribution volume

$$\left(V_T = \frac{K_1}{k_2} \left(1 + \frac{k_3}{k_4} \right) \right).$$

For subsequent group level analysis (e.g. TRT variability and ketamine effects), all scans were analyzed using the same, most preferred, tracer kinetic model. Non-displaceable distribution volumes ($V_{ND} = K_1 / k_2$) as well as K_1 and k_3 values are also reported separately.

Statistics

The absolute percentage TRT variability of kinetic parameters between test and retest scans was calculated using the equation TRT variability = 2·(pretest–ptest)/(ptest+pretest)·100, where p is the kinetic parameter of interest. The between-subject coefficient of variation was calculated as the standard deviation divided by the

sample mean $\cdot 100$. Areas under the curve (AUC) from 0-120 min (SUV_{AUC}) and plasma parent fractions (0-180 secs and 0-120 mins) were calculated with Graphpad Prism 7.0 (La Jolla California USA, www.graphpad.com). SUV from 90 to 120 min (SUV_{90-120}) was calculated as the mean of the last three mid-frame SUV values.

Results

Brain Images and Plasma analysis

Uptake images from a TRT subject are shown in Figure 1. Total GM TACs for all subjects are shown in Figure 2. Peak uptake occurred around 10 min p.i. and with a SUV between 3.6-5.7. Brain activity decreased to about 25-40% of the peak by 120 min. No radioactivity uptake was observed in the jaw and skull in the dynamic PET images, indicating no defluorination. Injected activity was similar between PET1 and PET2 in the TRT (subjects 1-5) and ketamine (subjects 6-10) groups (Table 1). Molar activity and injected mass differed on average ($\pm SD$) $50 \pm 40\%$ between PET1 and PET2. The radioactivity concentration of [^{18}F]PK-209 in plasma peaked with a mean SUV of 17.4 ± 2.8 and decreased to $\sim 7\%$ of the peak at 3 min (Figure 3). The AUC (0-180 sec) for both TRT and ketamine groups did not differ between PET1 and PET2 (paired Student's t-test $p=0.11$ and $p=0.20$, respectively). [^{18}F]PK-209 was rapidly metabolized (Figure 4). Mean parent fractions for all 20 scans were 77 ± 7 , 57 ± 9 , 34 ± 5 , 19 ± 3 and $14 \pm 3\%$ at 5, 10, 20, 60 and 120 min p.i., respectively.

HPLC analysis of the radioactivity in plasma demonstrated that one major metabolite accounted for $8 \pm 5\%$ at 5 min, $27 \pm 3\%$ at 20 min and $32 \pm 3\%$ at 120 min p.i. The remainder of the activity could not be extracted, constituting $15 \pm 3\%$ at 5 min and $54 \pm 4\%$ at 120 min p.i. Recovery from the incubated pre-PET arterial sample remained $> 90\%$. There was no significant difference in metabolism (AUC) of [^{18}F]PK-209 between test and retest scans. However, parent fractions in the baseline scans of subjects 6 to 10 were 8 to 15% lower than their ketamine scans and 16% lower (range -5 to -30%) than the test-retest group. Specifically, the parent fraction was significantly lower at 10, 20 and 80 min post [^{18}F]PK-209 injection (paired Student's t-test $p<0.05$). The difference in mean blood-to-plasma ratios between test-retest and between baseline-ketamine scans was $<3\%$ for all 8 measured timepoints.

Kinetic modelling

Best model fits, according to the AIC, were obtained using an irreversible two-tissue compartment model with blood volume parameter ($2T3k_{VB}$) in 8 out of the 10

FIGURE 1 Transaxial, coronal and sagittal views of MR images (A) and averaged pet images from 4.25-70 min for the test scan (B) and retest scan (C) of subject 1. Activity is expressed in $kBq \cdot mL^{-1}$.

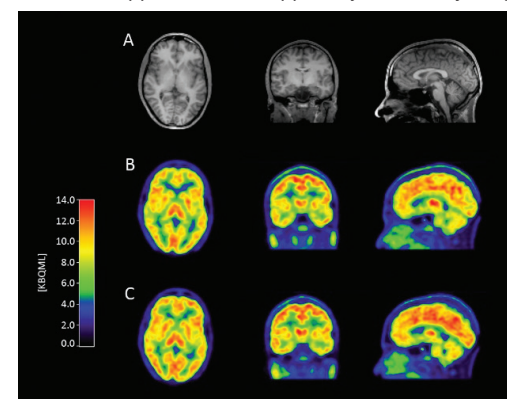


FIGURE 2 TAC for all subjects. A-E depict TEST-RETEST scans (closed and open circles respectively) of S1-5, and F-J depict baseline and ketamine scans (closed and open circles respectively) for S6-10.

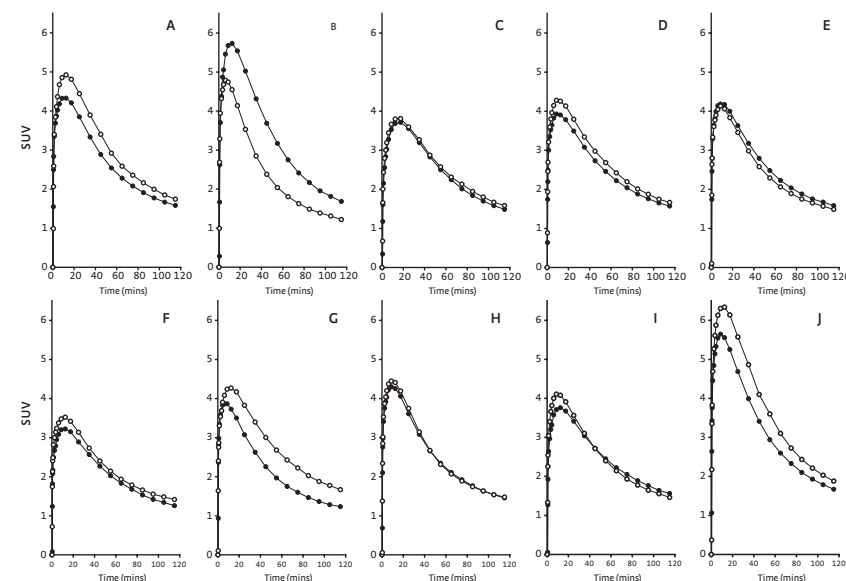


FIGURE 3 Concentration of total radioactivity in plasma following [^{18}F]PK-209 injection for subject 1-5 test scans (A) and retest scans (B) and subject 6-10 baseline scans (C) and ketamine scans (D).

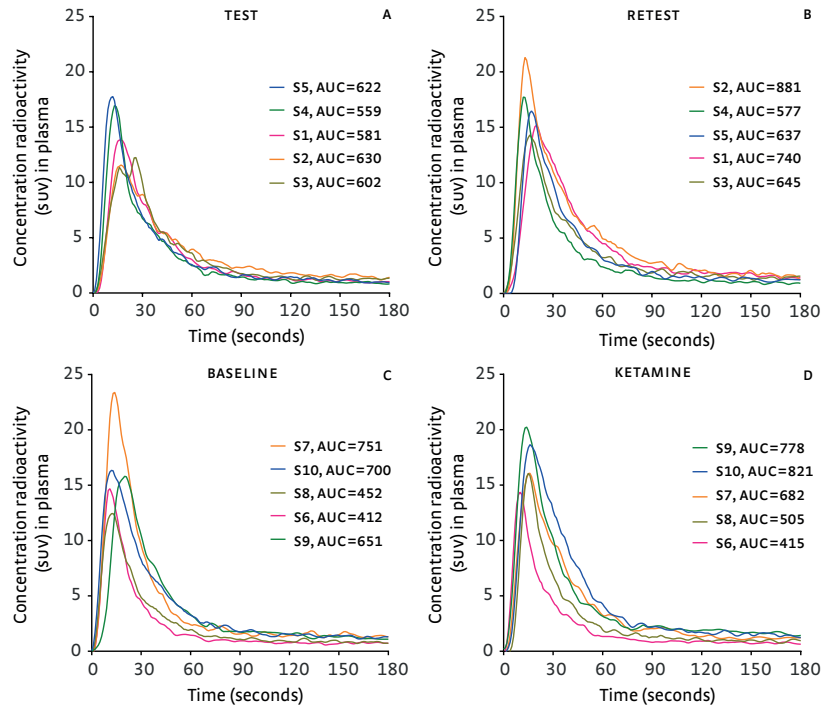
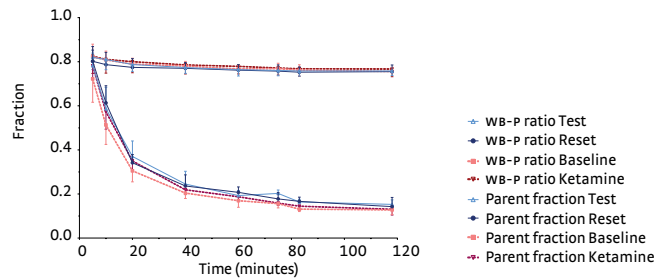


FIGURE 4 MEAN [^{18}F]PK-209 parent fractions in plasma and whole blood to plasma (WB-P) ratios of the 5 subjects in each group.



TRT scans and 6 out of the 10 ketamine group scans (see Table 2). Model preference between baseline and ketamine scans was different in 4 out of 5 subjects, but no consistent change in model preference was observed between pre- and post-ketamine scans. Fits of the 67 ROIs to the 2T3k_VB model in the 15 non-ketamine PET scans showed the highest consistency in the temporal lobe and cerebellum (12 out of 15 scans preferring 2T3k_VB) and lowest consistency in the thalamus and brainstem (7 and 8 out of 15 scans respectively). The correlation between model agreement and ROI size was significant ($r=0.33$, $p<0.01$) indicating less stable fits in smaller regions. The 2T4k_VB model was preferred in 25% of the ROIs, and no regions were identified that consistently favoured a model other than the 2T3k_VB model. Input functions that were averaged within-subjects increased the consistency in model preference, as 17 out of 20 PET scans showed best fits for the 2T3k_VB model. Considering the finding that the majority of scans as well as ROIs were fit best by the irreversible two-tissue compartment model, all scans were analyzed using the 2T3k_VB model. The primary outcome parameter was therefore the net influx rate constant K_i . Values of K_i for all 20 scans were calculated with three different plasma input functions and are presented in Table 2. The coefficient of variation of the baseline (PET1) K_i values ($N=10$) was 36% using the single scan input function, 37% using the within-subject input function, and 43% using the population average input function. Mean PET1 values of K_i in the nine volume-weighted ROIs, from low to high, were similar for all three input functions at approximately 0.008 in dorsal striatum, 0.010 in cerebellum, thalamus and insula, 0.015-0.018 in frontal, temporal, parietal and occipital cortices and 0.034-0.040 in brainstem. Correlations between K_i and SUV_{90-120} of the 10 PET1 scans, and between ΔK_i and $\Delta \text{SUV}_{90-120}$ were low for all three input functions (Spearman's $\rho<0.42$, $p>0.22$).

Test-retest group

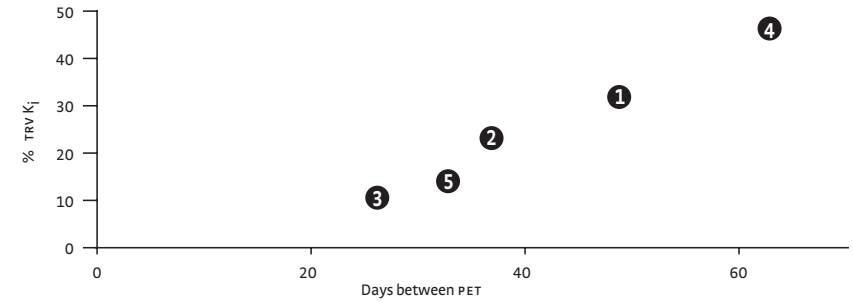
Mean TRT variability of whole brain GM K_i was 24% for scans analysed using individual metabolite corrected plasma input functions. A decrease in K_i was observed in retest scans for all subjects (range 8-37%). Across the 9 ROIs, differences between mean test-retest K_i ranged from -17% in thalamus to -36% in brainstem.

The Pearson correlation between scan interval in days and percentage difference in K_i was 0.99 ($p=0.002$) for whole brain GM (Figure 6) and 0.89 to 0.99 for individual ROIs. The TRT variability of K_1 , K_2 , K_3 and V_{ND} did not correlate with scan interval. Furthermore, the correlation of K_i TRT variability with scan interval was not significant ($p>0.05$) using within-subject and population averaged input functions.

TABLE 2 Rate constants obtained using a 2t3k_v8 model and three different plasma input functions (IF) for all subjects. TRTV = test-retest variability. $\% \Delta K_i$ = the percentage change from the baseline scan. The unit of K_1 is $\text{mL} \cdot \text{cm}^3 \cdot \text{min}^{-1}$ and the unit of k_3 and K_i is min^{-1} . VND equals K_1/k_2 .

		Single scan IF					Within-subject IF			Population IF			
		Pref. model	K_1	VND	k_3	K_i	K_i TRTV	Pref. model	K_i	K_i TRTV	Pref. model	K_i	K_i TRTV
S1	test	2T-3K	0.522	9.64	0.0016	0.0148	-32%	2T-3K	0.0118	6%	2T-3K	0.0136	4%
	retest	2T-3K	0.420	8.02	0.0014	0.0108		2T-3K	0.0126		2T-3K	0.0142	
S2	test	2T-4K	0.577	10.12	0.0016	0.0157	-23%	2T-3K	0.0131	-3%	2T-3K	0.0113	18%
	retest	2T-3K	0.407	5.90	0.0022	0.0125		2T-3K	0.0127		2T-3K	0.0136	
S3	test	2T-3K	0.341	7.33	0.0024	0.0166	-9%	2T-3K	0.0154	5%	2T-3K	0.0193	4%
	retest	2T-4K	0.347	6.14	0.0026	0.0152		2T-4K	0.0162		2T-4K	0.0201	
S4	test	2T-3K	0.473	9.73	0.0025	0.0235	-45%	2T-3K	0.0202	-17%	2T-3K	0.0147	-24%
	retest	2T-3K	0.490	9.34	0.0016	0.0148		2T-3K	0.0170		2T-3K	0.0115	
S5	test	2T-3K	0.451	8.64	0.0025	0.0208	-14%	2T-3K	0.0200	-5%	2T-3K	0.0170	-9%
	retest	2T-3K	0.465	7.29	0.0026	0.0182		2T-3K	0.0191		2T-3K	0.0156	
Mean TRTV			13%	21%	20%	24.3% ± 14.5		7.3% ± 5.6			11.9% ± 8.9		
Mean test			0.473	9.09	0.0021	0.0183		0.0161			0.0152		
Mean RETEST			0.426	7.34	0.0021	0.0143		0.0155			0.0150		
		Pref. model	K_1	VND	k_3	K_i	$\% \Delta K_i$	Pref. model	K_i	$\% \Delta K_i$	Pref. model	K_i	$\% \Delta K_i$
S6	baseline	1T-2K	0.528	9.78	0.0005	0.0046	182%	1T-2K	0.0038	237%	2T-4K	0.0071	113%
	ketamine	2T-3K	0.605	9.66	0.0014	0.0129		2T-3K	0.0128		2T-3K	0.0152	
S7	baseline	2T-4K	0.394	6.54	0.0029	0.0182	-35%	2T-4K	0.0170	0%	2T-4K	0.0150	8%
	ketamine	2T-3K	0.487	9.75	0.0012	0.0118		2T-3K	0.0169		2T-4K	0.0162	
S8	baseline	2T-3K	0.683	11.72	0.0007	0.0083	1%	2T-3K	0.0220	-9%	2T-3K	0.0183	-9%
	ketamine	2T-4K	0.559	10.30	0.0008	0.0084		2T-3K	0.0201		2T-3K	0.0167	
S9	baseline	2T-3K	0.368	7.74	0.0026	0.0193	-36%	2T-3K	0.0200	-41%	2T-3K	0.0114	-62%
	ketamine	2T-4K	0.328	6.56	0.0020	0.0124		2T-3K	0.0118		2T-3K	0.0044	
S10	baseline	2T-3K	0.488	10.51	0.0014	0.0143	30%	2T-3K	0.0105	83%	1T-2K	0.0011	-10%
	ketamine	2T-3K	0.600	9.84	0.0020	0.0186		2T-3K	0.0192		1T-2K	0.0010	
Mean baseline			0.492	9.25	0.0016	0.0129		0.0147			0.0106		
Mean ketamine			0.516	9.22	0.0015	0.0128		0.0162			0.0107		
% Change			5%	0%	-9%	-1%		10%			1%		

FIGURE 5 Scatterplot of the scan interval in days and percentage difference in K_i for subjects 1 to 5.

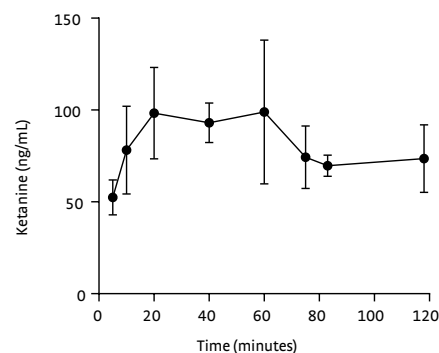


Duration of daylight correlated moderately with K_i ($r=0.54$, $p=0.11$). ROI size showed a weak correlation with TRT variability (Spearman's $\rho=-0.24$, $p=0.11$). The mean TRT variability was 13% for K_1 , 21% for V_{ND} , and 20% for k_3 . TRT variability of GM K_i generated using the within-subject input functions was markedly improved at 7%. The single population-averaged input function returned a K_i TRT variability of 12%. Analysis of the TACS (Figures 2A-E) showed that mean GM SUV_{AUC} of test scans was 316 ± 40 $SUV \cdot \text{min}$ and of retest scans 307 ± 31 $SUV \cdot \text{min}$. TRT variability of GM SUV_{AUC} was 13%, 33%, 4%, 8% and 6% for subjects 1 to 5, respectively (mean TRT variability 12%). Whole brain SUV_{90-120} was, on average, 1.68 and 1.64 in test and retest scans (-3% difference). Mean TRT variability of GM SUV_{90-120} was $12 \pm 12\%$, and the between-subject coefficient of variation of SUV_{AUC} and SUV_{90-120} for all 10 PET1 scans (including baseline scans in the ketamine group) was 15 and 11%, respectively.

Ketamine group

Ketamine administration led to whole brain GM K_i reductions in subjects 7 and 9, no change in subject 8, and increases in subjects 6 and 10 (data in Table 2). The effects of ketamine on K_i varied considerably between subjects, ranging from -36 to 182%. Model fits were unstable across ROIs and this was reflected in variable K_i changes between ROIs and subjects. The mean V_{ND} of whole brain GM did not change between baseline and ketamine scans. The mean rate of transport K_1 in the baseline scans ranged from 0.33 to 0.68 between subjects. After ketamine, K_1 increased in subjects 6, 7 and 10 by 15-24% and decreased in subject 8 and 9 with 18 and 11%, respectively, resulting in an overall mean increase of 5%. Within-subject input functions led to an increase in the difference of K_i between the baseline and ketamine

FIGURE 6 Mean plasma s-ketamine concentration during the course of the PET scan. Error bars represent standard deviations.



scans, ranging from -41 to 237% in the five subjects. The population averaged input function did not improve the consistency in change of K_i either. Analysis of TACS (Figures 2F-J) showed that whole brain SUV_{AUC} increased by 8, 27, 1, 1 and 17% following ketamine administration for subjects 6-10, respectively. Mean SUV_{AUC} of the baseline scans was $289 \pm 51 SUV \cdot min$ and of the ketamine scans $321 \pm 66 SUV \cdot min$. The mean SUV_{90-120} of baseline and ketamine scans was 1.53 and 1.68 respectively (10% increase, owing to subjects 6, 7 and 10).

Plasma ketamine concentration

Ketamine was well tolerated by all subjects. Feelings of dissociation were reported by all subjects at the start of PET scanning, but none showed loss of responsiveness or hypnosis. The plasma ketamine concentration could only be analysed for 3 out of 5 subjects and results are shown in Figure 5.

Discussion

Twenty PET scans were performed in 10 healthy subjects to evaluate [^{18}F]PK-209 brain kinetics, test-retest reproducibility and quantification of radiotracer binding to the intra-channel binding site of NMDA receptors. To this end, TRT variability was assessed in 5 subjects, followed by blocking experiments with intravenous $0.5 mg \cdot kg^{-1}$ S-ketamine administration in 5 different subjects. The kinetic profile of [^{18}F]PK-209 indicated irreversible binding, at least for the 120 min scan duration, suggesting a trapped binding mechanism or slow dissociation. The slow irreversible nature is in

accordance with in vivo behavior of [^{11}C]GMOM¹⁰, the carbon-11 labelled analogue of PK-209. [^{18}F]PK-209 readily entered the brain and displayed a fairly uniform pattern of uptake, with the rank-order of highest to lowest net influx constant (K_i) in the volume-weighted ROIs being brainstem > cortex > cerebellum-thalamus-hippocampus-insula > dorsal striatum. There were no ROIs which TACS consistently favoured a kinetic model other than the 2T3k_VB model. However, the significant correlation between 2T3k_VB model agreement and ROI size indicated that TACS in smaller brain ROIs were affected more by noise, and thus described adequately by several models. Previous kinetic analyses of PET scans with the structurally related radiotracer [^{11}C]GMOM have shown similar heterogeneity in model preference between and within subjects¹⁰.

Test-retest variability

The TRT variability of [^{18}F]PK-209 K_i calculated with single scan input functions was relatively large compared with reports of other radiotracers using similar equipment and techniques²¹, at 24% in whole brain GM K_i and 17% to 36% in individual ROIs. A closer examination of SUV_{AUC} showed good consistency between test and retest scans, with a mean 12% difference. Tracer uptake in the last 30 min of the scan, SUV_{90-120} , did not correlate with the irreversible rate of influx K_i in this group of subjects. Considering the small k_3 it is likely that the PET signal at 90 to 120 min p.i. is still dominated by free and non-specific binding. Furthermore, the TACS themselves showed clear dissociation and washout of [^{18}F]PK-209 during the course of the scan, suggesting that the ligand's trapping component within the ion-channel is relatively small. In the present study, a 'coffee-break' protocol with extended scanning up to four hours post radiotracer injection may have provided additional information on kinetics, such as the contribution of the ligand-binding site dissociation constant K_4 . However, tracer metabolism and low count rates at late timepoints would have complicated measurements of the input function.

Blood data from arterial measurements during the PET scan showed that there was rapid blood pool clearance combined with rapid tracer metabolism. Mean parent fractions were 57 and 34% at 10 and 20 min p.i., respectively, which is somewhat higher compared with non-human primate parent fractions¹⁵. Fast metabolism has also been shown in clinical PET studies of [^{11}C]ketamine²² and ligands from the class of bis(aryl)guanidines, i.e. [^{11}C]CNS-5161²³, [^{11}C]GMOM¹⁰, and [^{18}F]GE-179²⁴, which are structurally related to [^{18}F]PK-209. HPLC analysis showed that one [^{18}F]PK-209 metabolite accounted for approximately 30% of total plasma radioactivity from 20 min until the end of the scan. A limitation of the present study was that the fractional recovery of radioactivity from plasma declined over time, stabilizing at

approximately 45%. Arterial samples taken immediately before PET were incubated with [¹⁸F]PK-209 at 37°C and radioactivity recovery of these samples remained constant at approximately 90% during the 2-hour experiment. The difference between recovery fractions suggest that, during the scan, metabolites were formed in the body, which subsequently were retained within the pellet for corresponding samples. An influx of radiometabolites into the brain may have confounded [¹⁸F]PK-209 quantification and contributed to TRT variability. Ex vivo rodent studies have shown that polar metabolites only contribute 4% to total brain radioactivity at 60 min p.i. The non-polar metabolite fraction, however, was 18 and 25% at 15 and 60 min p.i., respectively¹³. Logan plots of [¹⁸F]PK-209 in non-human primates showed that linearity was attained from early to late time-points, arguing against the significant accumulation of radiometabolites in the brain. Furthermore, recovery of radioactivity in the present study was high at the start of the scan, indicating that the analytical methods to measure parent [¹⁸F]PK-209 and associated input functions provided reliable results. TRT variability was further examined as a function of parent fraction determination in plasma. To this end, TACS were modelled with arterial input functions using parent fractions that were averaged within-subjects and across the two samples of 5 subjects. Within-subject input functions led to a substantial reduction in K_i TRT variability from 24% to 7% and improved consistency of the 2T3k_V_B model preference from 14 to 17 (out of 20) PET scans.

Preliminary results showed a significant correlation between scan interval in days and reduction in K_i using the single scan input function, but not with subject- and population-averaged input functions. This correlation is likely due to either a systemic error in test or retest input function measurements or a true biological component resulting in lowered availability of the NMDA channel site for radiotracer binding during the second scan. In same-day test-retest studies with the metabotropic glutamatergic tracers [¹¹C]ABP688 and [¹⁸F]FPEB, it was shown that binding was significantly higher in the second scan, whereas two scans days to weeks apart showed good TRT variability²⁵. Diurnal and seasonal variation in receptor or endogenous ligand concentrations might be sources of increased TRT variability. In the present study, however, all scans were performed in the afternoon between 12:00 and 15:00 h, limiting diurnal effects on glutamatergic neurotransmission. The moderate correlation of K_i with duration of daylight and strong correlation of K_i with scan interval could be indicative of seasonal effects. These have been found previously in serotonin 5-HT_{1A} receptor PET studies²⁶. Finally, and taking into consideration the limitations of a small sample size, it is noteworthy that the two subjects aged 34 and 37 showed numerically higher TRT variability compared with

the three subjects aged 22-23. Future work is needed to understand the source of variability and a full validation of these findings will require a larger cohort.

Ketamine blocking studies

Despite good quality data for all [¹⁸F]PK-209 scans, there was no consistent effect of ketamine administration on the pharmacokinetic model parameters. Intravenous ketamine administration increased whole brain SUV_{AUC} and SUV₉₀₋₁₂₀ in three out of five subjects, whereas previous non-human primate experiments showed a 15% reduction in mean SUV_{AUC} after MK-801 administration¹⁵. The best PET model fits changed in 4 out of 5 subjects following ketamine administration, but not in a predictable manner. The unstable fits of [¹⁸F]PK-209 may be explained by changes in the arterial input function or brain pharmacokinetics of the tracer. For example, the increased SUV in subjects 6, 7 and 10, which is reflected in increased K₁ values, shows that the uptake of [¹⁸F]PK-209 is blood flow dependent. Ketamine is known to exert direct vasodilatory effects on the cerebral vasculature through a calcium-dependent mechanism. In a review of 20 human imaging studies, it was shown that plasma ketamine concentrations, comparable to those used in the present study, increased global and/or regional cerebral blood flow in human subjects²⁷. Contrasting results from a recent simultaneous PET and functional MRI imaging study in anesthetized non-human primates demonstrated that cerebral blood volume following administration of the PCP site blocker GE-179 was acutely reduced²⁸. In a bolus-plus-infusion paradigm, 'cold' GE-179 at a dose of 0.6 mg·kg⁻¹ was administered when [¹⁸F]GE-179 was at steady-state, which was expected to reduce the brain signal by competitive displacement at the PCP binding site. A short-term blood volume decrease was observed, however GE-179 did not significantly block the PET signal and had no effect on arterial plasma blood levels, indicating that the [¹⁸F]GE-179 signal is independent of flow²⁸. Ketamine may affect blood flow differently than GE-179, and a future study in humans with simultaneous [¹⁸F]PK-209 PET and fMRI could elucidate the relationship between NMDA-R blockers, blood flow and radiotracer binding.

The arterial plasma fractions of [¹⁸F]PK-209 in the baseline scans were on average 8 to 15% lower than in the ketamine scans (Figure 4), but also 16% lower compared with the TRT group. The small increase in baseline metabolism of subjects 6 to 10 may suggest an initial group difference which was normalized by ketamine administration. However, in non-human primates there was no effect of MK-801 on [¹⁸F]PK-209 metabolism, nor did ketamine administration affect [¹¹C]GMOM metabolism in humans. Systematic errors in the estimation of arterial blood

parameters or natural variability in metabolism may underlie the observed differences. Although the measurement error may have affected the model parameters, it is unlikely to explain the variability of [^{18}F]PK-209 K_i between subjects following ketamine administration.

The mean plasma ketamine concentrations plateaued at $\sim 100 \text{ ng}\cdot\text{ml}^{-1}$ between 20 and 60 min after the start of PET (40 min since the start of ketamine infusion) and decreased to $\sim 70 \text{ ng}\cdot\text{ml}^{-1}$ at the end of the scan, 160 min since the start of $0.5 \text{ mg}\cdot\text{kg}^{-1}$ ketamine infusion. As expected, the C_{max} in the current study was dose-proportionally higher than the $0.3 \text{ mg}\cdot\text{kg}^{-1}$ ketamine administered in the [^{11}C]GMOM blocking study¹⁰. Subjects in a SPECT study by Stone et al.²⁹ were administered $1.1 \text{ mg}\cdot\text{kg}^{-1}$ S-ketamine over 75 min, which led to a mean plasma concentration of $173 \text{ ng}\cdot\text{ml}^{-1}$ and displacement of the NMDA-R channel ligand [^{123}I]CNS-1261 in the brain. Preclinical in vivo studies have also demonstrated a strong and rapid temporal relationship between ketamine concentrations in plasma and radiotracer inhibition in brain tissue. For example, in rats, 67% inhibition of [^3H]MK-801 binding was observed at 1 min post-dosing with $3 \text{ mg}\cdot\text{kg}^{-1}$ racemic (\pm)ketamine IV, and the inhibition declined to 19% at 20 min post-dose³⁰. The plasma racemic ketamine concentration required to inhibit 50% of specific [^3H]MK-801 binding in vivo has been calculated in the range of $1.9\text{--}3.7 \mu\text{M}$ ³⁰. The present pharmacokinetic data show a concentration of ketamine in plasma of $0.3\text{--}0.4 \mu\text{M}$ during PET scanning, which may have been insufficient to unmask specific uptake of [^{18}F]PK-209. Nevertheless, S-ketamine at a lower plasma concentration of $0.26 \mu\text{M}$ was shown to reduce the K_i of the equipotent carbon-11 labelled analogue of PK-209, [^{11}C]GMOM, in humans¹⁰. The concentrations of unlabelled PK-209 and GMOM that inhibit specific binding of [^3H]MK-801 to rat forebrain membranes were shown to be similar at 18.4 and 21.7 nM respectively¹³. Furthermore, data from the preclinical [^{18}F]PK-209 PET study demonstrated that a dose of $0.3 \text{ mg}\cdot\text{kg}^{-1}$ MK-801 reduced the volume of distribution in two out of three rhesus monkeys compared with baseline [^{15}O]. In displacement binding studies, MK-801 is two orders of magnitude more potent than (\pm)ketamine at the ion-channel site³⁰, but the compound is not approved for human use and therefore could not be implemented in the present study design. Despite these reports of inhibition of NMDA-R activity by channel blockers, the recent preclinical in vivo evaluation of [^{18}F]GE-179 suggests that the PET signal is largely non-specific²⁸.

NMDA receptors are complex, highly modulated ligand gated ion channels bound in cell membranes that, in order to open, require activation of nearby AMPA and kainate receptors as well as co-activation by glutamate and D-serine or glycine. Recently, electron cryomicroscopy experiments revealed how small molecules

affect the NMDA-R structure and ion channel opening³¹. Many endogenous ligands acting at NMDA-Rs, such as Mg^{2+} , Zn^{2+} , H^+ , polyamine cations, neurosteroids and fatty acids, determine the in vivo binding properties of ligands targeted for NMDA receptors. For example, it has been shown that in native NMDA receptors of rat hippocampus CA1 pyramidal neurons, IC_{50} values of NMDA-R channel blockers are increased 1.5 to 5 times compared with magnesium-free conditions³². Variations in physiological Mg^{2+} or other endogenous ligands could have affected [^{18}F]PK-209 binding and may have contributed to the observed TRT variability and inconsistent ketamine effects. A second possibility is that ketamine and [^{18}F]PK-209 inhibit distinct populations of NMDA-Rs. Ketamine predominantly inhibits synaptic NMDA-Rs, whereas for example memantine primarily inhibits extrasynaptic NMDA-Rs³³, although more weakly³⁴. In this respect it may be valuable to investigate memantine as a pharmacological blocker in future PET studies with NMDA-R radiotracers to examine different domains of [^{18}F]PK-209 binding. A third possibility is that ion-channel ligands exhibit biexponential association kinetics with the NMDA ionophore and thereby complicate PET pharmacokinetic modelling. Very few studies have examined how the association rate constants of ion channel blockers change as a function of radioligand concentration, and there is evidence to suggest that the kinetics of channel blocker association with the NMDA ionophore do not follow the law of mass-action². Changing the ligand binding site accessibility can change the rate of association and dissociation, but has no effect on equilibrium affinity of ligand binding³⁵. One cannot exclude that the slightly different doses of [^{18}F]PK-209 injected in the baseline versus the blocking scans may have contributed to a noisy data set.

Conclusion

The establishment of a radiotracer for in vivo quantification of specific binding to the NMDA receptor remains challenging. The divergent clinical and preclinical behaviour of [^{18}F]PK-209 could be due to multiple differences in interactions between exogenous and endogenous glutamatergic ligands. There are plausible biophysical explanations that remain to be tested, which are pivotal for interpreting the ligand-NMDA-R interactions. The conclusion of the present study is that the molecular interaction between [^{18}F]PK-209 and the binding site within the NMDA-R ion channel was not shown to be reproducible or specific. It is possible that the typical study design for neuroreceptor PET tracers executed here is not applicable to such a dynamic and complex receptor system as the NMDA-R.

REFERENCES

- Paoletti P, Bellone C, Zhou Q.: NMDA receptor subunit diversity: impact on receptor properties, synaptic plasticity and disease: *Nature reviews Neuroscience*. 2013 Jun;14(6):383-400. Available from: <https://doi.org/10.1038/nrn3504>
- Javitt DC, Zukin SR.: Biexponential kinetics of [3H]MK-801 binding: evidence for access to closed and open N-methyl-D-aspartate receptor channels: *Molecular pharmacology*. 1989 Apr;35(4):387-93. Available from <https://molpharm.aspetjournals.org/content/35/4/387.long>
- Traynelis SF, Wollmuth LP, McBain CJ, Menniti FS, Vance KM, Ogden KK, Hansen KB, Yuan H, Myers SJ, Dingledine R.: Glutamate receptor ion channels: structure, regulation, and function: *Pharmacological reviews*. 2010 Sep;62(3):405-96. Available from: <https://doi.org/10.1124/pr.109.002451>
- Lee C-H, Lü W, Michel JC, Goehring A, Du J, Song X, Gouaux E.: NMDA receptor structures reveal subunit arrangement and pore architecture: *Nature*. 2014 Jun 22;511(7508):191-7. Available from: <https://doi.org/10.1038/nature13548>
- Danyisz W, Parsons CG.: Alzheimer's disease, β -amyloid, glutamate, NMDA receptors and memantine--searching for the connections: *British journal of pharmacology*. 2012 Sep;167(2):324-52. Available from: <https://doi.org/10.1111/j.1476-5381.2012.02057.x>
- Ametamey SM, Bruehlmeier M, Kneifel S, Kolic M, Honer M, Arigoni M, Buck A., Burger C, Samnick S, Quack G, Schubiger P.: PET studies of ^{18}F -memantine in healthy volunteers: *Nuclear Medicine and Biology*. 2002;29(2):227-31. Available from: [https://doi.org/10.1016/S0969-8051\(01\)00293-1](https://doi.org/10.1016/S0969-8051(01)00293-1)
- Asselin M, Hammers A, Turton D, Osman S, Koeppe M BD.: Initial kinetic analyses of the in vivo binding of the putative NMDA receptor ligand [C-11]CNS 5161 in humans: *NeuroImage*. 2004;22:137. Available from: <https://doi.org/10.1016/j.neuroimage.2004.09.006>
- Hartvig P, Valtysson J, Lindner KJ, Kristensen J, Karlsten R, Gustafsson LL, Persson J, Svensson JO, Oye I, Antoni G.: Central nervous system effects of subdissociative doses of (S)-ketamine are related to plasma and brain concentrations measured with positron emission tomography in healthy volunteers: *Clinical pharmacology and therapeutics*. 1995 Aug;58(2):165-73. Available from: [https://doi.org/10.1016/0009-9236\(95\)90194-9](https://doi.org/10.1016/0009-9236(95)90194-9)
- Klein PJ, Chomet M, Metaxas A, Christiaans JAM, Kooijman E, Schuit RC, Lammertsma AA, Berckel BNM Van, Windhorst AD.: European Journal of Medicinal Chemistry Synthesis, radiolabeling and evaluation of novel amine guanidine derivatives as potential positron emission tomography tracers for the ion channel of the N-methyl-D-aspartate receptor: *European Journal of Medicinal Chemistry*. 2016;118:143-60. Available from: <https://doi.org/10.1016/j.ejmech.2016.04.022>
- Doef TF van der, Golla SS, Klein PJ, Oropeza-Seguias GM, Schuit RC, Metaxas A, Jobse E, Schwarte LA, Windhorst AD, Lammertsma AA, Berckel BN van, Boellaard R.: Quantification of the novel N-methyl-d-aspartate receptor ligand [^{11}C]GMO M in man: *Journal of Cerebral Blood Flow & Metabolism*: 2016;36:1111-21. Available from: <https://doi.org/10.1177/0271678X15608391>
- Waterhouse RN, Slifstein M, Dumont F, Zhao J, Chang RC, Sudo Y, Sultana A, Balter A, Laruelle M.: In vivo evaluation of [^{11}C] N-(2-chloro-5-thiomethylphenyl)-N'-(3-methoxy-phenyl)-N'-methylguanidine ([^{11}C]GMO M) as a potential PET radiotracer for the PCP/NMDA receptor: *Nuclear medicine and biology*. 2004 Oct;31(7):939-48. Available from: <https://doi.org/10.1016/j.nucmedbio.2004.03.012>
- Van der Aart J, van der Doef TF, Horstman P, Huisman MC, Schuit RC, van Lingen A, Windhorst AD, van Berckel BNM, Lammertsma AA.: Human Dosimetry of the N-Methyl-D-Aspartate Receptor Ligand [^{11}C]GMO M: *Journal of Nuclear Medicine*. 2017;58(8):1330-3. Available from: <https://doi.org/10.2967/jnumed.116.188250>
- Klein PJ, Christiaans JAM, Metaxas A, Schuit RC, Lammertsma AA, van Berckel BNM, Windhorst AD.: Synthesis, structure activity relationship, radiolabeling and preclinical evaluation of high affinity ligands for the ion channel of the N-methyl-d-aspartate receptor as potential imaging probes for positron emission tomography: *Bioorganic & Medicinal Chemistry*. 2015;23(5):1189-206. Available from: <https://doi.org/10.1016/j.bmc.2014.12.029>
- Klein PJ, Schuit RC, Metaxas A, Christiaans JAM, Kooijman E, Lammertsma AA, van Berckel BNM, Windhorst AD.: Synthesis, radiolabeling and preclinical evaluation of a [^{11}C]GMO M derivative as PET radiotracer for the ion channel of the N-methyl-D-aspartate receptor: *Nuclear Medicine and Biology*. 2017;51:25-32. Available from: <https://doi.org/10.1016/j.nucmedbio.2017.05.003>
- Golla SSV, Klein PJ, Bakker J, Schuit RC, Christiaans JAM, van Geest L, Kooijman EJ, Oropeza-Seguias GM, Langermans JA. M, Leysen JE, Boellaard R, Windhorst AD, van Berckel BNM, Metaxas A.: Preclinical evaluation of [^{18}F]PK-209, a new PET ligand for imaging the ion-channel site of NMDA receptors: *Nuclear Medicine and Biology*. 2015;42(2):205-12. Available from: <https://doi.org/10.1016/j.nucmedbio.2014.09.006>
- Surti S, Kuhn A, Werner ME, Perkins AE, Kolthammer J, Karp JS.: Performance of Philips Gemini TF PET/CT scanner with special consideration for its time-of-flight imaging capabilities: *Journal of Nuclear Medicine*. 2007;48(3):471-80. Available from <http://jnm.snmjournals.org/content/48/3/471.long>
- Vollmar S, Michel C, Treffert JT, Newport DF, Casey M, Knöss C, Wienhard K, Liu X, DeFrise M, Heiss WD.: HeinzlCluster: accelerated reconstruction for FORE and OSEM3D: *Physics in Medicine and Biology*. 2002 Aug 7;47(15):307. Available from: <https://doi.org/10.1088/0031-9155/47/15/307>
- Zhang Y, Brady M, Smith S.: Segmentation of brain MR images through a hidden Markov random field model and the expectation-maximization algorithm: *IEEE transactions on medical imaging*. 2001 Jan;20(1):45-57. Available from: <https://doi.org/10.1109/42.906424>
- Hammers A, Allom R, Koeppe MJ, Free SL, Myers R, Lemieux L, Mitchell TN, Brooks DJ, Duncan JS.: Three-dimensional maximum probability atlas of the human brain, with particular reference to the temporal lobe: *Human brain mapping*. 2003 Aug;19(4):224-47. Available from: <https://doi.org/10.1002/hbm.10123>
- Akaike H.: Data Analysis by Statistical Models: *No To Hatatuse*. 1992;24(2):127-33. Available from: <https://doi.org/10.1125/01jscn1969.24.127>
- van Assema DM, Lubberink M, Boellaard R, Schuit RC, Windhorst AD, Scheltens P, van Berckel BN, Lammertsma AA.: Reproducibility of quantitative (R)-[^{11}C]verapamil studies: *EJNMMI Research*. 2012 Jan 17;2(1):1. Available from: <https://doi.org/10.1186/2191-219X-2-1>
- Kumlien E, Hartvig P, Valind S, Oye I, Tedroff J, Langstrom B.: NMDA-Receptor Activity Visualized with (S)-[N-Methyl- ^{11}C] Ketamine and Positron Emission Tomography in Patients with Medial Temporal Lobe Epilepsy: *Epilepsia*. 1999 Jan;40(1):30-7. Available from: <https://doi.org/10.1111/j.1528-1157.1999.tb01985.x>
- Schiffer WK, Pareto-Onghena D, Wu H, Lin K-S, Gibbs AR, Fowler JS, Logan J, Alexoff DL, Dewey SL, Biegon AR.: In vivo evaluation of [^{11}C]CNS-5161 as a use-dependent ligand for the NMDA glutamate receptor channel: *Journal of Cerebral Blood Flow & Metabolism*. 2005 Aug;25(1_suppl):S595-S595. Available from: <https://doi.org/10.1038/sj.cbfm.9591524.0595>
- McGinnity CJ, Hammers A, Riaño Barros DA, Luthra SK, Jones PA, Trigg W, Micallef C, Symms MR, Brooks DJ, Koeppe MJ, Duncan JS.: Initial evaluation of ^{18}F -GE-179, a putative PET Tracer for activated N-methyl D-aspartate receptors: *Journal of Nuclear Medicine*. 2014 Mar;55(3):423-30. Available from: <https://doi.org/10.2967/jnumed.113.130641>
- DeLorenzo C, Gallezot JD, Gardus J, Yang J, Planeta B, Nabusli N, Ogden RT, Labaree DC, Huang YH, Mann JJ, Gasparini F, Lin X, Javitch JA, Parsey RV, Carson RE, Esterlis I.: In vivo variation in same-day estimates of metabotropic glutamate receptor subtype 5 binding using [^{11}C]AP688 and [^{18}F]FPEB: *Journal of Cerebral Blood Flow and Metabolism*. 2017;37(8):2716-27. Available from: <https://doi.org/10.1177/0271678X16673646>
- Matheson CJ, Schain M, Almeida R, Lundberg J, Cselényi Z, Borg J, Varrone A, Farde L, Cervenka S.: Diurnal and seasonal variation of the brain serotonin system in healthy male subjects: *NeuroImage*. 2015;112:225-31. Available from: <https://doi.org/10.1016/j.neuroimage.2015.03.007>
- Zeiler FA, Sader N, Gillman LM, Teitelbaum J, West M, Kazina CJ.: The Cerebrovascular Response to Ketamine: A Systematic Review of the Animal and Human Literature. *Journal of Neurosurgical Anesthesiology*: 2016;28(2):123-40. Available from: <https://doi.org/10.1097/ANA.0000000000000234>
- Schoenberger M, Schroeder FA, Placzek MS, Carter RL, Rosen BR, Hooker JM, Sander CY.: In Vivo [^{18}F]GE-179 Brain Signal Does Not Show NMDA-Specific Modulation with Drug Challenges in Rodents and Nonhuman Primates: *ACS Chemical Neuroscience*. 2018;9(2):298-305. Available from: <https://doi.org/10.1021/acscchemneuro.7b00327>
- Stone JM, Erlandsson K, Arstad E, Squassante L, Teneggi V, Bresnan R., Krystal JH, Ell PJ, Pilowsky LS.: Relationship between ketamine-induced psychotic symptoms and NMDA receptor occupancy - A [^{11}C]CNS-1261 SPET study: *Psychopharmacology*. 2008;197(3):401-8. Available from: <https://doi.org/10.1007/s00213-007-1047-x>
- Fernandes A, Wojcik T, Baireddy P, Pieschl R, Newton A, Tian Y, Hong Y, Bristow L, Li YW.: Inhibition of in vivo [3H]MK-801 binding by NMDA receptor open channel blockers and GluN2B antagonists in rats and mice: *European Journal of Pharmacology*. 2015;766:1-8. Available from: <https://doi.org/10.1016/j.ejphar.2015.08.044>
- Zhu S, Stein RA, Yoshioka C, Lee CH, Goehring A, McHaourab HS, Gouaux E.: Mechanism of NMDA Receptor Inhibition and Activation: *Cell*. 2016;165(3):704-14. Available from: <https://doi.org/10.1016/j.cell.2016.03.028>
- Nikolaev M V., Magazanik LG, Tikhonov DB.: Influence of external magnesium ions on the NMDA receptor channel block by different types of organic cations: *Neuropharmacology*. 2012;62(5-6):2078-85. Available from: <https://doi.org/10.1016/j.neuropharm.2011.12.029>
- Johnson JW, Glasgow NG, Povyshva NV.: Recent insights into the mode of action of memantine and ketamine: *Current Opinion in Pharmacology*. 2015;20:54-63. Available from: <https://doi.org/10.1016/j.coph.2014.11.006>
- Song X, Jensen MØ, Jogini V, Stein RA, Lee C-H, Mchaourab HS, Shaw DE, Gouaux E.: Mechanism of NMDA receptor channel block by MK-801 and memantine: *Nature*. 2018 Apr 18;556(7702):515-9. Available from: <https://doi.org/10.1038/s41586-018-0039-9>
- Starmer CF, Packer DL, Grant AO.: Ligand binding to transiently accessible sites: mechanisms for varying apparent binding rates: *Journal of Theoretical Biology*. 1987 Feb 7;124(3):335-41. Available from: [https://doi.org/10.1016/S0022-5193\(87\)80120-0](https://doi.org/10.1016/S0022-5193(87)80120-0)

CHAPTER 6

**QUANTIFICATION OF HUMAN
BRAIN PDE4 OCCUPANCY
BY GSK356278: A [11C]
(R)-ROLIPRAM PET STUDY**

PUBLISHED IN JOURNAL OF CEREBRAL BLOOD FLOW & METABOLISM

Jasper van der Aart^{1,2}, Cristian Salinas¹, Rahul Dimber¹,
Sabina Pampols-Maso¹, Ashley A. Weekes¹, John Tonkyn⁴, Frank A. Gray⁴,
Jan Passchier¹, Roger N. Gunn^{1,3}, Eugenii A. Rabiner^{1,5}

1 Imanova (Invicro), London, UK

2 Department of Radiology and Nuclear Medicine, vu University Medical Center,
Amsterdam, the Netherlands

3 Division of Brain Sciences, Department of Medicine, Imperial College London, UK

4 GlaxoSmithKline, Stevenage, UK

5 Centre for Neuroimaging Sciences, Institute of Psychiatry, King's College,
London, UK

© 2017 The Authors. Open Access. This article is distributed under the terms of the Creative Commons
Attribution 4.0 International License. DOI 10.1177/0271678X17720868

Abstract

We characterized the relationship between the plasma concentration of the PDE4 inhibitor GSK356278 and occupancy of the PDE4 enzyme in the brain of healthy volunteers, using the PET tracer [¹¹C](R)-rolipram. To this end, PET scans were acquired in 8 males before and at 3 and 8 hours after a single 14 mg oral dose of GSK356278. A metabolite corrected arterial input function was used in conjunction with the dynamic PET emission data to estimate volumes of distribution (V_T) from a two-tissue compartment model. The administration of GSK356278 reduced [¹¹C](R)-rolipram whole brain (V_T) by 17% at 3 hours post-dose ($p=0.01$), and by 4% at 8 hours post-dose. The mean plasma C_{max} was 42.3 ng/ml, leading to a PDE4 occupancy of 48% at T_{max} . The in vivo affinity of GSK356278 was estimated as $EC_{50}=46 \pm 3.6$ ng/ml. We present the first report of a direct estimation of PDE4 blockade in the living human brain. In vivo affinity of GSK356278 for the PDE4, estimated in this early phase study, was combined with GSK356278 safety and tolerability data to decide on a therapeutic dose for future clinical development.

Introduction

Rolipram is a selective inhibitor of the enzyme phosphodiesterase (PDE)-4, a member of the PDE enzyme family which hydrolyse the second messenger cyclic adenosine monophosphate (cAMP). The carbon-11-labelled (R) enantiomer of rolipram has been demonstrated to be suitable for *in vivo* evaluation of PDE4 availability and activity with positron emission tomography (PET)^{1,2}. [¹¹C](R)-rolipram binding is sensitive to pharmacological challenges in rat³ and porcine brain⁴. However, to this point, no human blocking studies with PDE4 modulators have been published. GSK356278 is a potent, CNS penetrant inhibitor of cAMP hydrolytic activity⁵ that binds to the high-affinity rolipram binding site (HARBS) with a piC_{50} of 8.6 and is nonselective for the PDE4 A, B, and D isoforms⁶. In a model of anxiety in common marmosets, the therapeutic index for GSK356278 was > 10 versus < 1 for rolipram⁶, which may be explained by the faster HARBS dissociation rate compared to rolipram. The present study was designed to evaluate the relationship between the plasma GSK356278 concentration and the occupancy of the brain PDE4 enzyme in healthy male subjects. These data were to be utilized to optimize the dose range for future Phase 1 and 2 studies.

Methods

This was an open-label study in 8 healthy male volunteers with a mean (\pm standard deviation, SD) age of 34.4 ± 10.7 . This study was approved by the Edinburgh Independent Ethics Committee for Medical Research and the Administration of Radioactive Substances Advisory Committee (ARSAC) and conducted in accordance with ICH GCP and the 2008 revision of the Declaration of Helsinki. PET scanning was performed at Imanova, Centre for Imaging Sciences (Hammersmith Hospital, London, UK). All subjects gave written informed consent, tested negative for drugs in urine, and were free from clinically significant illness or disease as determined by their medical history, a full physical examination, blood laboratory tests and electrocardiography.

Radiopharmaceutical Preparation

[¹¹C](R)-rolipram was prepared by O-[¹¹C] methylation of its desmethyl analog (1 mg) in dimethylformamide (350 μ l) using [¹¹C] methyl iodide in the presence of tetrabutyl ammonium hydroxide (0.5 M, 4 μ l). The reaction mixture was heated to 85°C

for 5 min, diluted with HPLC mobile phase (1 ml) and loaded onto semi-preparative HPLC for purification (Agilent Eclipse XDB C18, 5 μ m, 250 \times 9.4 mm). The retention time of [11 C](R)-rolipram was 5.4 min through isocratic elution with a mixture of 10 mM ammonium formate buffer/acetonitrile (60/40, v/v) at a flow rate of 6 ml/min. The desired fraction was collected, diluted with water (20 ml) and loaded onto a SepPak[®] Classic C18 cartridge for reformulation. Following an initial wash with sterile water (10 ml), [11 C](R)-rolipram was eluted off the cartridge with ethanol (1 ml) and subsequently diluted with saline (10 ml). In a final step the resulting formulation solution was filtered through a 0.22 μ m sterile filter into a sterile, pyrogen free, vial. Typical synthesis from a 55 μ A, 30 min beam provided 3.35 ± 1.4 GBq (uncorrected) of [11 C](R)-rolipram in a total synthesis time of 35 min with a specific activity of 142 ± 133 GBq/ μ mol. Quality control showed that doses were obtained with radiochemical purities > 99% and that the final product for injection was sterile and pyrogen free.

Positron Emission Tomography Data Acquisition

In total, 22 [11 C](R)-rolipram PET scans were acquired on a Siemens Biograph HiRez XVI PET-CT scanner (Siemens Healthcare, Erlangen, Germany) of which 8 scans at baseline (PET 1) and 7 scans at approximately 3 and 8 hours post-dose each (PET 2 and PET 3 respectively). A CT scan of the head was acquired for attenuation and model-based scatter correction. Subjects were injected with an intravenous bolus of the radioligand and dynamic emission data were acquired continuously for 90 minutes. PET data were reconstructed using filtered backprojection with corrections for attenuation, dead time, random coincidences, and scatter. Dynamic data were binned into 26 frames (8*15 seconds, 3*1, 5*2, 5*5, and 5*10 minutes). A continuous sampling system (ABSS Allogg, Mariefred, Sweden) was used to measure whole blood activity for the first 15 minutes (sampled at 5 ml/minute). Discrete blood samples were acquired to measure blood and plasma radioactivity concentration at 5, 10, 15, 20, 30, 40, 50, 70, 90 min and to determine with HPLC the fraction of radioactivity corresponding to intact parent [11 C](R)-rolipram in arterial plasma. Plasma free fraction (f_p) was determined by ultrafiltration. The three discrete blood samples at 5, 10 and 15 min post-injection were used to calibrate the continuous blood data. The continuous and discrete datasets were used to form a whole-blood activity curve covering the duration of the scan. Radioactivity concentrations in discrete plasma samples were divided by the corresponding whole-blood samples to form plasma-over-blood (POB) data, and a constant POB model was fitted (i.e. average of

POB values). This POB value was then multiplied by the whole blood curve to generate a total plasma curve. Parent fraction data were fitted to a sigmoid model $f = ((1 - (t^3 / (t^3 + 10^0)))^b + c) / (1 + c)$ where t is time and a , b and c are fitted parameters. The resulting fitted parent fraction profile was multiplied by the total plasma curve and then smoothed post-peak using a tri-exponential fit to derive the required parent plasma input function. For each scan, a time delay was fitted and applied to the input function to account for any temporal delay between blood sample measurement and the tomographic measurements of the tissue data.

Image Analysis

T1-weighted magnetic resonance images (MRI) were acquired to aid in the definition of the anatomic regions of interest (ROIs) using a Siemens Magnetom Trio 3T MRI scanner at Imanova. Dynamic PET images were registered to each individual subject's MRI, and corrected for motion using a frame-to-frame registration process with a mutual information cost function. Regional analysis was facilitated by using a human brain atlas containing ROIs that had been manually delineated on a T1-MR image template according to strict anatomical criteria⁷. The target ROIs included the caudate, putamen, thalamus, hippocampus, frontal cortex, parietal lobe, temporal lobe, occipital pole and cerebellum. For each subject the template and the corresponding atlas were individually warped to the subject's anatomical MRI which was previously linearly registered to the PET images and used to generate time activity curves (TACs).

Compartmental modeling and specific signal estimation

The individual metabolite corrected arterial input function and the whole blood activity curve were used in conjunction with the dynamic PET data to estimate regional volumes of distribution (V_T) using a two-tissue compartment model. The blood volume component (V_B) was fixed at 5%.

The V_T is the sum of the tracer's specific (V_S) and non-displaceable (V_{ND}) binding. As there is no suitable (pseudo)reference region in the human brain, devoid of PDE4, it is not straightforward to estimate V_{ND} and calculate the non-displaceable binding potential (BP_{ND}). Target occupancy and V_{ND} may be estimated from V_T data and the related plasma concentration of GSK356278 if a sufficiently large reduction in V_T is observed post-block. However, we were not able to acquire data following high levels of PDE4 blockade due to the safety limitations on the maximal dose of GSK356278 we could administer. Therefore, an estimate of the average brain binding potential

$(BP_{ND}^{baseline})$ was used from the literature², acquired in an experiment where the binding of [¹¹C](R)-rolipram and the inactive enantiomer [¹¹C](S)-rolipram in the human brain was examined. The specific binding of [¹¹C](R)-rolipram was estimated by making explicit assumptions that the (S) enantiomer demonstrates only non-displaceable binding, and the magnitude of this non-displaceable component is similar for both stereoisomers. For each subject in the current study, an individual estimate of V_{ND} was made using $BP_{ND}^* = 0.5$ and the formula

$$V_{ND} = \frac{V_T^{baseline}}{1 + BP_{ND}^*},$$

where $V_T^{baseline}$ is the global average brain V_T before drug administration. In order to evaluate the sensitivity of our data to the assumption of the literature BP_{ND} estimate we repeated the process with BP_{ND}^* of 0.25 and 1. For each ROI, average V_T (\bar{V}_T) values per subject and scan were calculated as

$$\bar{V}_T = \frac{\sum_i \alpha_i \times V_{Ti}}{\sum_i \alpha_i},$$

where α_i is the volume (in mm³) of region i and V_{Ti} is the total volume of distribution of region i . Finally, GSK356278 occupancy of PDE4 was calculated as,

$$\text{occupancy} = 1 - \frac{BP_P^{drug}}{BP_P^{baseline}}, \text{ where } BP_P = \frac{K_1 k_3}{k_2 k_4}.$$

Plasma GSK356278 concentrations ($C_P^{GSK356278}$) were obtained from blood samples using mass-spectrometry with a lower limit of quantification of 0.3 ng/ml. Changes in [¹¹C](R)-rolipram specific binding following the administration of GSK356278 were related to plasma GSK356278 concentrations at the start of PET scanning using an E_{MAX} occupancy model. The model

$$OCC = \frac{C_P^{GSK356278}}{C_P^{GSK356278} + EC_{50}}$$

was fitted to the data to obtain estimates of the half maximal effective concentration (EC_{50}). A paired sample one-tailed t-test with a significance level of 0.05 was used, under the assumption that population is normally distributed, to assess V_T changes at 3h and 8h compared to baseline. Considering the small sample size the Wilcoxon signed rank test was also used to compare PET 1 with PET 2 and PET 3 with the critical value Wilcoxon $W \leq 3$ for $p \leq 0.05$. Six subjects completed both post-dose scans and two subjects completed only a single post-dose scan (one at 3h and one at 8h), therefore yielding $N=7$ for both post-dose t-tests.

FIGURE 1 A. Anatomical MRI and PET integrated activity from 30 to 90 minutes post [¹¹C](R)-rolipram injection at baseline, post-dose 1 (3h) and post-dose 2 (8h) for subject 2. Data for each scan have been normalized by the injected activity per liter (%ID/L). B. Regional measured data (circles) and model fits (lines) for subject 2. For each region the baseline (red), post-dose 1 (3h, green) and post-dose 2 (8h, blue) time activity curves are shown.

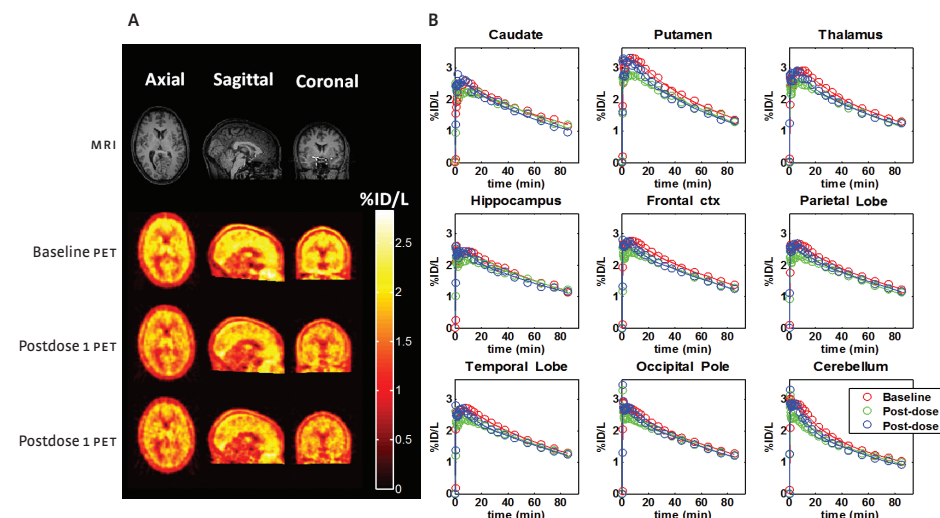
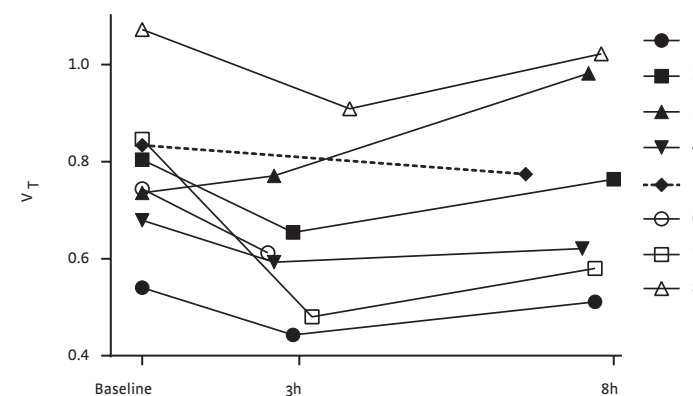


FIGURE 2 Global brain volumes of distribution (v_T) for baseline, 3h and 8h post-dose scan in all 8 subjects. Subjects 5 and 6 completed one post-dose scan.



Results

The mean (\pm sd) injected dose for the 22 PET scans in this study was 270 ± 61 MBq with specific activity of 76 ± 56 GBq/ μ mol. After injection, the tracer readily entered the brain and showed widespread distribution. The images and the regional TACs for a representative subject are presented in Figure 1a and 1b respectively.

A two-tissue compartment model using the metabolite-corrected plasma input function described the kinetics of [11 C](R)-rolipram well in all ROIs. The plasma free fractions (f_p) were similar in PET 1, 2 and 3 with mean (\pm sd) values of $7.4 \pm 3.4\%$, $7.5 \pm 2.6\%$ and $8.5 \pm 2.9\%$ respectively. [11 C](R)-rolipram V_T estimates are presented in Table 1 and Figure 2. The baseline [11 C](R)-rolipram V_T values seen in our study were consistent with those seen in previous human studies⁸. Intersubject variability (coefficient of variation) in the baseline V_T values (N=8) was 20%. Oral administration of 14 mg of GSK356278 led to a mean (\pm sd) reduction in V_T of $17.2 \pm 14.1\%$ at approximately 3h post-dose and $4.1 \pm 19.1\%$ at approximately 8h post-dose. The reduction in V_T was statistically significant at PET 2 ($p=0.012$, Wilcoxon $W=1$) but not at PET 3 ($p=0.271$, $W=6$). The magnitude of the decrease was similar across the 9 ROIs in the brain (range 16-20% for PET 2 and 0-8% for PET 3).

FIGURE 3 Individual plasma GSK356278 concentration-time curves. the dotted lines show the average time of the post-dose scans.

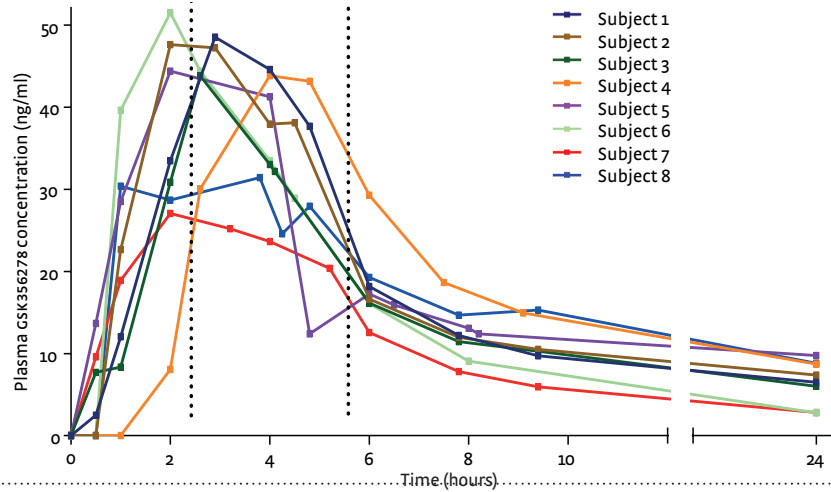
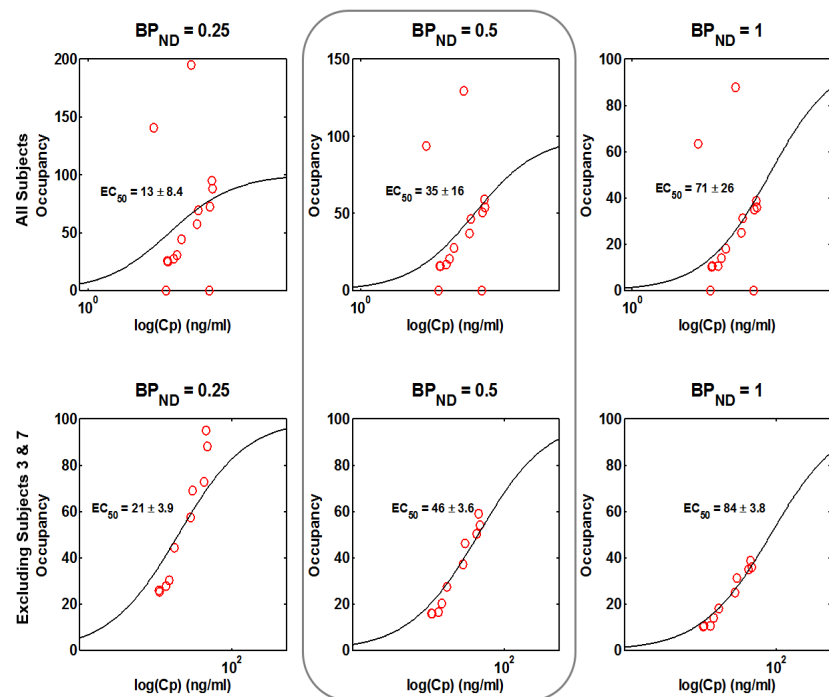


TABLE 1 [11 C](R)-rolipram binding in all 8 subjects expressed as v_T for the whole brain (global) and 9 regions of interest (ROI). Plasma GSK356278 concentration was measured at the start of PET. The bottom three rows show the column means for all subjects, i.e. N=8 for baseline scans and N=7 for post-dose scans. v_T , volume of distribution; v_{ND} , non-displaceable volume of distribution; BP^*_{ND} , estimated non-displaceable binding potential.

Subject	PET Time Post-dose (hr)	Whole brain	ROI VT													
		Global v_T	VT reduction Post-dose	Plasma 278 (ng/ml)	v_{ND} estimates and PDE4 occupancy			Caudate	Putamen	Thalamus	Hippocampus	Frontal Cortex	Parietal Lobe	Occipital Pole	Temporal Lobe	Cerebellum
					$BP^*_{ND} = 0.25$	$BP^*_{ND} = 0.5$	$BP^*_{ND} = 1$									
1	Pre	0.54			0.43	0.37	0.27	0.53	0.6	0.58	0.51	0.55	0.52	0.56	0.53	0.48
	2.9	0.44	18.0%	48.5	88%	54%	36%	0.43	0.50	0.46	0.43	0.44	0.42	0.47	0.45	0.39
	7.7	0.51	5.4%	12.2	25%	16%	11%	0.49	0.59	0.52	0.5	0.52	0.52	0.53	0.5	0.43
2	Pre	0.80			0.64	0.56	0.40	0.76	0.91	0.85	0.74	0.89	0.79	0.82	0.8	0.68
	2.9	0.65	18.7%	47.2	95%	59%	39%	0.62	0.73	0.68	0.64	0.7	0.62	0.69	0.66	0.55
	8	0.76	5.0%	12.0	26%	16%	10%	0.7	0.85	0.8	0.74	0.82	0.77	0.8	0.78	0.62
3	Pre	0.74			0.59	0.50	0.37	0.68	0.85	0.79	0.73	0.75	0.7	0.76	0.72	0.64
	2.6	0.77	-4.8%	43.8	0	0	0	0.76	0.90	0.79	0.72	0.8	0.76	0.81	0.76	0.64
	7.6	0.98	-33.5%	11.5	0	0	0	0.93	1.08	1.04	0.98	1.01	0.97	1.02	0.96	0.85
4	Pre	0.68			0.54	0.46	0.34	0.65	0.81	0.7	0.68	0.72	0.66	0.69	0.63	0.57
	2.6	0.60	12.6%	30.1	57%	37%	25%	0.56	0.69	0.63	0.59	0.62	0.56	0.63	0.57	0.49
	7.5	0.62	8.5%	18.6	44%	27%	18%	0.66	0.69	0.65	0.59	0.66	0.6	0.62	0.61	0.51
5	Pre	0.83			0.67	0.57	0.42	0.82	0.96	0.91	0.86	0.85	0.8	0.86	0.82	0.63
	6.6	0.77	7.2%	16.0	30%	20%	14%	0.8	0.88	0.82	0.81	0.8	0.73	0.78	0.78	0.57
6	Pre	0.74			0.60	0.50	0.37	0.75	0.91	0.8	0.76	0.73	0.68	0.78	0.71	0.58
	2.5	0.61	17.8%	44.4	73%	50%	35%	0.58	0.76	0.65	0.63	0.63	0.56	0.65	0.59	0.46
7	Pre	0.85			0.68	0.58	0.42	0.73	1.02	0.87	0.86	0.86	0.83	0.89	0.85	0.7
	3.2	0.48	43.2%	25.2	195%	130%	88%	0.42	0.55	0.5	0.48	0.51	0.47	0.51	0.5	0.38
	7.7	0.58	31.4%	7.8	141%	94%	63%	0.5	0.69	0.61	0.59	0.59	0.56	0.61	0.59	0.48
8	Pre	1.07			0.86	0.74	0.54	0.93	1.3	1.1	1.08	1.13	1.1	1.12	1.04	0.85
	3.8	0.91	15.2%	31.4	69%	46%	31%	0.8	1.07	0.95	0.88	0.95	0.93	0.96	0.93	0.71
	7.8	1.02	4.7%	14.7	28%	17%	11%	1.02	1.16	1.07	1.02	1.06	1.03	1.06	1.01	0.77
	Pre	0.78														
	2.9	0.64	17.2%	38.7		54%		17	19	18	18	17	18	16	16	20
	7.6	0.75	4.1%	13.3		27%		0	8	5	4	5	4	5	3	7

FIGURE 4 Model fits of the PET occupancy data and plasma GSK356278 concentration with estimated EC_{50} in all subjects examined (top row) and for the data set excluding subjects 3 and 7 (bottom row). Column 2 represents the most likely value of the non-displaceable binding potential (BP_{ND}) while the other two columns are intended to show the effect of a different estimate of BP_{ND} on the EC_{50} .



The individual plasma GSK356278 concentration-time curves are presented in Figure 3. The mean C_{MAX} was 42.3 ng/ml. Figure 4 shows plasma GSK356278-PDE4 occupancy plots using three different estimates of BP_{ND} . Visual inspection suggested that subjects 3 and 7 may be outliers, with ΔV_T (and occupancies) for these subjects being notably different from the mean ΔV_T of the sample as a whole. Plasma free fractions were similar between the three PET scans in subject 3 (range 6.3 to 9.3%) and subject 7 (range 11.8 to 12.0%). The modified Thompson Tau test was used to determine if the ΔV_T for these subjects were outliers. The method takes into account the sample mean, SD and N, and provides a statistically determined

rejection value. Subject 7's ΔV_T for both post-dose scans exceeded the rejection region of 1.7 SD. Subsequently the test was applied to ΔV_T with N=6 and identified both post-dose scans of subject 3 as outliers. The test on N=5 did not identify additional outliers. We therefore examined the group ΔV_T again without subjects 3 and 7. The reduction (\pm SD) in average V_T for N=5 was $16.4 \pm 2.5\%$ and $6.1 \pm 1.7\%$ for 3h and 8h data respectively ($p < 0.001$, $W=0$). The estimated mean PDE4 occupancy was $49 \pm 8\%$ at 3h, and $19 \pm 5\%$ at 8h. The *in vivo* affinity of GSK356278, excluding subjects 3 and 7, was estimated as $EC_{50} = 46 \pm 3.6$ ng/ml, leading to an estimated PDE4 occupancy of 48% at plasma T_{MAX} .

Discussion

To our knowledge, this is the first study to explore the blockade of the human PDE4 enzyme in the brain *in vivo*. Baseline V_T values obtained in this study were consistent with those seen in previous human studies^{2,8}. The between subject variability (coefficient of variation) of the baseline V_T was 20%, comparable to earlier reports of 25%⁸. Oral administration of the PDE4 inhibitor GSK356278 led to a mean V_T reduction of 17% around 3 hours post-dose compared to the baseline V_T , and a reduction of 4% around 8 hours post-dose, consistent with the hypothesis that GSK356278 enters the brain readily and binds to PDE4. V_T change in all subjects followed the plasma concentration of GSK356278, with ΔV_T PET 2 > ΔV_T PET 3. The estimated relationship between the plasma concentration of GSK356278 and PDE4 occupancy indicates that occupancies of close to 50% of PDE4 are achieved at T_{MAX} following the administration of single oral doses of 14mg of GSK356278. The available data provides no evidence for indirect pharmacokinetics for GSK356278 in the human brain, suggesting that the plasma EC_{50} (46 ng/ml) estimated in this study can be used to calculate PDE4 occupancy following repeat dose administration.

The assessment of the relationship between PDE4 occupancy and plasma GSK356278 concentration was complicated by our inability to estimate the [¹¹C] (R)-rolipram BP_{ND} directly from the study data, due to the relatively low levels of occupancy achieved. Our population estimate of BP_{ND} from the literature ignores between subject variability in PDE4 expression. Although an error in the estimate of BP_{ND} would lead to an error in the estimated EC_{50} , a relatively large range of BP_{ND} estimates (0.25 to 1) produced a modest difference in GSK356278 EC_{50} (21-84 ng/ml), indicating that our estimated EC_{50} is relatively robust to variability in assumed. In the absence of higher levels of occupancy or associated estimates with the inactive

enantiomer [¹¹C](S)-rolipram it is not possible to confirm individual variability in directly. GSK356278 EC₅₀ of 46 ng/ml with a plasma C_{max} of 42.3 ng/ml leads to an estimated PDE4 occupancy of 48% at T_{max}, with a range of 34% - 67% (depending on the BP_{ND} estimate).

Subjects 3 and 7 were identified as outliers based on abnormal post-dose V_T compared to the baseline. Specifically, subject 3 showed an increase in post-dose V_T, whereas subject 7 showed an exceptionally large reduction, leading to occupancy at 3h > 100%. The metabolite-corrected arterial input function and plasma free fraction of [¹¹C](R)-rolipram for these subjects did not differ between scans, making it unlikely that changes in blood flow or plasma protein binding could explain these findings. Variability in estimated parameters are thus the most likely explanation for the findings in these subjects. Test-retest variability of V_T in healthy humans was shown to be approximately 19% in an earlier study of 12 subjects⁸.

PDE enzyme activity dysfunction has been implicated in disease states such as asthma, ischemic stroke and CNS disorders. In a study of patients with major depressive disorder, [¹¹C](R)-rolipram binding was reduced by 18% compared to healthy control subjects, and could be partially normalized with selective serotonin reuptake inhibitor treatment⁹. PDE4 selectively metabolizes cAMP in the brain to the inactive monophosphate and is therefore an important component of the cAMP cascade. The enzymatic activity of PDE4 is regulated by protein kinase A (PKA) via a feedback mechanism, with high concentrations of cAMP stimulating PKA to phosphorylate PDE4, thereby increasing its enzymatic activity and returning the concentration of cAMP to steady state. Unilateral injection of a PKA activator and inhibitor into the rat striatum was shown to significantly increase and decrease, respectively, the binding of [¹¹C](R)-rolipram as measured with PET³. Upregulation of the cAMP cascade through long-term pharmacological inhibition of the PDE4 enzyme is a promising therapeutic intervention for a range of conditions. In preclinical studies, GSK356278 was shown to improve performance in an object retrieval test in cynomolgus macaques⁶, consistent with the reported effects of rolipram in various tests of cognition¹⁰. Despite the possible benefits of brain-penetrant PDE4 inhibitors, clinical use has been limited by mechanism-dependent adverse events such as nausea and emesis¹¹. The highest dose in this study was limited to 14 mg (equivalent to ~50% occupancy) by these adverse events in Phase I studies.

In conclusion, we present the first human report of PDE4 occupancy measured directly in the human brain with PET. Our data will be used in conjunction with the known plasma GSK356278 pharmacokinetics to determine optimal doses to be used in future clinical development.

REFERENCES

- 1 DaSilva JN, Lourenco CM, Meyer JH, Hussey D, Potter WZ, Houle S.: Imaging cAMP-specific phosphodiesterase-4 in human brain with R-[¹¹C]rolipram and positron emission tomography: *European Journal of Nuclear Medicine and Molecular Imaging*. 2002 Dec;29(12):1680-3. Available from: <https://doi.org/10.1007/s00259-002-0950-y>
- 2 Matthews, JC, Passchier J, Wishart MO, Martarello, L, Comley RA, Parker CA, Knibb ST, Hopper RV, Brown J, Gee AD.: The characterisation of both the R and S enantiomers of rolipram in man [abstract]: *Journal of Cerebral Blood Flow and Metabolism*. 2003;23 suppl:678J.
- 3 Itoh T, Abe K, Hong J, Inoue O, Pike VW, Innis RB, Fujita M.: Effects of cAMP-dependent protein kinase activator and inhibitor on in vivo rolipram binding to phosphodiesterase 4 in conscious rats: *Synapse*. 2010 Feb;64(2):172-6. Available from: <https://doi.org/10.1002/syn.20728>
- 4 Parker CA, Matthews JC, Gunn RN, Martarello L, Cunningham VJ, Dommett D, Knibb ST, Bender D, Jakobsen S, Brown J, Gee AD.: Behaviour of [¹¹C]R(-) and [¹¹C]S(+)-rolipram in vitro and in vivo, and their use as PET radiotracers for the quantitative assay of PDE4. *Synapse*. 2005 Mar 15;55(4):270-9. Available from: <https://doi.org/10.1002/syn.20114>
- 5 Guercio G, Castoldi D, Giubellina N, Lamonica A, Ribecai A, Stabile P, Westerduin P, Dams R, Nicoletti A, Rossi S, Bismara C, Provera S, Turco L.: Overall synthesis of GSK356278: Quick delivery of a PDE4 inhibitor using a fit-for-purpose approach: *Organic Process Research and Development*. 2010;14(5):1153-61. Available from: <https://doi.org/10.1021/op1001148>
- 6 Rutter AR, Poffe A, Cavallini P, Davis TG, Schneck J, Negri M, Vicentini E, Montanari D, Arban R, Gray FA, Davies CH, Wren PB.: GSK356278, a potent, selective, brain-penetrant phosphodiesterase 4 inhibitor that demonstrates anxiolytic and cognition-enhancing effects without inducing side effects in preclinical species: *The Journal of Pharmacology and Experimental Therapeutics*. 2014 Jul;350(1):153-63. Available from: <https://doi.org/10.1124/jpet.114.214155>
- 7 Tziortzi AC, Searle GE, Tzimopoulou S, Salinas C, Beaver JD, Jenkinson M, Laruelle M, Rabiner EA, Gunn RN.: Imaging dopamine receptors in humans with [¹¹C]-(+)-PHNO: dissection of D3 signal and anatomy: *NeuroImage*. 2011 Jan 1;54(1):264-77. Available from: <https://doi.org/10.1016/j.neuroimage.2010.06.044>
- 8 Zanotti-Fregonara P, Zoghbi SS, Liow J, Luong E, Boellaard R, Gladding RL, Pike VW, Innis RB, Fujita M.: Kinetic analysis in human brain of [¹¹C](R)-rolipram, a positron emission tomographic radioligand to image phosphodiesterase 4: a retest study and use of an image-derived input function: *NeuroImage*. 2011 Feb 1;54(3):1903-9. Available from: <https://doi.org/10.1016/j.neuroimage.2010.10.064>
- 9 Fujita M, Richards EM, Nicu MJ, Hines CS, Pike VW, Zarate Jr CA, Innis RB.: cAMP Signaling in Brain is Decreased in Unmedicated Depressed Patients and Increased by Treatment with a Selective Serotonin Reuptake Inhibitor: *Molecular Psychiatry*. 2017 May 22(5):754-759 Available from: <https://doi.org/10.1038/mp.2016.171>
- 10 Rutten K, Van Donkelaar EL, Ferrington L, Blokland A, Bollen E, Steinbusch HW, Kelly PA, Prickaerts JH.: Phosphodiesterase inhibitors enhance object memory independent of cerebral blood flow and glucose utilization in rats: *Neuropsychopharmacology*. 2009 Jul;34(8):1914-25. Available from: <https://doi.org/10.1038/npp.2009.24>
- 11 Spina D.: PDE4 inhibitors: current status: *British Journal of Pharmacology*. 2008 Oct;155(3):308-15. Available from: <https://doi.org/10.1038/bjpp.2008.307>

CHAPTER 7

DISCUSSION AND CONCLUSIONS



Four decades of multidisciplinary PET research has provided a wealth of studies that show the utility of molecular imaging for biomarker quantification and drug development (introduced in chapter 1). This thesis builds on that work with a literature review of dosimetry of carbon-11 labelled radiotracers (chapter 2) as well as four original PET studies describing the evaluation of novel radiotracers (chapters 3 to 6). The current chapter summarises the most important results of this thesis and places them in the context of recent developments in the field of PET imaging.

Dosimetry

In the development of novel drugs and radiotracers, studies into the timing, magnitude, and location of pharmacological effects are typically performed first in rodents¹ and/or non-human primates (NHP)², and subsequently in human subjects³. Prior to clinical implementation of novel PET radiotracers, national as well as local ethics and safety bodies require estimates of the radiation dose and associated risk arising from the intravenous administration of the radiopharmaceutical. In PET studies of the brain, there is usually a clear relationship between the amount of radioactivity injected and the accuracy and precision of imaging outcome measures. Quantification in regions with low radiotracer binding and/or low volumes requires injection of sufficient activity (expressed in megabecquerel) in order to obtain a good signal-to-noise ratio during the course of the PET scan. For example, a recent comparison of dynamic PET images of the D_2/D_3 radiotracer [^{11}C]PHNO that were reconstructed into images corresponding to injected activities of 212, 106, 53, 26 and 13 MBq showed that the estimated coefficient of variation of the [^{11}C]PHNO binding potential in the substantia nigra ranged from 13% for a 211 MBq scan to 48% for a 13 MBq scan⁴. In contrast, the larger putamen returned an acceptable coefficient of variation with injected activities as low as 13 MBq. With the current generation of PET scanners, the experimental study design and/or data quality still needs to be balanced against radiation limits. One megabecquerel corresponds to one million disintegrations of unstable atomic nuclei per second, exposing the subject to a source of ionising radiation until the radioisotope has decayed completely, which in the case of carbon 11 is approximately 5 half-lives or 100 minutes later. The total amount of radiation absorbed by the body divided by its mass (i.e. assuming homogeneous distribution) is not adequate to estimate the risks associated with exposure to radiation since it does not take into account non-uniform irradiation or differences in tissue sensitivity. The lung for example, is more sensitive to radiation than

the liver⁵. Tissue weighting factors enable the calculation of effective dose, which represents the relative risk contribution arising from each organ or tissue should the whole body be irradiated uniformly. In chapter 2, the methods to estimate radiation dose in animals and humans are reviewed, as well as the biological effects of the (relatively low levels of) radiation associated with carbon-11 labelled PET tracers. A literature review of 42 papers was performed and radiation burden was compared between tracers⁷.

The main finding in our review of human dosimetry studies was that the 95% confidence interval of the mean effective dose is small, with a range of 5.2-6.6 $\mu\text{Sv}\cdot\text{MBq}^{-1}$. Furthermore, inspection of ten animal studies suggested that preclinical dosimetry is not sufficiently reliable as a predictor for human dose estimates chiefly because of significant interspecies differences. Carbon-11 radiotracer dosimetry in animals prior to human imaging may therefore not offer significant value, and the benefit of animal dosimetry should be critically reviewed before experiments are committed to.

In a clinical setting, many PET centres in Europe follow the International Commission on Radiological Protection (ICRP) guidance that indicates a whole body effective dose constraint of 10 mSv (or less) per research subject, where they are not expected to benefit personally⁶⁵. The dosimetry data in chapter 2 show that up to four PET scans of 300 MBq can be acquired in a single subject for all radiotracers except one, while still staying below the 10 mSv constraint. For radiopharmaceuticals that are administered in the United States under an Investigational New Drug Application (IND), there are no specific radiation dose limits. In studies performed at institutions that follow U.S. Radioactive Drug Research Committee legislation where no IND has been obtained for the radiotracer, the maximum injected activity per scan is most likely limited by the so called critical organ, for which a maximum absorbed dose of 50 mSv is set. We show in chapter 2 that an organ limit of 50 mSv per scan corresponds to an injected dose of between 500 to 3000 MBq depending on the radiotracer. In clinical practice, the injected dose from carbon-11 labelled tracers rarely exceeds 400 MBq per scan as this provides a good signal-to-noise ratio for all regions of interest. However, PET protocols frequently include repeat scanning in a single subject, for example in receptor occupancy studies that provide a quantitative relationship of plasma and brain concentrations^{7,8}. Annual dose limits that cover the time frame of subjects' study enrolment are therefore more appropriate. The US regulations allow the annual absorbed radiation organ dose to be up to 150 mSv. Data show that this limit, translated into injected activity, is at least three

times higher than the ICRP recommendations of a 10 mSv whole-body maximum⁶. The radiation doses administered in PET studies are so low that any harmful effects are likely to be stochastic in nature, meaning that as the dose increases the probability of harm increases, rather than the severity of symptoms. In chapter 3, human PET experiments are presented that calculate the radiation risk for the novel NMDA receptor radiotracer [¹¹C]GMOM⁹. In these first-in-human PET experiments, [¹¹C]GMOM was shown to cross the blood-brain-barrier in all 5 subjects. Whole-body PET scans over 80 minutes allowed the visualisation of [¹¹C]GMOM distribution and elimination in each subject. Seven source organs were defined manually on the CT scans of three female and two male subjects. The radioactivity concentration-time course was measured to calculate carbon-11 residence times in the source organs and scaled to a gender specific reference. The effective dose (\pm SD) was $4.5 \pm 0.5 \mu\text{Sv}\cdot\text{MBq}^{-1}$, which is at the lower end of the range seen for other carbon-11 labelled ligands.

Radiation Considerations for Future Carbon-11 PET Studies

Compared with an effective dose of around 15 to 30 $\mu\text{Sv}\cdot\text{MBq}^{-1}$ for most fluorine-18 tracers¹⁰, carbon-11 tracers generally display a relatively modest radiation dose profile. Since all but one of the reviewed carbon-11 labelled PET tracers in chapter 2 have an effective dose under 9 $\mu\text{Sv}\cdot\text{MBq}^{-1}$, the data in this thesis support the notion that for first-time-in-human studies with a new carbon-11-labelled small molecule PET tracer where no human dosimetry data are available, one could assume an effective dose of 10 $\mu\text{Sv}\cdot\text{MBq}^{-1}$ (equal to the mean effective dose plus two standard deviations). A single PET scan of the region of interest would be possible while maintaining a wide radiation safety margin. Shortly after the publication of chapter 2, Zanotti-Fregonara and Innis¹¹ expanded on this advice by suggesting an experimental design to safely perform first-in-human studies of new carbon-11 labelled tracers:

- Perform one whole-body scan in a single human subject with a $\sim 370 \text{ MBq}$ (10 mCi) injected dose. If the radioactivity is fairly widely distributed in the body, it would negate the hypothesis that any organ dose is likely to exceed the theoretical maximal irradiation hypothesized by Gatley¹². In chapter 2 we describe how this model represents a worst-case scenario, assuming that the carbon-11 labelled compound is instantaneously distributed in the plasma and then transferred

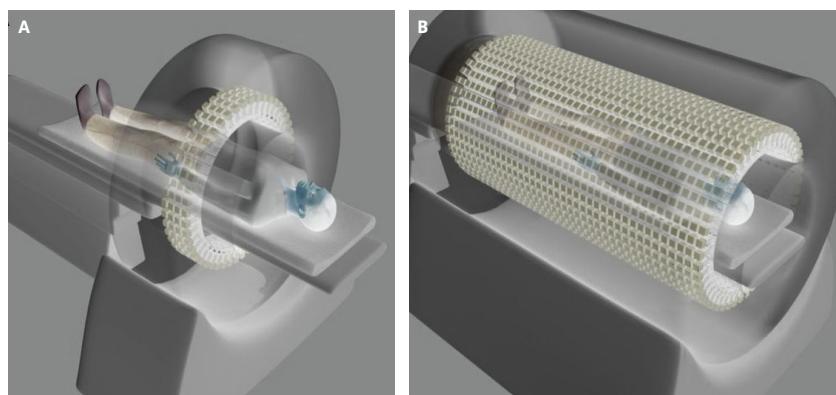
solely and irreversibly to a single organ. In reality however, the assumption of immediate uptake and trapping of the tracer until radioactivity has decayed never holds.

- To determine whether the radiotracer has a suitable pharmacokinetic profile in the organ of interest (e.g. brain), perform 5 to 10 scans using doses up to 740 MBq, which would allow two scans in a single subject. If a (specific) signal can be identified in the brain, it is important to assess its stability over time and effects of biological variability and measurement variability.
- If the radioligand looks promising, complete the human dosimetry study by acquiring a total of six to ten whole-body scans at 370 MBq (10 mCi) each.

An integral part of all PET activities in biomedical research are the two basic principles of radiation protection: Justification of irradiation and administration of a dose that is as low as reasonably achievable (ALARA) or practicable (ALARP) consistent with the aim of the investigation. It could be argued that in cases where a carbon-11-labelled radiotracer will not be administered more than twice in the same subject, the radiation dose is unlikely to exceed an effective dose of 10 mSv or an organ dose of 150 mSv. In fact, for 31 out of 32 radiotracers reviewed in chapter 2, the 10 mSv constraint will not be exceeded even if three 400 MBq PET-CT brain scans would be performed in the same subject (1200 MBq at $7.8 \mu\text{Sv}\cdot\text{MBq}$ equals 9.4 mSv). However, the reported effective doses are group means that can at best only be representative of a population and should not be used to calculate the risk to a particular individual. It has been suggested that biological half-life and fractional uptake differ across individuals with an estimated biokinetic variability factor of two¹³. Nevertheless, effective dose is less affected by individual variability in organ dose due to multiplication of the absorbed dose by tissue weighting factors. Considering that the radiation burden of carbon-11 labelled tracers is relatively low and serial PET scanning in the same subject is possible for all tracers, it could be argued that carbon-11 dosimetry studies in groups of healthy volunteers should only be performed if the radiotracer is foreseen to be repeatedly administered in large groups of subjects. Not only do whole-body PET-CT dosimetry scans expose subjects to potentially unnecessary radiation, they also put a burden on expensive resources such as clinical scanners, highly trained staff and laboratory equipment. In this respect, it is vital to have agreement between PET researchers that a new radiotracer is indeed promising enough to justify further irradiation of subjects in a dosimetry study.

Radiotracers are distributed throughout the entire body after intravenous administration (assuming blood-brain barrier penetration). However, current PET scanners only contain a small portion of the body within the field of view, generally approximately 20 cm. It has been estimated that no more than ~3-5% of the available photon pairs that escape the body without being attenuated or scattered can be detected by the scanner¹⁴. The first prototype total-body scanner has recently been developed, which increases the coverage of detector rings to encompass the entire body (Figure 1,¹⁵).

FIGURE 1 Whole-body pet (A) versus total-body pet (B).



The sensitivity can be significantly increased by a factor of ~24 for PET scans from the top of the head to the groin. This gain can be used in several ways, for example to (i) increase the signal-to-noise ratio, (ii) reduce imaging time, (ii) reduce the injected activity, or a combination of these. With a total-body PET scanner, a carbon-11 dosimetry scan could be performed with injections of just 20 MBq, resulting in negligible effective doses. Since multiple bed positions are not required anymore, total-body PET also opens up the possibility of pharmacokinetic scans of multiple organ systems after novel radiolabelled compounds have been administered not only intravenously, but also orally or intranasally. Furthermore, the increased signal-to-noise ratio allows radiotracers to be followed for significantly longer time courses than is currently possible. For example, it has been estimated that for ¹⁸F-labelled radiotracers, imaging could be conducted as late as ~18 hours before

the signal decays, and ~3 hours for carbon-11¹⁴. The large gain in sensitivity of the total-body PET/CT scanner will broaden the utility of PET for radiation biodistribution studies, but most importantly it will introduce a whole range of new impactful applications in medical research and drug development.

PET of Glutamate Receptor Pharmacology

The search for more efficacious pharmacotherapies for CNS disorders relies heavily on exploiting novel drug targets, such as glutamatergic receptors. Glutamate is the most abundant neurotransmitter in the vertebrate nervous system and the major mediator of excitatory signals. Brain tissue contains as much as 5 - 15 mmol glutamate per kg, depending on the region, more than of any other amino acid¹⁶. It has been estimated that 80% of the energy utilisation in the brain is for membrane repolarization after glutamate release¹⁷. There are more than 20 different glutamate receptors, including the ionotropic NMDA receptor which is permeable to calcium when activated. Pharmacological blockade of the ion channel and negative allosteric modulation of the GluN2B (NR2B) binding site of NMDA receptors may have therapeutic potential for the treatment of a wide range of CNS pathologies¹⁸. Although several molecules have been developed as CNS drugs for these targets¹⁹, the strict physiochemical and pharmacological characteristics that are required for radiotracers in order to be suitable for in vivo quantitative target binding have been challenging to perfect. In contrast to novel CNS therapeutics, where the elimination half-life would ideally allow for once-daily dosing, radiotracers benefit from medium-to-fast metabolism and elimination. A rapid reduction of the radiotracer concentration in the free compartment, in combination with low non-specific binding, minimises noise from the non-displaceable PET signal²⁰. The challenges in the radiotracer development process are akin to drug development in that there is considerable attrition of candidates during preclinical to clinical translational studies due to the narrow range of suitable attributes²⁰. In addition, PET studies must adhere to numerous complex regulations concerning toxicology, radiation exposure, manufacturing licenses, manufacturing practices, the type of approvals needed (depending on the objective of the investigation, the study population and whether or not it is considered to be a clinical trial) and the approval and conduct of clinical studies themselves. A successful PET ligand requires optimisation of many parameters such as affinity, selectivity, lipophilicity, stability, radiolabelling feasibility, blood-brain barrier penetration and pharmacokinetics²¹.

Radiotracer development programmes at the VU University Medical Center (Amsterdam UMC, The Netherlands) have shown significant advancements in the identification and synthesis of radioligands for the ion channel and GluN2B binding sites of the NMDA receptor^{22,23,24}. In chapter 4 and 5, two novel glutamatergic candidate radiotracers were evaluated in humans and non-human primates (NHP) by performing experiments that assessed the kinetic profile of the radiotracers and its metabolites in the brain, blood and plasma. In both studies, attempts were made to block the specifically bound fraction with intravenously administered pharmacological challenges that were expected to compete with the radiotracer at the NMDA receptor binding site. Target occupancy in NHP and humans are generally highly correlated, after adjusting for interspecies differences in plasma-free fraction and bioavailability. In addition, there is a strong scientific case for NHP studies when investigational compounds have not been approved (yet) for human administration, as is currently the case for GluN2B negative allosteric modulators.

In chapter 4, the initial PET assessment of [¹¹C]HACH242 in three NHPs is presented. A hybrid PET-MRI scanner was used in conjunction with an arterial input function in an attempt to quantify [¹¹C]HACH242 binding before and 10 minutes after administration of an intravenous dose of radiprodil. This negative allosteric modulator of the GluN2B receptor was expected to reduce the signal of [¹¹C]HACH242, which after modelling of the data could reveal the extent of specific radiotracer binding to the NMDA receptor in the brain. Results showed that [¹¹C]HACH242 enters the brain and produced time-activity curves (TACs) that showed appropriate reversible pharmacokinetics within the 90 minute duration of the PET scan. However, no consistent blocking effect was observed in the radiprodil condition. In chapter 4, a number of questions and issues which may explain these results have been addressed or proposed for investigation in future research. Amongst these are (i) whether changes in cerebral blood flow (CBF) underlie the lack of clear changes in [¹¹C]HACH242 TACs, (ii) the effect of radiprodil on the delivery of parent [¹¹C]HACH242 from blood to tissue, and other sources of variability in the input function, (iii) endogenous ligands competing with radiotracer acting at NMDA receptors that affect the in vivo binding properties of the radioligand, (iv) non-selectivity of [¹¹C]HACH242.

Reliable input functions for kinetic modelling could not be generated because of variability in the whole blood radioactivity measurement during the first minutes post tracer injection. A closer look at the individual TACs does not show a clear relationship between the area under curve of the standardised uptake values (SUV) in plasma and brain. Furthermore, although the metabolite analyses represent a useful approximation, more detailed studies are required to assess the contribution

of radiometabolites to the non-displaceable signal, preferably in humans. To minimise factors that could influence the PET signal, future attempts at visualising the GluN2B binding site of the NMDA receptor are preferably performed in humans. This may avoid potential CBF effects of anaesthetics and will allow for larger volumes of arterial blood to be drawn. First-in-human clinical trials with novel GluN2B specific ligands other than radiprodil will enable the clinical evaluation of [¹¹C]HACH242. Further assessment of test-retest variability and specific binding is therefore warranted.

The radiotracer [¹⁸F]PK-209, developed by VUMC radiochemists Pieter Klein and colleagues²², binds to the phencyclidine binding site of the NMDA receptor, which sits within the ion channel in the transmembrane domain. Preliminary evidence indicated that [¹⁸F]PK-209 exhibits quantifiable binding in non-human primates²⁵. Since PET in primates is highly amenable to clinical translation, glutamatergic neurotransmission in the human brain was investigated with [¹⁸F]PK-209 in a first-time-in-human PET study, presented in chapter 5. A radiotracer should provide a stable signal over a period of days and months in order to study drug occupancy, assuming that the density of the target remains relatively constant. Two aims of the PET study were to assess [¹⁸F]PK-209 test-retest (TRT) variability within subjects and to characterise the specific binding component by comparing the baseline scan results to those following intravenous ketamine infusion. The NMDA receptor is expressed throughout the CNS, hence a reference region devoid of NMDA receptors was not available. Arterial blood sampling was performed during each scan and a metabolite corrected input function generated.

With a scan time of 120 minutes, the best model fits to describe the in vivo kinetics of [¹⁸F]PK-209 were obtained using an irreversible two-tissue model with blood volume parameter (2T3k_VB) in 8 out of 10 test-retest scans and 6 out of 10 scans in the ketamine group. There were no brain regions of interest (ROIs) that consistently favoured a kinetic model other than the 2T3k_VB model. However, the significant correlation between 2T3k_VB model agreement and ROI size indicates that TACs in smaller brain ROIs were affected more by noise, and thus described adequately by several models. TACs showed that [¹⁸F]PK-209 readily entered the brain and displayed a fairly uniform pattern of uptake, with the rank-order of highest to lowest K₁ in ROIs being brainstem > cortex > cerebellum/thalamus/hippocampus/insula > dorsal striatum. This is partly consistent with the spatial distribution of [¹⁸F]PK-209 binding in the rhesus monkey brain²⁵, and approximately 50% higher in cortex compared with binding in the cerebellum, thalamus and dorsal striatum. The TRT variability however was relatively large, showing a mean 24% difference

in whole-brain grey matter K_i between test and retest PET scans. The irreversible binding component K_i did not correlate with the last 30 minutes of the time activity curve, SUV_{90-120} . Only small irreversibility was observed, therefore it is possible that the last 30 min is still dominated by free and non-specific binding. Irreversible binding prohibited the assessment of the equilibrium partition coefficient between radioligand in plasma and the total concentration of radioligand in the tissue. Model independent graphical analysis techniques such as Patlak and Logan methods were not investigated due to the uncertainty in the arterial plasma measurements.

The discussion of chapter 5 includes a thorough investigation of the PET and blood data to evaluate the factors that may have contributed to the high TRT variability and absence of a reliable reduction in [^{18}F]PK-209 signal despite high plasma ketamine concentrations. These factors include:

- Differences in subject characteristics such as age
- Differences in [^{18}F]PK-209 injectate such as activity and molar activity
- Diurnal and seasonal variation such as duration of daylight
- The interval between test and retest scans
- The relationship between non-displaceable distribution volumes ($V_{ND}=K_1/k_2$) as well as K_1 and k_3
- Radiotracer pharmacokinetics in blood, plasma and brain
- ROI size in relation to kinetic model fits
- Target density in brain ROIs in relation to [^{18}F]PK-209 binding
- [^{18}F]PK-209 radiometabolites and parent fraction variation within subjects and between subjects
- Recovery fractions of radioactivity from plasma
- Ketamine plasma concentrations and potency at the binding site
- Ketamine's potential cerebral blood flow effects
- In vivo NMDA receptor biology and pharmacology

Measurement errors in the input function were methodically investigated. Blood data from arterial measurements during the PET scan showed that there is rapid blood pool clearance, combined with quick tracer metabolism that is similar to the rate reported for a comparable PCP radiotracer, [^{18}F]GE-179²⁶. In our dataset there were no significant changes in parent fraction between the test and retest scans. TRT variability was further examined as a function of parent fraction determination in the plasma. To this end, TACs were modelled with arterial input functions using parent fractions that were averaged within-subjects and across the two samples of 5 subjects. Within-subject input functions led to a reduction in K_i TRT

variability from 24% to 7%. Population averaged parent fractions may provide an avenue for further investigation in future PET studies with [^{18}F]PK-209 since TRT variability of K_i using the population-averaged input functions was acceptable at 11%. Mixed effects modelling of the PET data could also offer new insights into the tracer pharmacokinetics and TRT variability. Non-linear mixed effects modelling on a population instead of individual level could resolve both intra- and intersubject variability²⁷ and might allow the estimation of covariate effects such as the factors listed above.

The unsuccessful translation of pre-clinical to clinical results might be related to pharmacological differences between the two blocking compounds, MK-801 and S-ketamine. However, S-ketamine at lower plasma concentrations than reported in chapter 5 have been shown to reduce K_i of the carbon-11 labelled analogue of PK-209, [^{11}C]GMOM, in humans²⁸. Considering the preliminary evidence of specificity of the [^{11}C]GMOM PET signal for the ion channel of the NMRA receptor, it is recommended that test-retest variability experiments are performed before further clinical application of the radiotracer.

The variable test-retest signal of [^{18}F]PK-209 and [^{11}C]HACH242 could indicate that the tracers are sensitive to fluctuations in endogenous ligand such as glutamate (via GluN2), D-serine or glycine (via GluN1 or GluN3), or cations such as Mg^{2+} and Zn^{2+} . In addition, NMDA receptor internalisation and/or different brain distributions of glutamatergic transporters could have affected the binding of [^{18}F]PK-209 and hence complicate the interpretation. Variations in presynaptic glutamate release, altered glutamate uptake and release by glial cells, and altered glutamate metabolism could be investigated in future multimodal imaging studies, for example by using a combination of PET with 1H and ^{13}C magnetic resonance spectroscopy (MRS). A major limitation of MRS however is that it cannot distinguish between glutamate located extracellularly or intracellularly (where it does not exert effects on the NMDA receptor or PET radiotracer).

Natural variability in the affinity of [^{18}F]PK-209 for the binding site or changes in the number of binding sites might add variability to the PET measurements. In our small sample of 5 test-retest subjects, preliminary results showed a significant correlation between the scan interval in days and the reduction in K_i using the single scan input function, but not with subject- and population-averaged input functions. The observed correlation is likely due to either a systemic error in test or retest input function measurement or a true biological component resulting in lowered availability of the NMDA channel site for radiotracer binding during the second scan.

Future work is needed to understand the source of the variability and a full validation of these findings will require a larger cohort.

Imaging PDE4 Occupancy in Humans

The ability to characterise brain binding in humans as early in the drug development process as possible is valuable decision making regarding compound progression²⁹. The relationship between target occupancy and the plasma concentration of the drug over time can guide dose selection for subsequent clinical trials. In chapter 6, a third pharmacological experiment is described that relies on competition between the PET radiotracer and an administered drug. In contrast to the two NMDA receptor targets described in chapter 4 and 5, the target that was studied in chapter 6, phosphodiesterase 4 (PDE4), is located intracellularly. The PET tracer must therefore cross the plasma membrane to bind the target. The carbon-11 labelled R-enantiomer of rolipram, [¹¹C](R)-rolipram, was used to investigate the PDE4 occupancy of the novel compound GSK356278 in healthy volunteers. The mechanism of action of GSK356278 is thought to underlie upregulation of the cAMP cascade through long-term pharmacological inhibition of the PDE4 enzyme. Upregulation of cAMP is a promising therapeutic intervention for a range of psychiatric and neurological conditions. For example, studies with PDE4 inhibitors (HT-0712, roflumilast and BPN14770) have shown preliminary evidence of memory improvements in healthy elderly with age-associated memory impairments³⁰. In line with these results, GSK356278 demonstrated anxiolytic and cognition-enhancing effects in pre-clinical species performance in an object retrieval test⁴ and displayed a therapeutic profile that supported further evaluation of GSK356278 in a clinical setting. The aim of chapter 6 was to evaluate the relationship between the concentration of GSK356278 in plasma and the occupancy of the brain PDE4 enzyme. By performing multiple PET scans at different time points it was possible to measure the kinetics of GSK356278 at its target site in relation to the plasma PK. This is important because an increased target residence time (measured with PET) would suggest indirect drug kinetics, which could lead to different estimations of IC₅₀ following single or (clinically more relevant) repeat dosing³¹.

This study presents the first human data of PDE4 occupancy measured directly in the human brain with PET. Oral administration of 14mg GSK356278 led to a mean occupancy of 49 ± 8% at 3h post-dose and 19 ± 5% at 8h post-dose. The in vivo affinity (EC₅₀) of GSK356278 was estimated at 46 ± 3.6 ng/ml. Despite the possible

benefits of brain-penetrant PDE4 inhibitors, the highest dose in our study was limited to 14 mg by mechanism-dependent adverse events such as nausea and emesis. The relatively low levels of occupancy achieved with 14 mg in combination with the absence of a suitable (pseudo)reference region in the human brain, devoid of PDE4, complicated the estimations of the [¹¹C](R)-rolipram non-displaceable binding potential (BP_{ND}) directly from the study data. Three non-displaceable (V_{ND}) binding values were calculated with BP_{ND} estimates of 0.25, 0.5 and 1, which were chosen based on published data from an experiment with [¹¹C](R)-rolipram and the inactive enantiomer [¹¹C](S)-rolipram. The assumptions were that the (S) enantiomer demonstrates only non-displaceable binding, and the magnitude of this non-displaceable component is similar for both stereoisomers. Consequently, the population estimate of BP_{ND} ignores between subject variability in PDE4 expression and non-displaceable radiotracer binding. Nevertheless, the relatively large range of BP_{ND} estimates produced only a modest difference in GSK356278 EC₅₀ of 21–84 ng/ml, indicating that the estimated EC₅₀ is relatively robust to variability in assumed BP_{ND}. The data from the occupancy plot did not show hysteresis or other evidence for indirect pharmacokinetics for GSK356278 in the human brain, suggesting that the plasma EC₅₀ could be used to calculate PDE4 occupancy following repeat dose administration.

Future work is needed to determine the minimum level of occupancy required to ensure clinical effects. The decision on what is the minimal occupancy level to aim for will need to be made with reference to clinical and pharmacodynamic parameters achieved at particular occupancy levels. In addition, studies are required to assess the occupancy at steady state plasma GSK356278 concentration following repeat dose administration. Alternative dosing strategies such as the use of an up-titration regimen may help patients become accustomed a higher therapeutic maintenance dose with lower treatment discontinuation and improved tolerability. In vivo occupancy of PDE4 at T_{max} higher than 60% (assuming BP_{ND}=0.5) has not been published yet. Recent experiments in NHP with the PDE4 inhibitor roflumilast confirm plasma concentration-dependent occupancy with a maximum occupancy of 50% even after the administration of up to 200 µg/kg roflumilast³². Repeat dose administration may lead to higher occupancy levels, and this merits further investigation. PET occupancy data that are correlated to safety and tolerability measures might help to stratify patients based on potential for treatment efficacy in late phase development. This could allow pharmacological differentiation of the asset from marketed drugs or new competitor compounds.

Conclusions

Dysfunctional brain NMDA receptors and aberrant PDE4 enzyme activity are implicated in various neurological and psychiatric disorders including Alzheimer's disease and major depressive disorder. The visualisation of these biomarkers in the living human brain could identify biological mechanisms of disease pathogenesis and the pharmacological modification of disease progression. The strength of imaging with PET lies in its excellent quantitative accuracy and high sensitivity that allows for measurement of interactions between the radiotracer, its target, and modulation of these binding processes by an administered drug. However, the development of radiotracers with the right physiochemical characteristics is a major challenge. In addition, in order to successfully bridge preclinical and early clinical drug development, the timing of novel radiotracer availability for Phase 1 implementation is paramount if PET is to be used optimally to de-risk drug development of novel CNS compounds.

This thesis aims to extend our understanding of the ligand-target interactions of four radiotracers with the use of PET imaging of the healthy living brain. Chapter 2 presents a review of radiation dosimetry methods and estimates from 42 scientific reports. The radiation risk arising from carbon-11 labelled PET tracers showed a relatively small range of effective dose estimates in humans, owing to the short half-life of carbon-11 and the absence of tracer accumulation in a single radiation sensitive organ. Furthermore, carbon-11 radiotracer dosimetry in animals prior to human imaging may not offer significant value. Therefore, the benefit of animal dosimetry should be critically reviewed before experiments are committed to. The findings of chapter 2 support the conclusion that carbon-11 dosimetry studies in groups of healthy volunteers only should be performed if the radiotracer is foreseen to be repeatedly administered in large groups of subjects. Chapter 3 presents dosimetry of the brain NMDA receptor radiotracer [^{11}C]GMOM. The effective dose was at the lower end of the range seen for other carbon-11 radiotracers, allowing serial PET scanning in the same subject.

The interest in glutamatergic compounds such as ketamine for the treatment of mood disorders has greatly expanded in the past years. Glutamate is the most abundant neurotransmitter in the vertebrate nervous system and crucial for synaptic transmission. Chapters 4 and 5 detail PET experiments of [^{11}C]HACH242 and [^{18}F]PK-209; two radiotracers for different binding sites of the NMDA glutamate receptor, GluN2B and the intrachannel (PCP) site, respectively. PET time-activity

curves showed that [^{11}C]HACH242 and [^{18}F]PK-209 entered the brain with kinetics that are appropriate for CNS radiotracers. HPLC analysis identified the fraction of unmetabolised parent tracer in arterial plasma and radioactivity in blood. Contrary to expectations based on prior rodent imaging studies with both ligands, no consistent blocking effect was observed following intravenous administration of the NMDA modulators ketamine and radiprodil. Glutamate receptors regulate widely different molecular events from a single chemical signal, which separates them from some other well-validated imaging targets in the brain. The challenges in radiotracer development are akin to drug development in that there is considerable attrition of candidates during preclinical to clinical translational studies due to the narrow range of suitable tracer attributes and discrepancy between animal and human biology. Chapter 4 and 5 present suggestions for further experiments in humans that may be required to progress the development of radiotracers for in vivo imaging of the ionotropic NMDA receptor.

Chapter 6 reports on a Phase 1 study of the novel compound GSK356278, wherein multiple [^{11}C]R-rolipram PET scans in the same subject were performed to measure GSK356278 exposure and binding over time at the PDE4 target site in the brain. The relationship between the concentration of GSK356278 in plasma and the occupancy of the brain PDE4 enzyme showed an occupancy in healthy volunteers of approximately 50% at the tested dose of 14mg. These results can guide dose selection for subsequent clinical trials which aim to demonstrate therapeutic efficacy in patients.

More hospitals are building PET centres, and breakthroughs in radio-chemistry help to drive down imaging costs. The implementation of PET imaging early on in drug development can provide dose ranges for first-in-human safety and tolerability studies, and increase confidence of CNS candidate drugs in clinical development by disregarding unsuitable molecules early on. However, the application of PET imaging in CNS drug development depends on the availability of suitable imaging probes for the right targets. We have shown that four novel PET radiotracers reach the brain tissue and exhibit appropriate kinetics. Two of these demonstrate potential for quantification of drug binding at the NMDA receptor and PDE4 enzyme, illuminating a more effective way to make drug development decisions.

REFERENCES

- Rutter AR, Poffe A, Cavallini P, Davis TG, Schneck J, Negri M, Vicentini E, Montanari D, Arban R, Gray FA, Davies CH, Wren PB: GSK356278, a potent, selective, brain-penetrant phosphodiesterase 4 inhibitor that demonstrates anxiolytic and cognition-enhancing effects without inducing side effects in preclinical species: *The Journal of pharmacology and experimental therapeutics*. 2014;350(1):153-63. Available from: <https://doi.org/10.1124/jpet.114.214155>
- Comley RA, van der Aart J, Gulyás B, Garnier M, Iavarone L, Halldin C, Rabiner EA: In vivo occupancy of the 5-HT_{1A} receptor by a novel pan 5-HT_{1A/B/D} receptor antagonist, GSK588045, using positron emission tomography: *Neuropharmacology*. 2015;92:44-8. Available from: <https://doi.org/10.1016/j.neuropharm.2014.11.017>
- Van der Aart J, Salinas C, Dimber R, Pampols-Maso S, Weekes AA, Tonkyn J, Gray FA, Passchier J, Gunn RN, Rabiner EA: Quantification of human brain PDE4 occupancy by GSK356278: A [¹¹C](R)-rolipram PET study: *Journal of Cerebral Blood Flow & Metabolism*. 2017;0271678X1772086. Available from: <https://doi.org/10.1177/0271678X17720868>
- Dimber R, Searle G, Keat N, Cunneen M, Hallett W: Estimating the impact of injected activity on quantitative outcome measures in PET radioligand studies in the human brain: *Journal of Nuclear Medicine*. 2010. p. 1292-1292.
- The 2007 recommendations of International the International Commission on Radiological Protection. *International Commission on Radiological Protection (ICRP) publication 103*:7-8.
- Van Der Aart J, Hallett WA, Rabiner EA, Passchier J, Comley RA: Radiation dose estimates for carbon-11-labelled PET tracers: *Nuclear Medicine and Biology*. 2012;39(2):305-14. Available from: <https://doi.org/10.1016/j.nucmedbio.2011.08.005>
- Abanades S, van der Aart J, Barletta JAR, Marzano C, Searle GE, Salinas CA, Ahmad JJ, Reiley RR, Pampols-Maso S, Zamuner S, Cunningham VJ, Rabiner EA, Laruelle M, Gunn RN: Prediction of repeat-dose occupancy from single-dose data: characterisation of the relationship between plasma pharmacokinetics and brain target occupancy. *Journal of Cerebral Blood Flow and Metabolism*. 2011 Mar;31(3):944-52. Available from: <https://doi.org/10.1038/jcbfm.2010.175>
- Takano A, Varrone A, Gulyas B, Salvadori P, Gee A, Windhorst A, Vercouillie J, Bormans G, Lammertsma AA, Halldin C: Guidelines to PET measurements of the target occupancy in the brain for drug development: *European Journal of Nuclear Medicine and Molecular Imaging*. 2016;43(12):2255-62. Available from: <https://doi.org/10.1007/s00259-016-3476-4>
- Van der Aart J, van der Doef TF, Horstman P, Huisman MC, Schuit RC, van Lingen A, Windhorst AD, van Berckel BNM, Lammertsma AA: Human Dosimetry of the N-Methyl-D-Aspartate Receptor Ligand 11 C-GMOM: *Journal of Nuclear Medicine*. 2017;58(8):1330-3. Available from: <https://doi.org/10.2967/jnumed.116.188250>
- Zanotti-Fregonara P, Lammertsma AA, Innis RB: Suggested pathway to assess radiation safety of ¹¹C-labeled PET tracers for first-in-human studies: *European journal of nuclear Medicine and Molecular Imaging*. 2013 Oct;40(11):1781-3. Available from: <https://doi.org/10.1007/s00259-013-2512-x>
- Zanotti-Fregonara P, Innis RB: Suggested pathway to assess radiation safety of ¹¹C-labeled PET tracers for first-in-human studies: *European Journal of Nuclear Medicine and Molecular Imaging*. 2012 Mar;39(3):544-7. Available from: <https://doi.org/10.1007/s00259-011-2005-8>
- Gatley SJ: Estimation of upper limits on human radiation absorbed doses from carbon-11-labeled compounds: *Journal of Nuclear Medicine*. 1993 Dec;34(12):2208-15.
- Stabin MG: Uncertainties in internal dose calculations for radiopharmaceuticals. *Journal of Nuclear Medicine*. 2008 May;49(5):853-60. Available from: <https://doi.org/10.2967/jnumed.107.048132>
- Cherry SR, Jones T, Karp JS, Qi J, Moses W, Badawi R: Total-Body PET: Maximizing Sensitivity To Create New Opportunities for Clinical Research and Patient Care: *Journal of Nuclear Medicine*. 2017;jnumed.116.184028 Available from: <https://doi.org/10.2967/jnumed.116.184028>
- Cherry SR, Badawi RD, Karp JS, Moses WW, Price P, Jones T: Total-body imaging: Transforming the role of positron emission tomography: *Science Translational Medicine*. 2017;(March 2017):1-4. Available from: <https://doi.org/10.1126/scitranslmed.aaf6169>
- Schousboe A: Transport and metabolism of glutamate and GABA in neurons and glial cells: *International review of neurobiology*. 1981. Vol. 22, 1-45. Available from: [https://doi.org/10.1016/S0074-7742\(08\)60289-5](https://doi.org/10.1016/S0074-7742(08)60289-5)
- Béllanger M, Allaman I, Magistretti PJ: Brain energy metabolism: Focus on Astrocyte-neuron metabolic cooperation: *Cell Metabolism*. 2011;14(6):724-38. Available from: <https://doi.org/10.1016/j.cmet.2011.08.016>
- Paoletti P, Bellone C, Zhou Q: NMDA receptor subunit diversity: impact on receptor properties, synaptic plasticity and disease: *Nature reviews Neuroscience*. 2013 Jun;14(6):383-400. Available from: <https://doi.org/10.1038/nrn3504>
- Danysz W, Parsons CG: Alzheimer's disease, β -amyloid, glutamate, NMDA receptors and memantine--searching for the connections: *British journal of pharmacology*. 2012 Sep;167(2):324-52. Available from: <https://doi.org/10.1111/j.1476-5381.2012.02057.x>
- Honer M, Gobbi L, Martarello L, Comley RA: Radioligand development for molecular imaging of the central nervous system with positron emission tomography: *Drug discovery today*. 2014 Aug 27. Available from: <https://doi.org/10.1016/j.drudis.2014.08.012>
- Gruber S, Ametamey SM: Imaging the glutamate receptor subtypes—Much achieved, and still much to do: *Drug Discovery Today: Technologies*. 2017;25:27-36. Available from: <https://doi.org/10.1016/j.ddtec.2017.10.006>
- Klein PJ, Christiaans JAM, Metaxas A, Schuit RC, Lammertsma AA, van Berckel BNM, Windhorst AD: Synthesis, structure activity relationship, radiolabeling and preclinical evaluation of high affinity ligands for the ion channel of the N-methyl-D-aspartate receptor as potential imaging probes for positron emission tomography: *Bioorganic & Medicinal Chemistry*. 2015;23(5):1189-206. Available from: <https://doi.org/10.1016/j.bmc.2014.12.029>
- Christiaans JAM, Klein PJ, Metaxas A, Kooijman EJM, Schuit RC, Leysen JE, Lammertsma AA, van Berckel BNM, Windhorst AD: Synthesis and preclinical evaluation of carbon-11 labelled N-((5-(4-fluoro-2-[¹¹C]methoxyphenyl)pyridin-3-yl)methyl)cyclopentanamine as a PET tracer for NR2B subunit-containing NMDA receptors: *Nuclear Medicine and Biology*. 2014;41(8):670-80. Available from: <https://doi.org/10.1016/j.nucmedbio.2014.04.131>
- Klein PJ, Schuit RC, Metaxas A, Christiaans JAM, Kooijman E, Lammertsma AA, van Berckel BNM, Windhorst AD: Synthesis, radiolabeling and preclinical evaluation of a [¹¹C]GMOM derivative as PET radiotracer for the ion channel of the N-methyl-D-aspartate receptor: *Nuclear Medicine and Biology*. 2017 Aug;51:25-32. Available from: <https://doi.org/10.1016/j.nucmedbio.2017.05.003>
- Golla SSV, Klein PJ, Bakker J, Schuit RC, Christiaans JAM, van Geest L, Kooijman EJM, Oropeza-Seguias GM, Langermans JAM, Leysen JE, Boellaard R, Windhorst AD, van Berckel BNM, Metaxas A: Preclinical evaluation of [¹⁸F]PK-209, a new PET ligand for imaging the ion-channel site of NMDA receptors: *Nuclear Medicine and Biology*. 2015;42(2):205-12. Available from: <https://doi.org/10.1016/j.nucmedbio.2014.09.006>
- McGinnity CJ, Hammers A, Riaño Barros DA, Luthra SK, Jones PA, Trigg W, Micallef C, Symms MR, Brooks DJ, Koeppe MJ, Duncan JS: Initial evaluation of ¹⁸F-GE-179, a putative PET Tracer for activated N-methyl D-aspartate receptors: *Journal of Nuclear Medicine*. 2014 Mar;55(3):423-30. Available from: <https://doi.org/10.2967/jnumed.113.130641>
- Zamuner S, Rabiner EA, Fernandes SA, Bani M, Gunn RN, Gomeni R, Ratti E, Cunningham VJ: A pharmacokinetic PET study of NK₁ receptor occupancy: *European journal of nuclear medicine and molecular imaging*. 2012 Feb;39(2):226-35. Available from: <https://doi.org/10.1007/s00259-011-1954-2>
- Van der Doef TF, Golla SS, Klein PJ, Oropeza-Seguias GM, Schuit RC, Metaxas A, Jobse E, Schwarte LA, Windhorst AD, Lammertsma AA, van Berckel BN, Boellaard R: Quantification of the novel N-methyl-d-aspartate receptor ligand [¹¹C]GMOM in man: *Journal of Cerebral Blood Flow & Metabolism*. 2016;36:1111-21. Available from: <https://doi.org/10.1177/0271678X15608391>
- Comley RA, Salinas CA, Slifstein M, Petrone M, Marzano C, Shotbolt P, Van der Aart J, Neve M, Iavarone L, Gomeni R, Laruelle M, Gray FA, Gunn RN, Rabiner EA: Monoamine transporter occupancy of a novel triple reuptake inhibitor in baboon and human using Positron Emission Tomography: *The Journal of Pharmacology and Experimental Therapeutics*. 2013; 346(2), 311-317. Available from: <https://doi.org/10.1124/jpet.112.202895>
- Prickaerts J, Heckman PRA, Blokland A: Investigational phosphodiesterase inhibitors in phase I and phase II clinical trials for Alzheimer's disease: *Expert Opinion on Investigational Drugs*. 2017;26(9):1033-48. Available from: <https://doi.org/10.1080/13543784.2017.1364360>
- Shotbolt P, Tziortzi AC, Searle GE, Colasanti A, van der Aart J, Abanades S, Plisson C, Miller SR, Huiban M, Beaver JD, Gunn RN, Laruelle M, Rabiner EA: Within-subject comparison of [(11)C]-(-)-PHNO and [(11)C]raclopride sensitivity to acute amphetamine challenge in healthy humans: *Journal of Cerebral Blood Flow and Metabolism*. 2012 Jan;32(1):127-36. Available from: <https://doi.org/10.1038/jcbfm.2011.115>
- Takano A, Uz T, Garcia-Segovia J, Tsai M, Lahu G, Amini N, Nakao R, Jia Z, Halldin C: A Nonhuman Primate PET Study: Measurement of Brain PDE4 Occupancy by Roflumilast Using (R)-[¹¹C]Rolipram: *Molecular Imaging and Biology*. 2018;1-8. Available from: <https://doi.org/10.1007/s11307-018-1168-0>

CHAPTER 8

SUMMARY IN DUTCH
NEDERLANDSE SAMENVATTING



Het primaire doel van het onderzoek in dit proefschrift is de *in vivo* evaluatie van nieuwe positron emissie tomografie (PET) moleculen die kwantitatieve moleculaire beeldvorming mogelijk maakt van de glutamaatreceptor in de humane hersenen. De belangstelling voor glutamaterge geneesmiddelen zoals ketamine voor de behandeling van stemmingsstoornissen is de afgelopen jaren enorm toegenomen. Glutamaat is een belangrijke lichaamseigen stof; de meest voorkomende neurotransmitter in het vertebrale zenuwstelsel en cruciaal voor synaptische transmissie. Het bindt aan NMDA-receptoren, waarvan is aangetoond dat de functie verstoord is in verschillende neurologische en psychiatrische ziektebeelden, waaronder de ziekte van Alzheimer en depressieve stoornissen. De visualisatie en kwantificatie van NMDA-receptoren in het levende menselijke brein zou de identificatie van biologische mechanismen van ziektepathogenese mogelijk maken. Daarnaast kan met PET de farmacologische modificatie van biomarkers worden gemeten, zoals bijvoorbeeld doelbezetting van receptoren na toediening van een bepaalde dosis van een geneesmiddel. De kracht van medische beeldvorming met PET ligt in de uitstekende kwantitatieve nauwkeurigheid en hoge gevoeligheid van de techniek, zodat dynamische interacties tussen de PET-ligand (ook wel radiotracer genoemd) en het doelwit kunnen worden gemeten tijdens de scan.

De mogelijkheid om met behulp van PET de receptoren, transporters en enzymen in het brein te meten is echter niet vanzelfsprekend. De ontwikkeling van PET-radiotracers met de juiste fysicochemische eigenschappen is namelijk een grote uitdaging. Een radiotracer wordt zorgvuldig geselecteerd voor klinische implementatie na een reeks succesvolle preklinische experimenten waarin de optimalisatie van talrijke parameters centraal staat, zoals affiniteit, selectiviteit, lipofiliciteit, stabiliteit, radiochemisch potentieel, penetratie van de bloed-hersenbarrière, distributie in het weefsel en farmacokinetiek. De uitdagingen in het ontwikkelingsproces van radiotracers zijn vergelijkbaar met de ontwikkeling van geneesmiddelen; er is in beide gevallen sprake van een aanzienlijke afname van kandidaatmoleculen tijdens radiochemische, preklinische, en translationele experimenten. Er zijn tot op heden nog geen gevalideerde PET-radiotracers beschikbaar die betrouwbaar de binding aan NMDA-receptoren in het menselijke brein kunnen meten. Onderzoeksprogramma's van het VU Universitair Medisch Centrum te Amsterdam hebben significante vooruitgang laten zien in de identificatie en synthese van radiotracers voor twee verschillende bindingsplaatsen van de NMDA-receptor, namelijk [¹¹C]HACH242 voor GluN2B en [¹⁸F]PK-209 voor het ionkanaal.

Bij de ontwikkeling van nieuwe geneesmiddelen en radiotracers worden onderzoeken naar de farmacokinetiek en farmacodynamiek meestal eerst uitgevoerd

bij knaagdieren en/of primaten, en vervolgens bij mensen. De farmacokinetiek van onderzoeksmiddelen voor het centraal zenuwstelsel is normaalgesproken sterk gecorreleerd in primaten en mensen, mits verschillen tussen de twee soorten in biologische beschikbaarheid en plasmaconcentratie in acht worden genomen. Bovendien is beeldvorming in primaten wetenschappelijke te rechtvaardigen wanneer onderzoeksmiddelen (nog) niet zijn goedgekeurd voor menselijke toediening, zoals momenteel het geval is voor liganden met GluN2B-negatieve allosterische modulatie. In hoofdstuk 4 wordt de evaluatie van de radiotracer [¹¹C]HACH242 in drie primaten gepresenteerd. Een hybride PET-MRI-scanner werd gebruikt in combinatie met arteriële bloedafnames in een poging om [¹¹C]HACH242 binding te kwantificeren vóór en 10 minuten na toediening van een intraveneuze dosis radioprodil. Verwacht werd dat deze negatieve allosterische modulator van de GluN2B-receptor door middel van bindingscompetitie het signaal van [¹¹C]HACH242 in het brein zou verminderen. Dit zou een indicatie kunnen geven voor de mate van specifieke binding van beide stoffen aan de GluN2B NMDA-receptoren. De resultaten toonden aan dat [¹¹C]HACH242 in de hersenen werd opgenomen en de tijd-activiteitscurven (TACS) vertoonden reversibele farmacokinetiek binnen de 90 minuten durende PET-scan. In tegenstelling tot de verwachtingen op basis van eerdere preklinische studies werd er geen consistent blokkerings-effect waargenomen na toediening van radioprodil. In hoofdstuk 4 worden een aantal verklaringen voor de resultaten aangedragen, die in toekomstig onderzoek hiaten in kennis over de GluN2B radiotracers kunnen opvullen. Bijvoorbeeld (i) de bijdrage van radioprodil en anesthesie op veranderingen in hersendoorbloeding, (ii) het effect van radioprodil op de afgifte van [¹¹C]HACH242 van bloed naar weefsel, en andere bronnen van variabiliteit in de arteriële invoerfunctie, (iii) lichaamseigen liganden die de binding van [¹¹C]HACH242 aan NMDA-receptoren beïnvloeden, (iv) affiniteit van de radiotracer voor bindingsplaatsen benevens GluN2B, zoals sigma-1. In toekomstig PET-onderzoek kunnen de eerste twee versturende factoren worden geminimaliseerd door PET in mensen uit te voeren, zodat algehele anesthesie niet noodzakelijk is en er een groter volume arterieel bloed kan worden afgenomen. Nieuwe GluN2B-specifieke liganden die momenteel in ontwikkeling zijn zullen de klinische evaluatie van [¹¹C]HACH242 in de nabije toekomst mogelijk maken. Verdere beoordeling van de test-hertest-variabiliteit en specifieke GluN2B binding is daarom gerechtvaardigd.

De radiotracer [¹⁸F]PK-209 toonde in eerder primaatonderzoek kwantificeerbare specifieke binding aan NMDA-receptoren. De volgende stap in de validatie van de radiotracer is beschreven in hoofdstuk 5, namelijk de eerste toediening van [¹⁸F]-PK-209 in de mens. Een betrouwbare radiotracer moet een stabiel signaal geven bij

herhaalde metingen, ervan uitgaande dat de concentratie van het doelwit constant blijft. Verschillende farmacokinetische modellen werden in hoofdstuk 5 toegepast om de PET-data te analyseren, met als primaire doel om de test-hertest variabiliteit in gezonde proefpersonen te meten. Het secundaire doel omvatte de kwantificatie van de specifieke bindingscomponent. Hiertoe werd een vergelijking gemaakt tussen de farmacokinetiek van [¹⁸F]PK-209 vóór en na intraveneuze toediening van S-ketamine. In elk hersengebied bevinden zich neuronen met NMDA-receptoren, derhalve was een referentiegebied zonder NMDA-receptoren voor PET-modellering niet beschikbaar. Arterieel bloed werd daarom afgenomen tijdens elke scan, zodat een metaboliet-gecorrigeerde invoerfunctie kon worden gegenereerd.

De resultaten van deze studie laten zien dat [¹⁸F]PK-209 net als in niet-humane primaten goed opgenomen werd in de hersenen. De tijd-activiteitscurven tijdens de 120 minuten durende scan werden voor de meeste scans het beste beschreven met een irreversibel twee-compartimentenmodel met een extra correctie voor bloedvolume. De schatting van de irreversibele parameter k_3 was echter onnauwkeurig vanwege de kleine inhibitieconstante. De discussie van hoofdstuk 5 omvat een grondig onderzoek van de PET- en bloedresultaten om factoren te evalueren die mogelijk hebben bijgedragen aan de hoge test-hertest variabiliteit, alsmede de afwezigheid van een betrouwbare verlaging van het [¹⁸F]PK-209 signaal ondanks hoge plasma ketamine concentraties. Deze factoren omvatten:

- Verschillen in kenmerken van proefpersonen, zoals leeftijd.
- Verschillen in [¹⁸F]PK-209-injectaat, zoals radioactiviteit en molaire activiteit.
- Variatie in de tijd waarop de PET-scan werd uitgevoerd, alsmede seizoen effecten.
- Het interval tussen test- en hertestscans.
- De relatie tussen niet-verplaatsbare distributievolumes ($V_{ND} = K_1/k_2$) en K_1 en k_3 .
- Farmacokinetiek van de radiotracer in bloed, plasma en hersenen.
- Grootte van de hersengebieden en het effect hiervan op de kinetische modellering.
- Expressie van NMDA-receptoren in hersengebieden in relatie tot [¹⁸F]PK-209 binding.
- Variatie in radiometalieten en concentratie binnen en tussen proefpersonen.
- Herstelfracties van radioactiviteit uit plasma.
- Ketamine plasmaconcentraties en affiniteit voor de NMDA-receptor.
- Potentiële effecten van ketamine op hersendoorbloeding.
- In vivo NMDA-receptorbiologie en farmacologie.

Glutamaatreceptoren reguleren veelzijdige moleculaire processen via talrijke bindingsplaatsen op het neuron. Er zijn meer dan 20 verschillende glutamaatreceptoren, zoals de ionotrope NMDA-receptor, die alleen onder bepaalde omstandigheden doorlaatbaar is voor calciumionen. Toekomstig werk is nodig om de werking van de receptor in het levende brein beter te begrijpen en voor verdere toetsing van hypothesen is een groter cohort van proefpersonen vereist. De in dit proefschrift beschreven studies in primaten en gezonde vrijwilligers zijn niet alleen belangrijk voor de ontwikkeling van een volgende generatie NMDA-radiotracers, maar geven ook suggesties voor verder onderzoek met NMDA-radiotracers die (met beperkt succes) reeds klinisch zijn toegepast, zoals [¹¹C]GMOM en [¹⁸F]GE179.

Voorafgaand aan de klinische implementatie van nieuwe PET-radiotracers, vereisen zowel lokale als nationale ethische toetsingscommissies vanwege veiligheidsredenen een schatting van de stralingsbelasting van het radiofarmacon en het bijbehorende risico voor de proefpersoon dat voortvloeit uit de intraveneuze toediening ervan. Het secundaire doel van dit proefschrift, beschreven in hoofdstuk 2 en 3, is de kwantificatie en evaluatie van de stralingsdosis van radiotracers die met koolstof-11 gemarkeerd zijn. Omdat de tracer radioactief is, zendt die gammastraling uit die door de PET-scanner kan worden gedetecteerd. In hoofdstuk 2 worden de methoden voor het schatten van de stralingsdosis bij dieren en mensen besproken, evenals de biologische effecten van de gebruikelijke dosis in PET-onderzoek met koolstof-11 tracers.

De belangrijkste bevinding van het literatuuronderzoek was het smalle 95% betrouwbaarheidsinterval van de gemiddelde effectieve dosis van 5,2 tot 6,6 μ Sv per geïnjecteerde MBq. De twee belangrijkste verklaringen zijn de relatief korte halfwaardetijd van koolstof-11 en de spreiding van radioactieve moleculen in het lichaam, waardoor ophoping in een enkel stralingsgevoelig orgaan wordt voorkomen. Resultaten van tien dierstudies toonden bovendien aan dat preklinische dosimetrie niet voldoende betrouwbaar is als voorspeller voor humane dosimetrie. Dit is grotendeels het gevolg van de anatomische verschillen tussen dieren en mensen die niet correct kunnen worden gemodelleerd. De voordelen van dosimetrie in dieren moet daarom kritisch worden beoordeeld voordat de experimenten worden uitgevoerd.

De stralingsdosissen die in PET-onderzoeken worden toegediend zijn zo laag dat eventuele schadelijke effecten stochastisch van aard zijn. Met andere woorden, naarmate de dosis toeneemt, neemt *de kans* op schade toe, in plaats van de ernst van de symptomen. In hoofdstuk 3 worden PET-experimenten gepresenteerd

waarin het stralingsrisico in mensen wordt gekwantificeerd voor de nieuwe NMDA-receptor radiotracer [¹¹C]GMOM. In deze eerste humane PET-scans met [¹¹C]GMOM bleek de stof zoals verwacht de bloed-hersenbarrière te passeren in alle vijf proefpersonen. PET-scans van het hoofd tot en met het bovenbeen met een totale duur van 80 minuten maakten de visualisatie mogelijk van absorptie, distributie en eliminatie van de intraveneus geïnjecteerde [¹¹C]GMOM. Zeven bronorganen werden handmatig gedefinieerd op de CT-scans van de drie vrouwelijke en twee mannelijke proefpersonen. Het concentratie-tijdsverloop van koolstof-11 werd in deze organen gemeten en vervolgens geschaald naar een geslacht specifiek referentiemodel. De effectieve dosis (\pm standaarddeviatie, SD) was $4,5 \pm 0,5$ μ Sv per MBq. Zoals aangetoond in hoofdstuk 2 is de effectieve dosis van [¹¹C]GMOM relatief laag in vergelijking met andere koolstof-11 gemarkeerde liganden. Dit onderzoek kreeg de Alavi-Mandell Award toebedeeld door *The Society of Nuclear Medicine and Molecular Imaging* (SNMMI).

Een belangrijk onderdeel van PET in biomedisch onderzoek zijn de twee basisprincipes van stralingsbescherming: rechtvaardiging van bestraling en toediening van een dosis die zo laag als redelijkerwijs haalbaar is, zonder dat het doel van het onderzoek gecompromitteerd wordt. Desalniettemin is er in PET-studies van de hersenen een verband tussen de hoeveelheid geïnjecteerde radioactiviteit en de nauwkeurigheid van metingen. Voor kwantificatie van het PET-sigitaal in regio's met een klein volume of een lage binding van de radiotracer, is injectie van voldoende radioactiviteit vereist om een goede signaal-ruisverhouding te verkrijgen. De resultaten uit hoofdstuk 2 ondersteunen de stelling dat wanneer een met koolstof-11 gemerkte radiotracer niet meer dan tweemaal in dezelfde persoon zal worden toegediend, het zeer onwaarschijnlijk is dat het limiet van 10 mSv of een orgaandosis van 150 mSv per onderzoek wordt overschreden. Voor 31 van de 32 radiotracers die in hoofdstuk 2 worden besproken, wordt het limiet van 10 mSv zelfs niet overschreden als drie 400 MBq PET-CT-hersenscans in dezelfde proefpersoon worden gedaan. De gerapporteerde effectieve doses zijn echter groepsgemiddelden die alleen representatief zijn voor een populatie. Ze kunnen niet worden gebruikt om het risico voor een individu te berekenen omdat de biologische halfwaardetijd en opname tussen individuen significant kan verschillen. Niettemin worden in de berekening van de effectieve dosis de individuele verschillen in de orgaandosis afgezwakt door vermenigvuldiging van de geabsorbeerde dosis met een weefsel-factor, die de gevoeligheid van organen voor straling in acht neemt. Aangezien de stralingsbelasting van koolstof-11 tracers relatief laag is, moet de toegevoegde

waarde van dosimetriestudies in gezonde vrijwilligers goed overwogen worden. Alleen als wordt voorzien dat de radiotracer herhaaldelijk zal worden toegediend in grote groepen proefpersonen is het van belang uit te sluiten dat de radiotracer een uitzonderlijk hoge stralingsbelasting geeft. PET-CT-scans voor dosimetrie belasten namelijk niet alleen de proefpersoon, maar ook de bezetting van klinische scanners, goed opgeleid personeel en laboratoriumapparatuur. In dit opzicht is het essentieel om overeenstemming te bereiken tussen PET-onderzoekers dat een nieuwe radiotracer inderdaad onderzoek potentieel heeft dat extra bestraling van proefpersonen in dosimetrie-onderzoek rechtvaardigt.

De succesvolle integratie van verschillende onderzoek disciplines in PET, zoals chemie, fysica, biologie, en farmacologie, kan uiteindelijk leiden tot nieuwe toepassingen die een positief effect kunnen hebben op het leven van talrijke patiënten. Een betrouwbare radiotracer voor een relevante biomarker kan het ontwikkelingsproces van nieuwe geneesmiddelen bespoedigen door belangrijke klinisch farmacologische vragen te beantwoorden. Zoals, komt het onderzoeksmiddel op de plaats waar het zijn optimale biologische activiteit kan inzetten? Bindt het aan de juiste receptor, en veroorzaakt het middel een farmacologisch effect in gezonde vrijwilligers? PET-studies kunnen in een vroeg stadium van geneesmiddelontwikkeling een antwoord verschaffen op deze vragen, waardoor middelen die geen activiteit hebben direct kunnen worden gediscontinueerd. Dit vermindert de kans dat een primair onderzoeksdoel zoals effectiviteit niet wordt gehaald in fase 2 klinisch onderzoek.

Voor de mogelijkheid om binding van een onderzoeksmiddel in de hersenen vroeg in het ontwikkelingsproces te meten, is een waardevolle toepassing van PET. De relatie tussen doelbezetting en de plasmaconcentratie van het geneesmiddel over de tijd kan onderzoeksteams informeren over de juiste dosis voor verdere klinische ontwikkeling. In hoofdstuk 6 wordt het derde farmacologische experiment van dit proefschrift beschreven: Een fase 1-studie van het nieuwe onderzoeksmiddel GSK356278, een antidepressivum met procognitieve eigenschappen. In dit onderzoek zijn drie [¹¹C]R-rolipram PET-scans in dezelfde gezonde proefpersoon uitgevoerd zodat binding van GSK356278 aan het PDE4-enzyme in de hersenen gemeten kon worden op twee tijdstippen na inname in relatie tot de farmacokinetiek in het plasma. Wanneer de relatie tussen plasmaconcentratie en binding aan PDE4 (gemeten met PET) verandert over de tijd suggereert dit indirecte kinetiek tussen plasma en doelweefsel. Dit zou kunnen leiden tot afwijkende schattingen van IC₅₀ na eenmalige en herhaalde dosering. De relatie tussen de concentratie

van GSK356278 in plasma en de bezetting van het PDE4-enzym in de hersenen toonde een directe relatie over de tijd, met een PDE4 bezetting van ongeveer 50% rond de piek plasmaconcentratie (~3u na inname) bij de geteste dosis van 14 mg. Deze resultaten dienden als leidraad voor de beslissing over de dosis GSK356278 in vervolgonderzoek dat was gericht op therapeutische werkzaamheid in patiënten.

Vier decennia van multidisciplinair PET-onderzoek heeft een weelde aan data opgeleverd die tot substantiële vooruitgang heeft geleid in kennis over klinische farmacologie en geneesmiddelontwikkeling (geïntroduceerd in hoofdstuk 1). Dit proefschrift bouwt voort op dat werk met een literatuuroverzicht van dosimetrie van koolstof-11 gemarkeerde radiotracers (hoofdstuk 2) evenals vier originele PET onderzoeken waarin nieuwe radiotracers worden geëvalueerd (hoofdstuk 3 t/m 6). Tenslotte vat hoofdstuk 7 de belangrijkste resultaten van dit proefschrift samen en plaatst deze in de context van recente ontwikkelingen op het gebied van PET-beeldvorming. PET is uniek omdat het de mogelijkheid biedt om niet-invasief de concentratie van een geneesmiddel, de interactie met het doelweefsel, en de farmacodynamische effecten te kwantificeren in het levende menselijk brein. Hoewel de juiste toepassing van PET een gespecialiseerd multidisciplinair team vereist, en daarom relatief duur is, openen meer en meer ziekenhuizen PET-centra vanwege de toegevoegde waarde voor de gezondheidszorg en (pre)klinisch onderzoek. Naast het schaalvoordeel helpt ook vooruitgang in radiochemische technieken om de kosten van een PET-scan te drukken. En bovendien, de informatie die PET biedt kan de omvang en de duur van klinische onderzoek in geneesmiddelontwikkeling aanzienlijk verminderen door ongeschikte moleculen vroeg uit bedrijf te nemen, waardoor de kosten van het PET-onderzoek gemakkelijk kunnen worden gecupereerd. De waarde van PET bij de ontwikkeling van geneesmiddelen voor het centrale zenuwstelsel hangt echter af van de beschikbaarheid van geschikte radiotracers. We hebben aangetoond dat vier nieuwe radiotracers het hersenweefsel bereiken en adequate farmacokinetiek vertonen. Twee tracers hebben potentieel voor kwantificering van geneesmiddelbinding aan de NMDA-receptor en het PDE4-enzym. Moleculaire beeldvorming is een waardevol onderdeel geworden van farmacologisch onderzoek, en PET in het bijzonder kan het proces van geneesmiddelontwikkeling verlichten.



CURRICULUM VITAE

Jasper van der Aart was born on 27 December 1982 and raised in Lisse, the tulip capital of the Netherlands. After completing school (gymnasium level) in 2001 he went on to study Psychology at Leiden University. Jasper became intrigued by the measurement of neuropsychological functions whilst participating as a volunteer in a clinical trial at the Centre for Human Drug Research (CHDR). He continued his studies at Utrecht University, which offered a leading neuroscience programme, and obtained his Bachelor of Science degree in 2005. He was admitted to the research master Neuroscience & Cognition and graduated cum laude in 2008. During this period, he completed internships in Utrecht at the departments of Psychopharmacology and the University Medical Center, as well as at Cambridge University (UK) where he studied patients with ADHD and impulsive personality using PET imaging and neuropsychological test batteries. It was during this internship that Jasper's interest in CNS PET imaging was ignited.

About 100 km south, GlaxoSmithKline and Imperial College London had just opened the Clinical Imaging Centre (CIC) where Jasper was hired as an Imaging Scientist in 2008. In 2011, he helped transition the CIC into the privately held company Imanova (now Invicro), where imaging studies were performed in collaboration with three major London universities and several pharmaceutical companies. Having spent 6 years in the UK, Jasper returned to the Netherlands in 2013 to start a combined position at the CHDR and at the VU University Medical Center in Amsterdam as a PhD candidate under the supervision of prof.dr. Adriaan Lammertsma and prof.dr. Bart van Berckel. He has presented most of the work in this thesis at conferences such as BrainPET, BPS, BAP, and NeuroReceptor Mapping.

In 2015, Jasper joined the CHDR full-time as project leader of commercial Phase 1 clinical trials under the supervision of prof.dr. Joop van Gerven and dr. Geert Jan Groeneveld. Whilst working at the CHDR, he trained in clinical pharmacology and led first-in-human, single and multiple ascending dose studies with novel compounds for the treatment of mood and neurodegenerative disorders. In 2018, Jasper moved to Cambridge (UK) to join AstraZeneca as an Associate Director, working on late phase clinical development of the medicine Tagrisso in patients with lung cancer.

In his spare time, Jasper is an avid musician and has written and released more than 30 songs under his artist moniker Vandera. He has performed to large audiences around the world and is a household name to many with followers globally. His music can be found on vinyl, and streamed through online platforms such as Spotify, iTunes and YouTube. It is with his dedication and passion to every pursuit that he has accomplished these achievements in his work and hobbies.

PUBLICATIONS 2011-2019

J. van der Aart, M. Yaqub, E. Kooijman, J. Bakker, J. Langermans, R. Schuit, M. Hofman, J. Christiaans, A. Lammertsma, B. van Berckel, A. Windhorst. Evaluation of the novel PET tracer [^{11}C]HACH242 for imaging the GluN2B NMDA receptor in non-human primates. *Molecular Imaging & Biology*, 2019, 21(4), 676-685.

J. van der Aart, S. Golla, M. van der Pluijm, L. Schwarte, P. Schober, R. Schuit, P. Klein, A. Lammertsma, A. Windhorst, R. Boellaard, B. van Berckel. Test-retest reproducibility and specific binding of the NMDA receptor ligand [^{18}F]PK209 in humans. *EJNMMI Res*, 2018, 8(1):69.

J. van der Aart, D. Richards, G. Searle, C. Bishop, S. Shabbir, S. Zamuner, K. Edwards, P. Hawkins, E. Rabiner. Evaluation of [^{18}F]flutemetamol as a PET imaging agent in AL amyloidosis. 2019, in preparation.

J. van der Aart, C. Salinas, R. Dimber, S. Pampols-Maso, A. Weekes, J. Tonkyn, F. Gray, R. Gunn, E. Rabiner. Quantification of Human Brain PDE4 Occupancy by GSK356278: A [^{11}C](R)-Rolipram PET Study. *Journal of Cerebral Blood Flow & Metabolism*, 2018 Nov;38(11):2033-2048.

J. van der Aart, K. Recourt, G. Jacobs, M. de Kam, A. Khoshchin, K. Kanhai, P. Siebenga, R. Zuiker, E. Vets, M. Timmers, P. de Boer, J.M. van Gerven. Pharmacodynamic effects of the P2X7 receptor antagonist JNJ-54175446 in a translational human dexamphetamine challenge model. Abstract BAP conference 2017. Manuscript in preparation.

J. van der Aart, T. van der Doef, P. Horstman, M. Huisman, R. Schuit, A. van Lingen, A. Windhorst, B. van Berckel, A. Lammertsma. Human Dosimetry of the NMDA Receptor Ligand [^{11}C]GMOM. *The Journal of Nuclear Medicine*, 2017, 58 (8),1330-3.

J. van der Aart, H. van Gorsel, M. de Kam, M. Yaqub, A. Lammertsma, B. van Berckel, M. Timmers, P. de Boer, J. van Gerven. Amphetamine Induced Psychomotor Improvement in Relation to Striatal Dopamine Release in Healthy Subjects. Abstract. *J of Cerebral Blood Flow & Metabolism*, 2016, 36, 735-6.

C. Bakker, **J. van der Aart**, E. 't Hart, D. Kay, G. Groeneveld, A. Maelicke. Safety, pharmacokinetics and pharmacodynamics of repeat doses of intranasal Memogain[®], a prodrug of galantamine, in healthy elderly subjects. Abstract at BPS2017, manuscript in preparation.

R. Comley, **J. van der Aart**, B. Gulyas, M. Garnier, L. Iavarone, C. Halldin, E. Rabiner. In vivo occupancy of the 5-HT_{1A} receptor by a novel pan 5-HT_{1A}(A/B/D) receptor antagonist, GSK588045, using positron emission tomography. *Neuropharmacology*, 2015, 92: 44-8.

R. Comley, C. Salinas, M. Slifstein, M. Petrone, C. Marzano, P. Shotbolt, **J. van der Aart**, M. Neve, L. Iavarone, R. Gomeni, F. Gray, R. Gunn, E. Rabiner. Monoamine transporter occupancy of a novel triple reuptake inhibitor using Positron Emission Tomography. *J Pharmacol Exp Ther*, 2013, 346(2), 311-7.

F. Klumpers, D. Denys, **J. van der Aart**, L. Kenemans, J. Baas. Testing the effects of Δ^9 -THC and D-cycloserine on extinction of conditioned fear in humans. *J of Psychopharmacology*, 2012, 26(4):471-8.

P. Shotbolt, A. Tziortzi, S. Miller, **J. van der Aart**, S. Abanades, C. Plisson, M. Huiban, J. Beaver, R. Gunn, M. Laruelle, E. Rabiner. Within- subject comparison of the sensitivity of [^{11}C]-(+)-PHNO and [^{11}C]raclopride to amphetamine induced changes in endogenous dopamine in healthy human volunteers. *Journal of Cerebral Blood Flow & Metabolism*, 2012, 32(1):127-36.

S. Abanades, **J. van der Aart**, J. Barletta, C. Marzano, G. Searle, C. Salinas, J. Ahmad, S. Zamuner, V. Cunningham, E. Rabiner, M. Laruelle, R. Gunn. Characterising the relationship between plasma pharmacokinetics and brain target occupancy following single dose allows prediction of repeat dose target occupancy. *Journal of Cerebral Blood Flow & Metabolism*, 2011, 31:944-52.

J. van der Aart, W. Hallett, E. Rabiner, J. Passchier, R. Comley. Radiation Dose Estimates for Carbon-11 Labelled PET tracers. *Nuclear Medicine & Biology*, 2011, 39(2):309-14.

ACKNOWLEDGEMENTS

I would like to thank and acknowledge many colleagues, friends and family across the world who have contributed so generously to the work presented in this thesis.

Profound gratitude goes out to the volunteers and everyone who was involved in the projects, starting with colleagues and friends at the VU medical centre.

prof.dr. Adriaan Lammertsma	dr. 'PK-209' Pieter Klein	dr. Jaco Bakker
prof.dr. Bart van Berckel	dr. Athanasios Metaxas	dr. Ramsha Iqbal
prof.dr. Ronald Boellaard	dr. 'HACH242' Johannes Christiaans	Esther Kooijman
prof.dr. Albert D. Windhorst	dr. Thalia van der Doef	Patricia McCarthy
dr. Sandeep Golla	dr. Eline Verwer	Marieke van der Pluijm
dr.ir. Maqsood Yaqub		

I would like to extend my thanks to colleagues at the CHDR who provided a high performing and intellectually stimulating environment to work in, through their management, teaching and regular project leader socials.

prof.dr. Adam Cohen	dr. Rob Zuiker	dr. Marieke de Kam
prof.dr. Joop van Gerven	dr. Kasper Recourt	dr. Geretta Hogendoorn
dr. Geert Jan Groeneveld	dr. Charlotte Bakker	Ania Chaudhuri
dr. Gabriel Jacobs	dr. Kawita Kanhai	Folkert van Meurs
dr. Willem Birkhoff	dr. Jules Heuberger	Abdelrahman Elsharkawy

I would like to thank everyone at the Clinical Imaging Centre (London) for their inspiration and guidance in the field of translational imaging. A special mention for their wit and wisdom goes to:

dr. Ilan Rabiner	dr. Khanum Ridler	dr. Alessandro Colasanti
prof.dr. Roger Gunn	dr. John Beaver	dr. Matthew Wall
dr. Andy Brown	dr. Rob Janiczek	dr. Lisa Wells
dr. Rob Comley	dr. Qi Guo	
dr. Jan Passchier	dr. Sergio Abanades	

I remain grateful to mentors and friends at Utrecht University who encouraged me to embark on the pharmacology path.

prof.dr. Joke Baas	dr. Koen Bocker	dr. Natalia del Campo
prof.dr. Leon Kenemans	dr. Floris Klumpers	

My deepest love and thanks go out to friends and family who kept me smiling and sane. Especially Teije, Floris, my sister-in-law Kiran, my parents Ben & Jose, my sister, nieces and nephew Sigrid, Dali, India and Levi. Lastly, this thesis would not have been possible without the selfless time and care of Pav, who I am lucky enough to call my wife and mother of our son Rohan. They are the most important people in my world and I dedicate this thesis to them.

